IMPACT OF THE TUMOR EXTRACELLULAR MATRIX NICHE ON ACUTE MYELOID LEUKEMIA DRUG SENSITIVITY: A COMPARATIVE SCREENING STUDY

SAMIRA KABIR

A THESIS SUBMITTED TO THE FACULTY OF GRADUATES STUDIES IN PARTIAL FULFILMENT OF THE REQUIREMENTS FOR THE DEGREE OF MASTER OF SCIENCE

GRADUATE PROGRAM IN BIOLOGY

YORK UNIVERSITY

TORONTO, ONTARIO

APRIL 2026

ABSTRACT

Acute myeloid leukemia (AML) progression and drug resistance are strongly shaped by interactions between leukemic cells and the extracellular matrix (ECM) within the bone marrow niche. These ECM-driven signals promote cell survival and reduce therapeutic sensitivity, contributing to treatment failure and relapse. Traditional two-dimensional polystyrene cultures do not recapitulate these microenvironmental cues, limiting their predictive value for preclinical drug screening. Scaffold-based culture systems offer a more physiologically relevant model by mimicking ECM architecture and enabling cell–matrix interactions. However, quantifying drug responses in these complex systems is challenging, as conventional assays including plate-based viability, flow cytometry and high-content imaging, have distinct limitations.

In this study, we optimized and compared these methods to evaluate AML drug responses in both polystyrene and ECM-mimicking scaffolds. Flow cytometry enabled reliable assessment of cell viability and revealed clear differences in drug sensitivity between the two platforms. This comparative approach highlights the impact of the ECM microenvironment on therapeutic responses, improving the evaluation of candidate AML drugs.

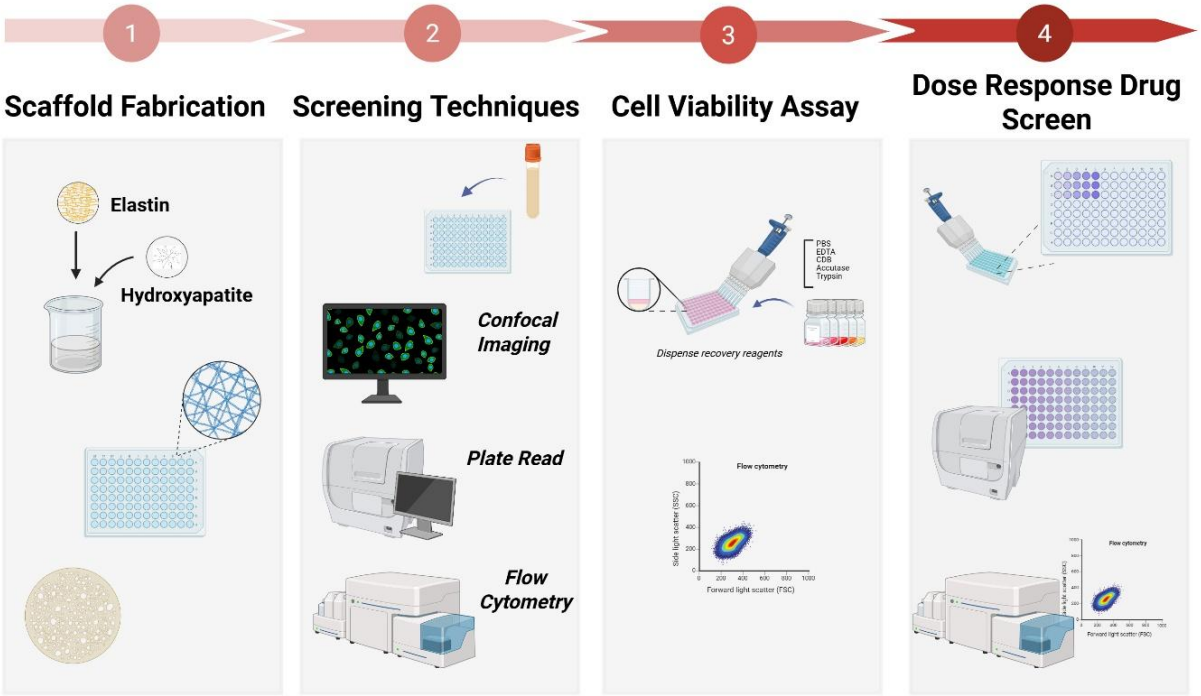

ACKNOWLEDGEMENTS

First and foremost, I would like to sincerely thank Dr. Eleftherios Sachlos for welcoming me into his lab and providing me the opportunity to pursue this research. I am deeply appreciative of his guidance, patience, and unwavering support throughout my graduate journey, his mentorship has been truly formative in shaping both my research and personal growth.

I would like to express my genuine gratitude to my supervisory committee Dr. Yuqing Feng for her thoughtful critique and words of wisdom for navigating through this process as well as my external examiners for their invaluable time. Additionally, this research was made possible through the generous support of CIHR and a NSERC Discovery Grant.

My heartfelt appreciation especially goes to Milad Falahat Chian for generously giving his time whether through meticulous training or invaluable advice for every single one of my experiments; I am incredibly grateful for his support. To my cherished friend Zhaklina, I will not forget the great friendship we built in our time forged through the long and grueling hours of our experiments, I could not have endured the hardships of research without you. Special thanks to Farrah Sawh for her constant companionship as well as Adriana Pagnani for her uplifting words. I would like to acknowledge the remaining members of the Stem Cell Engineering Lab, Joab Ogato and Ife Adeniyi, for their support and encouragement. Each member of the lab has contributed to my growth, fostering an inspiring research environment.

Lastly, I would like to thank my parents for giving me the freedom to pursue my passions and encouraging my academic growth through their limitless love. I am truly thankful to my sister for her endless belief in me and for always being there as a pillar of support in every aspect of my life. To my lifelong friends, thank you for standing by me throughout this degree and for your enduring love, patience, and encouragement. I would not be where I am today without all of you.

TABLE OF CONTENTS

LIST OF ABBREVIATIONS

2D	Two-Dimensional
5-FU	5-Fluorouracil
7-AAD	7-Aminoactinomycin D
αMEM	Alpha Minimum Essential Medium
AML	Acute Myeloid Leukemia
Ara-C	Cytarabine
BM	Bone Marrow
C	Collagen Type I
CD34	Cluster of Differentiation 34
CD38	Cyclic ADP Ribose Hydrolase
CD44	Cluster of Differentiation 44
CD45	Protein Tyrosine Phosphatase, Receptor Type C
CD49f	Integrin α6
CFU	Colony-Forming Unit
CSC	Cancer Stem Cell
CXCL12	C-X-C Motif Chemokine Ligand 12
CXCR4	C-X-C Chemokine Receptor 4
DAU	Daunorubicin
DMSO	Dimethyl Sulfoxide
DRD2	Dopamine Receptor D2
E	Elastin
ECM	Extracellular Matrix
ECs	Endothelial Cells
EDC	1-Ethyl-3-(3-Dimethylaminopropyl) Carbodiimide Hydrochloride
EDTA	Ethylenediaminetetraacetic Acid
FAB	French-American-British Classification
FBS	Fetal Bovine Serum
FIL	Filanesib

FN	Fibronectin
HA	Hydroxyapatite
HCS	High-Content Screening
Hoechst 33342	Fluorescent DNA-Binding Nuclear Stain
HSC	Hematopoietic Stem Cell
HSPC	Hematopoietic Stem and Progenitor Cell
HTS	High-Throughput Screening
LSC	Leukemia Stem Cell
MSC	Mesenchymal Stromal Cells
NHS	N-Hydroxysuccinimide
PBS	Phosphate Buffered Saline
PCR	Polymerase Chain Reaction
PEF	PBS, EDTA, FBS
PS	Polystyrene
SOR	Sorafenib
TDZ	Thioridazine
VEGF	Vascular Endothelial Growth Factor
VLA-4	Very Late Antigen-4
ZSQ	Zosuquidar

LIST OF FIGURES

CHAPTER 1

INTRODUCTION

1.1 Hematopoiesis and the Bone Marrow Niche

1.1.1 The Hematopoietic System

Hematopoiesis is a regulated biological process responsible for the continual renewal of an organism's blood cellular constituents, sustaining tissue maintenance through the production of diverse, specialized blood and bone marrow cells[118]. Critical physiological roles such as oxygen transport, platelet-mediated coagulation and immune defence are mediated by diverse cell types including erythrocytes, monocytes, lymphocytes, granulocytes and platelets[84]. These functions occur predominantly within the bone marrow (BM), a specialized and highly vascularized tissue that provides the structural and biochemical niche for the hematopoietic stem cell (HSC)[73]. In this niche, HSCs reside in close proximity to the stromal and endothelial components, promoting mutual survival[60].

1.1.2 Bone Marrow Microenvironment

The bone marrow microenvironment coined the "bone marrow niche" was conceptualized by Raymond Schofield in 1978 as important domain required for hematopoietic stem cell (HSC) maintenance. It is responsible for governing hematopoietic stem cell (HSC) fate by integrating structural, biochemical and mechanical cues that collectively maintain homeostasis[74]. Its role extends beyond serving as a physical habitat for the cells, as this complex framework provides a highly organized three-dimensional framework in which HSCs interact with stromal, endothelial, and bone-associated cells. Adhesion molecules, growth factors, and chemokines comprise this matrix and influence HSC behaviour through diverse signaling pathways, from these interactions HSC quiescence, self renewal, lineage commitment and mobilization are regulated[116].

The bone marrow microenvironment can be divided into the endosteal domain adjacent to bone-lining osteoblasts and the vascular domain enriched in sinusoidal endothelial and perivascular cells[119]. The endosteal niche is composed of osteoblasts, osteoclasts, sinusoidal endothelial cells, and stromal populations located along the bone surface. Together, these cells create a microenvironment that supports quiescent, long-term HSCs, with direct HSC–osteoblast interactions maintaining stem cell dormancy. Experimental

ablation of osteoblasts induces previously quiescent HSCs to enter the cell cycle, demonstrating their essential role in preserving stem cell quiescence and pool size. Expansion of osteoblast populations enhances hematopoiesis through Notch signaling, whereas osteoblast depletion disrupts marrow hematopoiesis and promotes extramedullary blood formation. Osteoblast-derived Wnt and BMP signaling pathways further contribute to HSC maintenance and long-term reconstitution capacity. Adhesion molecules such as N-cadherin, β-catenin, CD44, VCAM-1, cadherin-11, and ALCAM anchor HSCs within the niche and support stem cell preservation[68]. In addition, osteoblasts influence lineage production, including erythropoiesis and B-lymphopoiesis, while factors such as osteopontin can suppress HSC proliferation, indicating that the endosteal niche exerts both supportive and inhibitory regulation of hematopoiesis.

In contrast, the vascular niche is formed by arterioles, capillaries, sinusoidal vessels and surrounded by specialized endothelial cells, CXCL12-abundant reticular (CAR) cells in specific[77]. This compartment supports HSC activation, proliferation and differentiation and is associated with hematopoietic regeneration following physiological stress or transplantation. Endothelial cells influence HSC fate through angiocrine signaling and direct homing and trafficking via CXCR4/CXCL12 and RANK/RANKL pathways. CAR cells, which highly express VCAM-1, selectins, CD44, cytokines, and platelet-derived growth factor[52], additionally modulate HSC adhesion, migration, and vascular remodeling. Collectively, the endosteal and vascular compartments operate as a coordinated regulatory network in which HSC localization dictates functional state, maintaining hematopoietic homeostasis while enabling adaptive responses to stress.

1.1.3 Hematopoietic Stem Cells (HSCs)

At the apex of this hierarchical system reside hematopoietic stem cells (HSCs), first identified by Till and McCulloch for their defining capacities of self-renewal and to generate multiple hematopoietic lineages through multipotent differentiation[107]. Their work revealed HSCs are capable of fully restoring the hematopoietic system after sustaining damage by holding the capacity for transplantation and multilineage hematopoietic reconstitution.

Through asymmetric division, HSCs both preserve the long-term self-renewing stem cell pool and produce hematopoietic progenitor cells[86]. These progenitors undergo successive proliferative divisions and lineage commitment steps, forming precursor populations that ultimately mature into fully differentiated somatic blood cells. It encompasses the full spectrum of mature blood cells spanning both myeloid and lymphoid lineages. The myeloid lineage is comprised of (red blood cells), granulocytes, macrophages, and megakaryocytes whereas the lymphoid lineage generates T lymphocytes, B lymphocytes, and natural killer (NK) cells[42]. These properties allow for HSCs to regulate and maintain immune function while simultaneously recovering from injury regulating tissue regeneration and repair.

Although the abilities of HSCs are remarkable, and considerable effort is given towards exploiting HSCs for therapeutic applications, research is constrained by progressive loss of stemness and cell viability over time. These challenges arise primarily from HSCs struggling to maintain themselves outside of their physiological microenvironment, the bone marrow (BM) niche[129].

1.2 Extracellular Matrix (ECM) and Its Components

Within the bone marrow niche, the extracellular matrix (ECM) serves as a critical structural and regulatory component, providing both physical support and a reservoir of biochemical cues that influence hematopoietic stem and progenitor cell fate. This intricate network, composed of structural proteins, glycoproteins and signaling molecules[56], governs processes such as cell adhesion, proliferation, differentiation, and survival. The ECM further regulates cell behaviour through its mechanical properties, including stiffness and elasticity, and by controlling growth factor availability via binding, sequestration, and presentation[48].

1.2.1 Collagen

Extracellular matrix (ECM) components from all three major classes, collagen proteoglycans, and glycoproteins, are present within the bone marrow microenvironment and contribute to a variety of biological functions. These include the regulation of cell growth, mediation of cell adhesion and anti-adhesion processes, and the binding and

presentation of cytokines[19]. Within the bone marrow, two primary niches have been described: the endosteal (osteoblastic) niche, which supports hematopoietic stem cell quiescence and self-renewal, and the vascular or perisinusoidal niche, which is more closely associated with cellular proliferation and differentiation[49].

Collagen represents a major structural component of the bone marrow ECM and is predominantly localized within the endosteal osteoblastic niche. In addition to providing mechanical support, collagen contributes to the sequestration and presentation of growth factors within the niche. Analyses of ECM composition have identified Type VI collagen as the most abundant form (approximately 60% of total collagen), followed by Type I collagen (approximately 30%), while Types IV and V are detected primarily in bone marrow–derived ECM[33]. These collagen components have also been shown to influence mesenchymal stromal cell (MSC) differentiation toward osteogenic lineages[57].

Importantly, ECM collagen is significantly downregulated within the pre-leukemic bone marrow niche, suggesting that ECM remodeling is an early event in acute myeloid leukemia (AML) development. This remodeling is associated with reduced expression of several collagen genes, including Col1a1, Col1a2, Col3a1, Col4a1, and Col6a1[33]. Such alterations to ECM composition are proposed to play a critical role in reshaping the bone marrow microenvironment in a manner that promotes leukemogenesis and therefore are one of the primary proteins utilized in our ECM mimicking scaffold.

1.2.2 Hydroxyapatite

Similar to collagen, hydroxyapatite is an inorganic mineral constituent of the bone marrow niche that contributes to the rigidity and mechanical stability of the endosteal surface, where hematopoietic stem cells (HSCs) and stromal cells reside. In addition to its structural role, hydroxyapatite can bind and localize proteins, growth factors, and cytokines, thereby influencing signaling within the microenvironment and regulating the activity of osteoblasts and mesenchymal stromal cells (MSCs). Stromal cell–derived ECM generated within a collagen–hydroxyapatite (Col/HA) scaffold designed to mimic the bone marrow niche has been shown to promote MSC proliferation while preserving their differentiation potential. In

this system[7], MSCs synthesize ECM components that help reconstitute a tissue-specific three-dimensional microenvironment in vitro. This reconstructed environment has also been associated with enhanced angiogenic properties in vascularized bone tissue models, which is particularly important because a well-developed vascular network supports hematopoietic cell maintenance, migration, and signaling[43].

As hydroxyapatite can bind and present growth factors and cytokines that regulate stromal and osteoblastic cells, interactions within the niche can be modified in ways that favor leukemic cell survival. Through these interactions, leukemic cells can influence stromal and osteoblastic elements to generate an altered microenvironment that supports disease progression. For this reason, hydroxyapatite is frequently incorporated into biomaterial scaffolds to more accurately replicate the physical and biochemical properties of the bone marrow niche.

1.2.3 Elastin

Elastin is an extracellular matrix (ECM) protein that contributes to the elasticity and structural resilience of tissues, including those within the bone marrow (BM) niche. It is found within both the ECM and vascular structures, where it helps maintain tissue flexibility and mechanical integrity. These elastic properties are important for accommodating cellular movement, vascular expansion, and the dynamic remodeling that occurs within the niche[76]. Such flexibility is essential for regulating interactions between stromal and hematopoietic cells. However, during malignancy, these mechanical and structural properties can become altered in ways that favor leukemic cell survival and proliferation. Previous studies have suggested that reduced elastin levels within the bone marrow niche can promote cell proliferation in multiple myeloma, with proteomic and cell culture experiments demonstrating that decreased elastin correlates with increased proliferation, while supplementation with elastin can mitigate pro-myeloma effects[134]. Given its crucial role in maintaining the extracellular matrix and influencing cell behavior, elastin is often incorporated into scaffolds.

In acute myeloid leukemia (AML), interactions between leukemic cells and ECM components, such as collagen, fibronectin, hydroxyapatite and elastin, are essential not only for maintaining the structural integrity of the niche but also for mediating cell–matrix interactions that regulate cell–cell contact, migration, and spatial organization[111]. The ECM influences cellular behavior through multiple mechanisms including the presentation of bound growth factors, cytokines and adhesion ligands that signal via cell surface receptors like integrins[72]. AML cells can actively remodel the ECM by downregulating specific proteins, a process that contributes to disease progression. Even in the absence of niche cells, ECM characteristics such as mechanical stiffness, ligand availability and growth factor presentation[131] can independently modulate cell survival and responses to chemotherapeutic agents.

These ECM-mediated signals are particularly relevant in AML, where they can alter sensitivity to chemotherapeutic agents and contribute to therapy resistance[80]. Understanding how AML cells interact with the bone marrow ECM is therefore essential for developing physiologically relevant in vitro models and enhancing the predictive accuracy of drug screening platforms[18].

1.3 Hematopoietic Malignancies

1.3.1 Acute Myeloid Leukemia (AML)

Acute myeloid leukemia (AML), an aggressive hematologic malignancy characterized by the rapid expansion of abnormal myeloid cells in the bone marrow and peripheral blood. Acute myeloid leukemia (AML) is the most common acute leukemia in adults, comprising approximately 80% of cases in this population. Disease occurrence rises markedly with age, increasing from roughly 1.3 per 100,000 in individuals younger than 65 years to more than 12 per 100,000 among those older than 65[53]. The disease arises from somatic mutations in HSCs or early progenitor cells, which impair regular differentiation and results in an uncontrolled proliferation of immature myeloid blasts. Anemia, thrombocytopenia and increased susceptibility to infections are common symptoms of AML and present similarly to bone marrow failure, reflecting its disruption of hematopoiesis[85].

Current therapeutic approaches for AML include chemotherapy, radiation therapy, targeted therapies, and stem cell transplants. However, despite advancements in treatment, the disease remains associated with high relapse rates and limited overall survival, partially due to the malignancy's heterogeneity. Genetic alteration such as FLT3-ITD, NPM1, or TP53 mutations directly influence treatment response and overall survival[40]. Variability in molecular alteration and cytogenetic abnormalities contributes to disease presentation, progression, and treatment response[38]. To understand the complexity, a classification system based on genetic, morphologic, immunophenotypic, and clinical features was constructed worldwide by different countries to categorize patients into risk and outcome probabilities. These classifications are critical to guide diagnosis and therapeutic course of action.

Despite classification and treatment efforts, AML remains challenging to treat due to persistence of leukemic stem cells (LSCs) which can not be targeted by most existent chemotherapeutics. These LSCs possess stem cell-like properties including quiescence and self renewal, therefore repopulating the bone marrow with therapy resistant cells and driving relapse[16]. The heterogeneous nature of AML combined with LSCs ability to evade standard therapies through interactions with the bone marrow niche, emphasizes their central role in disease persistence and highlights the need to better understand their biology[106].

1.3.2 Leukemic Stem Cells (LSCs)

Leukemic stem cells (LSCs) are a functionally critical population in acute myeloid leukemia (AML) that drive disease initiation, progression, and relapse. LSCs are thought to originate through the stepwise accumulation of somatic mutations in HSCs or early progenitor cells, they possess a unique self-renewal capacity and block normal myeloid differentiation. These LSCs undergo clonal expansion and overcrowd the bone marrow with immature myeloid blasts that suppress hematopoietic stem and progenitor cell production and function (Fig. 1). In vivo studies show that LSC-enriched fractions defined by a $CD34^{+}CD38^{-}$ phenotype possess elevated stemness characteristics and survive chemotherapy, contributing to poor patient survival[5].

Studies exhibited phenotypic characterization of LSCs to typically express high levels of CD33 and CD45RA, expressing themselves as CD43+CD38-CD90- correlating to a unique profile that distinguishes them from normal HSCs[45]. They demonstrate developmental plasticity underlying leukemogenesis, however as the links between specific mutation profiles to leukemia manifestations cannot be defined clearly, they require further investigation.

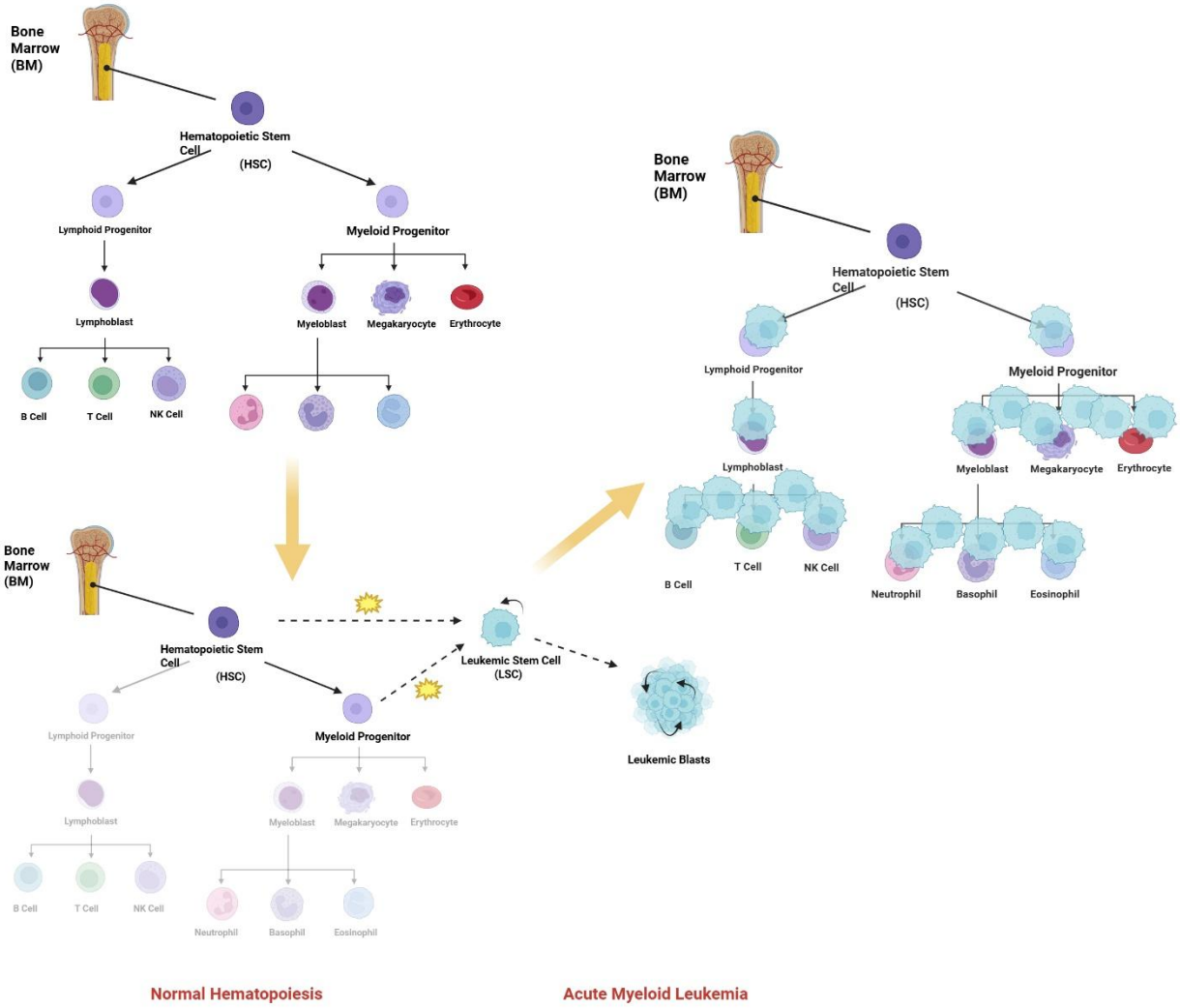

Figure 1. Comparison of normal hematopoiesis and leukemic transformation in acute myeloid leukemia (AML). Under normal conditions (left), hematopoietic stem cells (HSCs) in the bone marrow differentiate through tightly regulated lineage pathways into lymphoid and myeloid progenitors. In AML (right), genetic and molecular alterations disrupt this hierarchical differentiation process, leading to the formation of leukemic stem cells (LSCs). These cells exhibit uncontrolled self-renewal and give rise to an accumulation of immature leukemic blasts while impairing normal hematopoietic development.

1.3.3 The Leukemic Niche

In addition to genetic dysregulation, numerous studies show that the pathologically altered bone marrow microenvironment substantially contributes to leukemogenesis in AML[128]. Leukemic blasts and adjacent stromal components dynamically influence one another via interconnected signaling pathways. The leukemic niche contains several important components that contribute to the interplay between LSCs and their microenvironment such as metabolism, hypoxia, inflammation, secreted factors, cellular components and the extracellular matrix.

LSC behaviour is sustained through both intrinsic oncogenic signaling and external microenvironmental influences that mirror those governing HSCs. Regulatory pathways such as those responsible for Wnt/β-catenin signaling preserve LSC quiescence, self-renewal, and proliferative potential and can promote the conversion of HSCs and its progenitors into leukemia-initiating cells[133]. Genetic abnormalities frequently observed in AML, such as Mixed-Lineage Leukemia (MLL) rearrangements, can reprogram mutated progenitor cells towards stem-like states, strengthening LSC maintenance and highlighting their significance in chemoresistant relapse[81]. Through this interaction between LSCs and the bone marrow microenvironment, the niche can be remodelled into a specialized leukemic niche that aids in protecting LSCs, promotes survival signaling, and contributes to therapeutic resistance and relapse. Xenograft transplantation experiments reveal that LSCs rely on niche-derived cues, which direct their engraftment, resistance to chemotherapy, and regulation of cell cycle activity[59].

1.4 Niche Remodeling and Hijacking in AML

Chemotherapy resistance, leukemic survival and disease relapse in AML are increasingly attributed to the capacity of leukemic stem cells (LSCs) to remodel and exploit the bone marrow (BM) microenvironment. By reprogramming niche components, LSCs establish conditions that preferentially support leukemic survival and self-renewal while suppressing normal hematopoietic stem and progenitor cells (HSPCs)[112]. In healthy hematopoiesis, vascular and endosteal niches regulate HSC fate through coordinated chemokine, growth

factor and adhesion signaling[55]. During leukemogenesis, however, stromal, osteoblastic, and endothelial cells adopt a leukemia-supportive phenotype, while LSCs manipulate local signaling networks through cytokine secretion, receptor engagement and activation of pro-survival pathways. These interactions modulate key signaling proteins and confer protection from cytotoxic stress, limiting therapeutic efficacy.

1.5 Drug Resistance

As therapeutic agents target distinct receptors, kinases, and intracellular signaling pathways, their resistance mechanisms and interactions with the BM niche differ substantially[51]. This highlights the need to evaluate drugs with diverse mechanisms of action and compare their preliminary research data to their clinical outcome to characterize BM-mediated chemoresistance in AML.

1.6 Resistance Mechanisms and Clinical Relevance of Chemotherapeutics

1.6.1 5-Flourouracil

5-Flourouracil (5-FU) is an antimetabolite chemotherapeutic agent widely used in the treatment of a diverse array of cancers that is especially effective in treating breast and gastrointestinal cancers[113]. 5-FU is reputed as being most effective when administered through prolonged intravenous infusions against advanced, slow-growing tumors characterized by low proliferation fractions and extended doubling times[36]. Despite its established role in improving response rates and survival in other malignancies, 5-FU is not a first-line treatment for AML because its therapeutic ability is hindered by challenges such as off-target toxicities, lack of selectivity, and the development of chemoresistance[66]. Efforts to characterize tumor specificity may help determine genes, microRNAs, and cytokines involved in 5-FU toxicity and therapeutic response, however, these mechanisms are not yet fully defined due to tumor heterogeneity and variability in patient responses[21]. Elucidating the mechanism of action of 5-FU is essential for understanding its therapeutic effects and improving clinical outcomes.

5-Flourouracil exerts its anticancer effects by disrupting nucleic acid synthesis following intracellular conversion to active metabolites. These metabolites inhibit thymidylate

synthase (TS), leading to thymidine depletion and impaired DNA synthesis and are incorporated into RNA and DNA thus interfering with transcription and replication[130]. These actions inhibit cell proliferation, promote cell death and selectively target rapidly dividing cancer cells.

Although 5-fluorouracil (5-FU) is widely used as a standard chemotherapeutic agent in the treatment of several solid malignancies, its application in acute myeloid leukemia (AML) remains limited[104]. Due to a lack of robust clinical evidence demonstrating efficacy against AML, it has not been incorporated into standard treatment regimens. While early experimental studies reported reductions in leukemic growth in animal models of myeloid leukemia, suggesting potential antileukemic activity under certain conditions, these findings have remained preclinical and have not translated into clinical use[27]. Within laboratory settings, 5-Flourouracil has been utilized primarily as a research tool to investigate chemotherapy resistance including selection and characterization of primitive or stem-like leukemic subpopulations that exhibit intrinsic drug tolerance. While established AML treatment protocols primarily rely on cytarabine-based combination regimens, additional antimetabolite agents such as fludarabine, may be incorporated for selected patients with high-risk or relapsed disease[105]. Such studies contribute to understanding leukemic cell hierarchies and resistance mechanisms rather than serving as a foundation for therapeutic application.

1.6.2 Daunorubicin

Daunorubicin is a cornerstone anthracycline chemotherapy agent commonly used in the treatment of acute myeloid leukemia (AML), acute lymphoblastic leukemia (ALL) and Kaposi's sarcoma. In AML, Daunorubicin is frequently administered in combination with Cytarabine as part of the standard "7+3" induction regimen, in which Cytarabine is given as a continuous infusion for seven days while Daunorubicin is delivered as short intravenous infusions on each of the first three days[91]. Using this regimen, complete remission is achieved in 70-80% of patients however this varies depending on patient age, disease stage and cytogenic risk[35]. These factors highlight the importance of understanding the

mechanisms underlying daunorubicin's cytotoxic activity, as such insight may guide optimization of dosing strategies and therapeutic efficacy.

Daunorubicin exerts antimitotic and cytotoxic effects through multiple mechanisms including intercalation into DNA and topoisomerase II inhibition, with additional mechanisms involving transcription suppression and pathway modulation via production of DNA- damaging free radicals[14]. The agent halts DNA replication and transcription by causing double stranded breaks via topoisomerase IIα inhibition[108]. Additionally, it has been suggested there may be interactions between daunorubicin and cell membranes altering membrane fluidity and impacting signaling protein activity[6]. These diverse mechanisms contribute to its antileukemic effect and emphasizes its continued clinical use as a central component of AML therapies.

Recent advancements in remission rates and overall survival have largely relied on dose intensification of established chemotherapeutic agents rather than the introduction of novel therapies. Several clinical studies suggest that increasing Daunorubicin dosing during induction therapy may enhance therapeutic outcomes. In a randomized trial of younger patients with AML (17–60 years), high-dose daunorubicin significantly improved complete remission rates (70.6% vs. 57.3%) and prolonged overall survival (23.7 vs. 15.7 months) compared with standard dosing[28]. Similarly, dose escalation to 90 mg/m^2 has been associated with improved remission and survival outcomes relative to lower-dose regimens (45 mg/m^2), with remission rates increasing from 54% to 64% in older patients without additional toxicity[67]. Although dose intensification of Daunorubicin has been associated with improved remission rates in specific AML patient populations, the benefits of high-versus-low dose administration needs to be weighed against the well-established risk of cumulative anthracycline-associated cardiotoxicity[93], which may limit tolerability and long-term outcomes. Therefore, defining the optimal Daunorubicin dose remains a clinical challenge and reaffirms the need for individualized treatment strategies based on patient age, comorbidities and genetic risk factors.

1.6.3 Sorafenib

Sorafenib, an oral multikinase inhibitor, was developed as a targeted anticancer agent by exhibiting antiproliferative and antiangiogenic effects. It is currently only FDA approved for the treatment of patients with advanced or progressive renal cell carcinoma, hepatocellular carcinoma, and differentiated thyroid carcinoma[30]; however, sorafenib is being investigated in hematologic malignancies particularly in FLT3-mutated acute myeloid leukemia, where kinase signalling contributes to leukemic progression. It functions by inhibiting several intracellular and receptor tyrosine kinase pathways that are frequently dysregulated in malignancy, notably the Raf-Ras signalling cascade, the vascular endothelial growth factor (VEGF) pathway, and FMS-like tyrosine kinase 3 (FLT3)[39]. Through the blockade of these signaling pathways, sorafenib suppresses cellular proliferation, induces apoptosis and impairs tumor-associated angiogenesis. To understand these inhibitory effects, the molecular mechanisms underlying therapeutic activity and its role in AML can be further examined.

Sorafenib targets signaling pathways critical for cellular proliferation, survival and angiogenesis. It inhibits key upstream kinases within the Ras/Raf/MEK/ERK (MAPK) pathway, including wild-type and mutant B-Raf and C-Raf, thereby reducing downstream MEK and ERK phosphorylation and suppressing proliferative signalling[2]. In AML, particularly in FLT3-mutated cases, constitutive activation of kinase signaling pathways plays a critical role in disease progression. In addition, Sorafenib inhibits multiple receptor tyrosine kinases frequently dysregulated in AML, including FLT3, VEGFR-1, -2, and -3, PDGFR-β, FGFR1, c-KIT, and RET, contributing to impaired angiogenic and growth factor-mediated signaling. In AML, MAPK pathway suppression has been shown to promote activation of intrinsic mitochondrial apoptotic pathway through upregulation of pro-apoptotic proteins such as Bim and downregulation of anti-apoptotic regulators including MCL-1, thereby facilitating leukemic cell death [132].

Sorafenib has advanced through phase I and phase II clinical trials in combination with Cytarabine and Idarubicin for younger patients with acute myeloid leukemia (AML), demonstrating successful complete response (CR) rates, particularly in individuals

harboring FLT3 mutations[87]. In FLT3-ITD–positive AML, Sorafenib has been shown to effectively reduce bone marrow myeloblasts however resistance frequently develops through the emergence of mutant subclones expressing genes such as ALDH1A1, JAK3, and MMP15[70]. Studies have identified aberrant activation of alternative survival pathways, including PI3K/Mtor signaling, in both resistant cell lines and blasts derived from Sorafenib-resistant patients, suggesting pathway activation as a contributor to therapeutic failure[64]. Additionally, Sorafenib has been associated with activation of the JAK-STAT3 pathway, leading to upregulation of the anti-apoptotic protein BCL2 further promoting resistance. Targeting these adaptive mechanisms has shown promise, inhibition of BCL2 with Venetoclax has restored treatment sensitivity in resistant AML models[126]. Given the molecular heterogeneity of AML, Sorafenib resistance is still frequently observed in clinical settings and the mechanisms underlying this resistance present itself in diverse signaling pathways therefore developing uniformly effective strategies to overcome it remain difficult to determine.

1.6.4 Filanesib (ARRY-520)

Filanesib is a selective inhibitor of kinesin spindle protein (KSP/Eg5), a motor protein responsible for mitotic spindle assembly and chromosome segregation during cell division. Inhibition of KSP by Filanesib disrupts bipolar spindle formation, inducing mitotic arrest at the metaphase stage and subsequent activation of apoptotic pathways (programmed cell death)[102]. Filanesib has demonstrated clinical efficacy in multiple myeloma (MM), proceeding to phase III clinical trials with its mechanism of action prompting investigation in other hematological malignancies[31]. Cancers that depend on the short-lived anti-apoptotic protein myeloid cell leukemia-1 (MCL-1), as observed in MM shows marked sensitive to KSP inhibition in preclinical models[98]. Given that AML is characterized by rapid proliferation of leukemic blasts and reliance on survival signaling, disruption of mitotic progression provides a strong rationale for evaluating Filanesib as a therapeutic treatment for AML.

Filanesib exerts its effects through selective inhibition of KSP/EG5, leading to the disruption of mitotic spindle assembly and the formation of abnormal monopolar spindles. This

spindle defect induces cell cycle arrest at the G2/M phase, the prolonged mitotic arrest results in loss survival signaling and initiation of apoptosis[124]. In AML models, Filanesib-induced apoptosis proceeds via the intrinsic mitochondrial pathway, marked by upregulation of the pro-apoptotic protein Bim, independent of p53 activation or extrinsic death receptor signaling. As KSP expression is restricted to actively dividing cells, this allows for targeting against proliferating leukemic cells, providing for selectivity for malignant over normal tissues[3].

In AML cell models such as HL-60, Filanesib treatment demonstrated mitotic arrest followed by mitochondrial apoptosis, exhibited by increased Bim expression, and suppressed leukemic blast growth with the exclusion of normal hematopoietic colony formation[22]. These findings supported a therapeutic rationale and led to early-phase clinical evaluation in AML. In a Phase I study in relapsed or refractory disease, preclinical analyses confirmed target engagement consistent with KSP inhibition; however, patient response did not reflect the preclinical success as dose-limiting mucosal and hematologic toxicities had arisen[46]. As a result, further single-agent development of Filanesib in AML was discontinued. Its ability to enhance apoptotic priming in leukemic cells is further explored in combination regimens[99] to administer in lower doses to minimize toxicity while increasing susceptibility to other therapeutic agents, although these studies have been largely restricted to multiple myeloma.

1.6.5 Zosuquidar Hydrochloride

Zosuquidar hydrochloride is a third-generation potent inhibitor of P-glycoprotein (P-gp/ABCB1) developed to combat chemotherapeutic resistance. P-glycoprotein, a drug efflux transporter encoded by the MDR1/ABCB1 gene, is overexpressed in AML with nearly 30-50% of AML patients displaying increased P-gp expression characterizing it as a hallmark of multidrug resistance[100]. Lower complete remission rates and poor survival following standard treatment are associated with the transporter, making it a therapeutic resistance target. First generation and second generation of P-gp inhibitors caused adverse effects following induction, and thus the third generation of the drug was developed to posses' specific affinity for P-gp, lacking the off-target toxicities and avoiding pharmacokinetic

interactions[103]. By restoring drug sensitivity and retention of chemotherapeutic agents in resistant leukemic cells, Zosuquidar can be administered alongside conventional AML chemotherapy and enhance the efficacy of the regimen, especially in P-gp-expressing cells. Due to these factors, it has been primarily investigated as an adjunct to standard induction chemotherapy rather than as a standalone anticancer agent.

For Zosuquidar to increase the efficacy of chemotherapeutic agents it must inhibit P-glycoprotein (P-gp), a transmembrane efflux pump that is responsible for transporting cytotoxic substrates out of malignant cells. By binding to P-gp and blocking its ATPase-driven transport, drug efflux across the cell membrane is prevented[92]. Retention of chemotherapeutic agents such as anthracycline and cytarabine increase in efficacy by accumulation[89], thereby re-establishing effective intracellular drug–target engagement and promoting apoptosis in leukemic blasts while maintaining minimal pharmacokinetic interference.

While Zosuquidar is not considered as a standalone chemotherapeutic agent induction in AML, it has been investigated as a chemosensitizing agent to standard anthracycline-cytarabine chemotherapy. In a Phase I/II clinical study involving older patients with P-gp positive AML, intravenous infusion of Zosuquridar for 72 hours in combination with the "7+3" regimen was well tolerated and produced a response rate of approximately 48%[58]. 90% of P-gp inhibition occurs within 2 hours of Zosuquidar administration at an effective dose of 700 mg/day[71]. The clinical evidence supports that modulation of drug efflux is significant in improving sensitivity in resistance AML and the drug can be utilized as a resistance-targeting adjunct, even if it does not function effectively independently.

1.6.6 Thioridazine

Thioridazine (TDZ) is a dopamine receptor D2 (DRD2) antagonist that was originally used as an antipsychotic but has been repurposed into an anti-leukemic agent due its cytotoxic effects. It selectively acts against leukemic stem and progenitor cells by disrupting survival signalling and differentiation pathways[8]. Thioridazine demonstrates a particular efficacy against AML harboring an MLL-AF6 rearrangement, a poor-prognosis molecular subtype,

where DRD2 antagonism induces differentiation on malignant cells capable of being leukemia-initiating while sparing hematopoietic steam cells[94]. This approach suppresses leukemic clonogenicity and capacity to produce leukemic blasts.

Its therapeutic activity is exerted by disruption of cytoskeletal integrity and targeting dopamine receptor-mediated survival signaling in diseased cells. Thioridazine negatively impacts maintenance and survival signaling pathways in leukemia stem cells. One of the mechanisms by which Thioridazine acts is through cytoskeletal remodeling to promote an intracellular Ca^{2+} influx, mitochondrial depolarization, and reactive oxygen species accumulation, activating apoptotic pathways[110]. This impacts the clonogenic capacity and stem-cell potential of leukemic stem cells. This mechanism to have specific selectivity is associated to cytoskeletal regulation in MLL-AF6 positive AML, where the protein is unable to stabilize the cytoskeleton and renders malignant cells vulnerable to apoptosis and other chemotherapeutic agents.

Thioridazine, in particular, is a compound of interest due to earlier research from our group that established its capacity to target and effectively eliminate drug-resistant AML populations. As Thioridazine displayed promise in preliminary studies, in vivo phase I clinical studies validated its selective toxicity with a 19-55% blast reduction at a 50 mg dose in patients with DRD2 expressed-leukemic cells[10], when given alongside Cytarabine. Thioridazine differs from other chemotherapeutics because it is able to target cancer stem cells that give rise to blasts across multiple malignancies including glioblastoma and breast cancer, through cell cycle modulation and regulation of signaling pathways[121]. Dopaminergic signaling has been increasingly implicated in cancer stem cell (CSC) biology with evidence indicating the dopamine receptor may be a biomarker and a therapeutic vulnerability across other cancers as well[23]. Although these studies demonstrate promising therapeutic activity for thioridazine, their conclusions are constrained by small patient cohorts and the predominance of early-phase clinical trial data. Even so, with Thioridazine's unique ability to target cancer stem cells, its potential to be utilized in aggressive stem-cell driven AML subtypes or other cancers makes it significant to investigate.

1.6.7 Cytarabine

Cytarabine (cytosine arabinoside, Ara-C) is an antimetabolite pyrimidine analogue that undergoes intracellular activation to compete with deoxycytidine, thereby disrupting DNA synthesis[69]. Cytarabine remains the gold standard therapy in both induction and consolidation settings[120]. As noted previously, Cytarabine is administered as a standalone or incorporated in combination regimens with anthracyclines such as Daunorubicin or Idarubicin[79]. For decades, it's been used as a first line treatment for AML due its selective nature against myeloid blasts and its ability to accumulate to high intracellular concentrations. While most chemotherapeutic compounds may target specific manifestations of AML, Cytarabine is able to work across multiple AML risk groups and age categories making it the primary chemotherapeutic to utilize and develop combination approaches with.

Cytarabine disrupts DNA synthesis during the S-phase of the cell cycle by incorporating into the DNA of the leukemic cell[114]. Following nucleotide transporter uptake, Cytarabine undergoes phosphorylation to form an active metabolite cytarabine triphosphate (Ara-CTP). Ara-CTP competes nucleotide deoxycytidine triphosphate to incorporate into newly synthesized DNA by DNA polymerase[54]. This results in termination of production of the DNA strand. Thus, hindering DNA replication, damaging DNA and inducing apoptosis in leukemic cells. Due to its fast proliferation rate, leukemic cells uptake Cytarabine at higher rates than its healthy counterpart and suffer cell death in the malignant population.

Although the standard "7+3" induction regimen achieves complete remission rates of approximately 65–80%, relapse or refractory disease frequently develops within two years indicating the cancer evolves to become resistant to treatment[24]. One study associated resistance in AML to a defect in the expression of deoxycytidine kinase (Dck), the enzyme required for cytarabine activation[97], whereas other studies implicate metabolic adaptations such as increased oxidative phosphorylation[47]. Due to the heterogeneous nature of AML, even though cytarabine is employed across all AML subtypes, resistance mechanisms vary amongst patients. Increased cytarabine dosing has not consistently restored

responsiveness, suggesting that intrinsic cellular mechanisms rather than drug exposure alone drive resistance.

Table 1. Summary of Chemotherapeutic Agents Selected for Drug Screening. A table of small molecule compounds selected for dose response assay highlighting the class of drug, mechanism of action, its relevance to AML and the clinical phase the drug is currently in.

Class of Drug	Drug	Mechanism of Action	Relevance	Clinical Phase
Antimetabolites	5-Flourouracil	Inhibits DNA synthesis	Non-AML Treatment	NA
	Cytarabine		Standard AML Treatment	Approved
Anthracycline	Daunorubicin	DNA damage (Topo II inhibition)		Approved
Kinase, Efflux, Mitotic Inhibitors	Sorafenib	Block signaling pathways	Non-AML Treatment	Phase II
	Zosuquidar	Overcome drug resistance		Phase I/II
	Filanesib	Block cell division		Phase I
Repurposed Agent	Thioridazine	Target LSCs / signaling		Phase III

1.7 Translating Chemotherapeutic Efficacy from Preclinical Models to Clinical AML

A study reported that only 7% of AML drugs successfully progress through all clinical trial phases to receive FDA approval[62]. This low success rate is largely attributed to the immune evasion of leukemic stem cells (LSCs) within the bone marrow (BM) niche, meaning treatments that show efficacy in preclinical research often fail to translate to human trials, hindering progression to later clinical phases. Common contributors to failed AML trials include patient heterogeneity, selection bias, absence of control groups and high drug development costs[115]. Optimizing trial design should be prioritized to improve the success of drug discovery efforts.

Particularly when researchers utilized engineered scaffolds to support hematopoietic stem cell (HSC) survival co-cultured with stromal cells, the HSCs exhibited superior engraftment and long-term maintenance in vivo[1]. Similarly, a 3D scaffold derived from human bone

marrow stromal cells (BMSCs) was developed to replicate the BM microenvironment, allowing engrafted AML cells to be studied for leukemic cell development and progression within the niche[4], demonstrating increased viability in cells on the scaffold. This alludes that altering culture platforms can help maintain the cells' intrinsic characteristics and stem-like properties.

These promising findings indicate that scaffolds present a more physiologically relevant ex vivo model for evaluating potential therapeutic strategies [15]. For example, AML KG1 cells cultured on fibronectin coated scaffolds, a component of the ECM, revealed stronger adhesion and increased resistance to Cytarabine and Daunorubicin as observed in vivo in patients[75]. Such models provide insight into mechanisms by which leukemia stem cells are protected within the BM niche and improve the development of strategies to enhance the cytotoxicity against AML cells. Importantly, scaffolds create a versatile platform for identifying these interactions while screening additional therapeutic candidates[29], including those still in preclinical development or previously unsuccessful in clinical trials and serve as a preclinical test to evaluate their potential for future in vivo studies.

CHAPTER 2

AIMS AND OBJECTIVES

Acute myeloid leukemia (AML) cells, including leukemic stem cells (LSCs), interact dynamically with the bone marrow extracellular matrix (ECM), which has been implicated in disease progression, chemoresistance, and the persistence of therapy-resistant blasts leading to relapse[109]. The niche's properties critically regulate cell survival, adhesion, mobilization, proliferation, lineage commitment, differentiation, and apoptosis[50]. Emerging evidence suggests that ECM components such as fibronectin and hyaluronan not only provide structural support but also actively maintain LSCs in a stem-like state, influencing drug resistance and cell morphology[63]. Despite these insights, most AML drug screening studies continue to rely on two-dimensional polystyrene cultures, which fail to recapitulate ECM-mediated protection and the complexity of the leukemic niche.

To address this gap, ECM-enriched scaffold cultures provide a more physiologically relevant model, recreating structural and biochemical aspects of the niche and enabling closer examination of how ECM interactions influence leukemic cell survival and drug response. However, transitioning from conventional polystyrene to scaffold-based 2D cultures introduces technical challenges, particularly in drug screening and accurate cell quantification. **It is proposed optimization of high-throughput screening approaches will enable precise measurement of AML drug responses in ECM-mimicking scaffold cultures and the identification of effective small-molecule chemotherapeutics, while capturing niche-mediated differences in chemoresistance.** The overarching aim of this work is to optimize AML drug screening in ECM-relevant culture systems by:

Aim 1: Design and Optimize an Effective Cell Quantification Assay

The primary goal of the first aim is to develop a reliable and reproducible method for quantifying cells, which is critical for all subsequent analyses. To achieve this, we established a cell counting protocol using the Cytation C10, leveraging fluorescent staining for precise microscopy-based imaging. This allows accurate identification and enumeration of cells across different culture conditions. In parallel, we modified and optimized a cell viability procedure using the Cytation C10 in fluorescence plate reader mode, providing an alternative high-throughput approach. Together, these methods ensure that both cell

number and health can be assessed consistently, offering flexibility in experimental design and robustness in quantification across various conditions.

Aim 2: Assessment of Cell Recovery and Baseline Viability in 2D Scaffold and Polystyrene Cultures

The second aim addresses the challenge of efficiently recovering cells from engineered scaffolds while establishing baseline viability data across culture systems. By investigating different recovery agents and varying scaffold conditions, we aimed to optimize cell retrieval without compromising cell integrity. Establishing a baseline for cell viability on standard polystyrene plates and 2D scaffold cultures is equally important, as it provides reference points for evaluating the effects of drug treatments in subsequent experiments. This aim ensures that observed differences in cell response are reflective of treatment effects rather than technical variability in recovery or culture conditions.

Aim 3: Evaluate the Efficacy of Selected Chemotherapeutic Compounds on OCI-AML2 Leukemic Cells across Culture Conditions using Dose–Response Analysis

The third aim focuses on assessing the effects of small molecule compounds on a human OCI-AML2 acute myeloid leukemia (AML) cell line. Using flow cytometry, we measure changes in cell viability and behavior in both 2D scaffold and polystyrene cultures, providing detailed insight into drug responses under different conditions. In addition, by comparing results obtained through flow cytometry with those from fluorescence plate reader assays, we aim to evaluate the consistency, sensitivity, and suitability of these screening approaches. This aim builds on the optimized quantification and recovery protocols from the first two aims, ensuring that observed responses accurately reflect cellular effects rather than technical variability as well identification of effective therapeutics.

CHAPTER 3

MATERIALS AND METHODS

3.1. Scaffold Fabrication

To mimic the bone marrow niche, a physical structural scaffold is fabricated using collagen with the addition of extracellular matrix components as displayed in Figure 1. Collagen is identified as one of the extracellular matrix proteins that are abundant in the bone marrow niche and assist in the HSC adhesion to the bone surface, making it vital addition in creating the 2D scaffold[37].

A mixture of type I collagen (Cat.# C9879) was measured out in relation to a solution containing a dilution of acetic acid at a concentration of 0.05M. The mixture was sealed to swell the collagen for 8-48 hours at 4℃, which allows the collagen to rehydrate and form a thick gel-like slurry. The slurry was blended, over ice to prevent overheating and destroying the integrity of the collagen, removing any remaining collagen flakes. Using a bell jar, the slurry was degassed to eliminate air bubbles that may be present in the films. In the optimal scaffold used for the drug screen, a ratio of hydroxyapatite (mHA, 10 μm, Cat.# 900203) (mHA) and elastin (Cat.# E1625) (from Sigma-Aldrich Co.) were added. Hydroxyapatite and elastin were weighed out appropriately and added before titrating the mixture with glacial acetic acid. Blending was repeated before degassing the mixture once more, reassuring no air bubbles can persist in the films. 50 μL of the slurry were distributed into each well of a 96-well plate.

To produce 2D films, the 96-well plate containing the scaffold are left to evaporate for 24 hours, which differs from the 3D scaffold that is freeze dried over the same course of time. Once the plate is dried, the plate is sterilized using x-ray technology in an x-ray irradiator for 36 hours as seen in Figure 2.

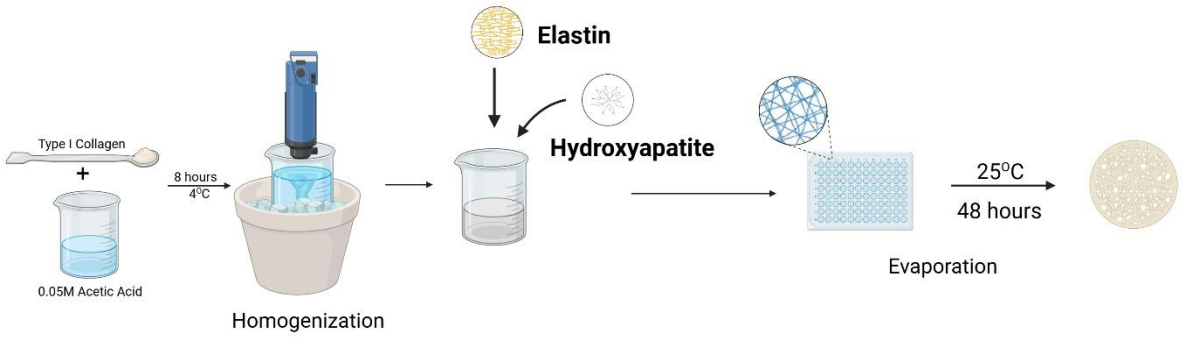

Figure 2. 2D Scaffold Fabrication Process. Type I Collagen flakes are rehydrated for 8 hours in an acetic acid solution and homogenized by blending. ECM components: Elastin and Hydroxyapatite are mixed in and the mixture is degassed. The collagen slurry is dispensed into a 96-well flat bottom plates and spread evenly through centrifugation to produce films. In biosafety cabinets (BSCs), scaffolds are left to evaporate for 24-48 hours.

3.2. Crosslinking of 2D Collagen Scaffolds

Crosslinking is a significant process to improve the structural and mechanical stability of the collagen-based scaffold under cell culture conditions[127]. Prior to seeding scaffolds with cells, a crosslinking solution was prepared consisting of N-hydroxysuccinimide (NHS; Cat. #6066-82-6, Sigma-Aldrich Co. Ltd., UK) and 1-ethyl-3-(3-dimethylaminopropyl) carbodiimide hydrochloride (EDC; Cat. #161462, Sigma-Aldrich Co. Ltd., UK) at a molar ratio of 5:2:1 (EDC:NHS:collagen), where the crosslinking solution was prepared by dissolving 1.15 mg EDC and 0.276 mg NHS in 80% (v/v) ethanol per 1 mg of collagen. The solution was dispensed onto 2D scaffolds to submerge them and incubated for 3 hours at room temperature while agitated on a microplate shaker (FisherBrand, USA) at 200 rpm.

Following incubation, the scaffolds were washed 3 times with phosphate-buffered saline (PBS; Dulbecco's phosphate-buffered saline powder, Cat. #D5652, Sigma-Aldrich Co. Ltd., UK, diluted in Milli-Q water and sterilized) to remove residual crosslinking reagents. After the final wash, scaffolds were stored in PBS at room temperature until further use.

3.3 Cell Culture

The leukemic cell line acute myeloid leukemia (AML) OCI-2 were obtained from Dr. Mark Minden's laboratory. Cells were expanded and maintained in α-minimum essential medium without phenol (αMEM; Cat.# 41061029, Thermo Fisher Scientific) supplemented with 10%

fetal bovine serum (FBS; Cat. #12483-020, Thermo Fisher Scientific, USA), 1% penicillin–streptomycin (Cat. #10378-016, Thermo Fisher Scientific, USA), and 1% L-glutamine (Cat. #25030164, Thermo Fisher Scientific, USA).

3.4 CFU Assay

A colony forming unit (CFU) assay assesses the clonogenic potential of cells by measuring their ability to proliferate, survive and form colonies. It is utilized in determining the progenitor function, differentiation and treatment response in leukemic and haemopoietic cells. OCI AML-2 cells cultured on polystyrene dishes were counted to suspend 500 cells in 50µl of media mixed with 500µl of MethoCult (Cat.# 4434, Stem Cell Technologies) and dispensed into each of the inner wells of a 24-well plate. The remaining wells were filled with 1 mL of PBS maintain hydration of the methylcellulose. The cells were incubated for 14 days, with images taken periodically throughout the growth period using a phase-contrast microscope to monitor and identify colony growth.

3.5 Cell Counting using Automated Imaging

For high-content screening (HCS), automated fluorescence imaging was used to assess cells cultured on polystyrene and scaffolds at multiple time points and dye concentrations. OCI AML-2 cells suspended in 1 mL of phenol-free OCI AML-2 media were counted with Trypan Blue using the Countess machine and a dilution to achieve 3.6x10^6 cells in 4 mL of media. Cells were seeded at volume of 100µL/well with a cell number of 10,000 cells/well. An DMSO-free cell tracking red dye (Cat.# ab269446, abcam) 1:20 labelling solution was made to be a 2X stock stain. This stain was further diluted to various stain concentrations — 1:100, 1:1,000, and 1:10,000. The total volume was brought up to 200 µL by adding 100 µL of the red dye stain concentrations.

The 96-well plate was divided for the time intervals of T0 and T24, each column containing 2 replicates had a differing stain concentration. Cells were seeded onto a standard polystyrene 96-well plate as well as a 96-well plate containing the 2D scaffold. Hoechst 33342 (Cat.# H3570, Invitrogen) was added to the wells on the day they were imaged, a 5X

stock was made for a 1:10,000 stain concentration in a 50 µL volume to be added into each well bringing the total volume per well up to 250 µL.

Confocal microscopy imaging was performed on the Agilent BioTek Cytation C10 Confocal Imaging Reader, confocal imaging was utilized to obtain clear images of the cells seeded. This experiment established a protocol that could be followed and further optimized to create a baseline for the best staining conditions as well as effectively imaging on the scaffolds, using imaging can quantify cells to cell count for the drug screen.

3.6 Establishing Cell Counting Procedure via Plate Reader

To determine a reliable cell counting method for a high-throughput drug screen (HTS), a plate reader was selected to perform a cell count by generating a standard curve and test various cell concentrations to assess accuracy. OCI-AML2 cells were seeded onto 96-well flat bottom plates, in standard polystyrene and scaffold conditions at varying concentrations of 12500, 25000, 50000 and 100000 cells per well. A standard curve in polystyrene was generated using cell concentrations ranging from 1,000,000 to 3,125 cells per well in a 96-well black plate with a clear bottom, plated in triplicate.

The cells for the standard curve and cell concentrations samples were stained with AlamarBlue (cat. #DAL1025, Thermo Fisher Scientific), incubated for 1 hour and centrifuged to pellet the cells. The supernatant was collected and transferred to a 96-well black plate with a clear bottom for a plate read in the Agilent BioTek Cytation C10 Confocal Imaging Reader. The resulting cell pellets were resuspended in PEF (PBS, FBS, and EDTA) and stained with Hoechst 33342 (1:5,000 dilution in PEF; Cat. #H3570, Invitrogen) and 7-AAD (1:25 dilution in PEF; Cat. #6996-50, Fisher Scientific). Following staining, cells used for the standard curve and varying cell concentrations were washed once with PEF, resuspended in fresh PEF and transferred to a 96-well (clear bottom) black plate for fluorescence measurement for total cell and dead cell counts.

3.7 Cell Recovery Optimization

As recovery is determined to be the primary method of harvesting cells from the scaffold, cell recovery methods are assessed with various recovery agents and testing this on the

control and with varying preparation of the scaffold, crosslinked versus non-crosslinked. Five recovery agents — PBS, EDTA (cat.# T9285,Sigma Aldrich), Cell Disassociation Buffer (Cat. # 100-0485, Stem Cell Technologies), Accutase and Trypsin (Figure 3) were dispensed at 20 uL per well in a 96-well flatbottom plate with cultured cells on polystyrene and scaffolds following 1 hour and 72 hours incubations. 60 uL of media/PBS were added on to all samples to deactivate enzyme activity for reagents requiring deactivation. Remaining solution is collected and transferred to a 96-well round bottom plate. The plate was centrifuged at 300X G for 5 minutes to collect a cell pellet, the supernatant is discarded for the cell pellet to be resuspended in 100 uL of PEF. Hoechst 33342 and 7-AAD were added for live/dead discrimination to assess which recovery agent resulted in the highest cell viability.

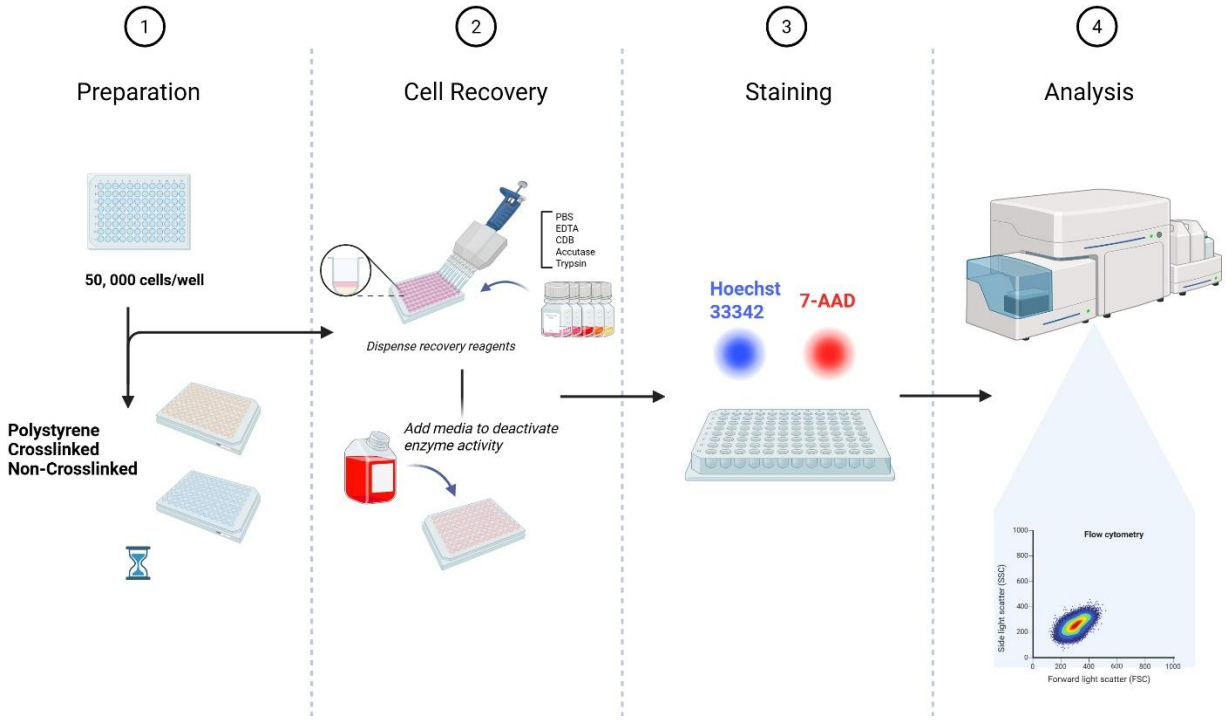

Figure 3. Schematic overview of the experimental workflow used to evaluate cell viability in scaffolds vs. polystyrene in AML cells with various cell recovery agents. Cells are seeded at 50,000 cells per well in either standard polystyrene plates or ECM-mimetic scaffolds (crosslinked or non-crosslinked). Following treatment, cells are retrieved from scaffolds using recovery reagents (e.g., PBS, EDTA, Accutase, or trypsin). Recovered cells are stained with Hoechst 33342 to label nuclei and 7-AAD to assess cell viability.

3.8 Implementation of Flow Cytometry for Cell Quantification

To obtain accurate and reliable cell counts, flow cytometry was applied as an alternative technique using the Agilent NovoCyte Opteon Spectral Flow Cytometer. OCI-AML2 cells were cultured in a 96-well plate for both polystyrene and in scaffolds, designed to mimic the bone marrow niche to assess potential differences between the two culture conditions on cell viability. Furthermore, establishing a baseline of the OCI-AML2 cell viability on polystyrene and scaffold without undergoing treatment is important in understanding how the cell populations behave in response to the two conditions and how interventions affect cell viability.

Figure 4. displays culture conditions with standard media and media with 0.1% DMSO, which were tested to determine cell survival before adding any drug treatment through staining with membrane integrity dyes: Hoechst 33342 and 7-AAD. Media containing 0.1% DMSO was being evaluated due to DMSO being used to dissolve small-molecule drugs at this concentration and considered the standard in drug testing without compromising cells[83]. OCI-AML2 cells were seeded onto polystyrene and crosslinked 2D scaffolds and incubated over a period of 72 hours. Cells were recovered by washing three times with PBS, resuspended in PEF and stained with dyes to be quantified on the flow cytometer.

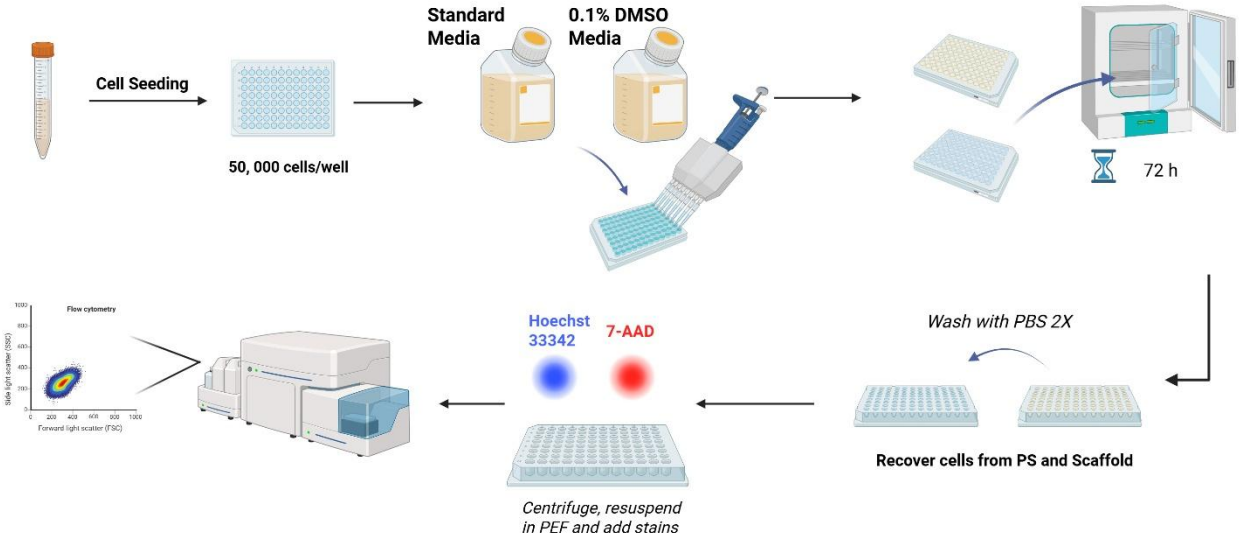

Figure 4. Protocol for baseline cell viability assay using OCI AML-2 cells following 72 hours incubation. OCI AML-2 cells are treated in two conditions: untreated and untreated with 0.1% DMSO concentration (standard in drug screening), following 72 hour incubation cells are recovered and stained with Hoechst 33342 and 7AAD for live/dead discrimination then analyzed on flow cytometer.

3.9 High-Throughput Dose Response Drug Screen

OCI-AML2 cells were utilized as a model to exhibit how chemotherapeutic drugs impact cell viability. 5-Flourouracil (Cat, # F6627-1G, Sigma Aldrich), Daunorubicin (Cat.# AAJ60224MA, Thermo Fisher Scientific), Sorafenib (Cat.# SML2653, Sigma Aldrich), Filanesib (Cat.# HY-15187, MedChemexpress CO.,Ltd), Zosuquidar Hydrochloride (Cat.# SML1044, Sigma Aldrich), Cytarabine (Cat.# 449560010, Thermo Fisher Scientific), and Thioridazine (Cat. # T9025, Sigma Aldrich) were dissolved in DMSO to a 10 mM concentration (Fig. 5).

For dose response assays, the 10 mM drug stocks were diluted further to concentrations of 0.001 uM, 0.01 uM, 0.1uM, 1 uM, and 10 uM. OCI-AML2 cells with drug treatment were cultured on both a 96-well flatbottom plate for polystyrene and scaffold conditions by adding the 10x drug stocks to cell suspension and incubated over a period of 72 hours. Following the 72-hour incubation, cell suspension was recovered utilizing the optimized cell recovery method. PEF was used for resuspension and staining with our membrane integrity dyes — Hoechst 33342 and 7-AAD. Results were analyzed by flow cytometry to quantify live and dead cell counts, with gating and data interpretation carried out in the NovoExpress software.

To compare a high-throughput versus high-content drug screening, a parallel experiment was run simultaneously on the plate reader of the Agilent BioTek Cytation C10 Confocal Imaging Reader via AlamarBlue staining. The daughter plate produced from the master plate with drug treatment was stained with AlamarBlue alongside a standard curve covering the expected range of cells. Cells were incubated at 37℃ for 1 hour, following incubation cells were centrifuged and supernatant was transferred to a 96-well optical-bottom black plate for analysis on the plate read function.

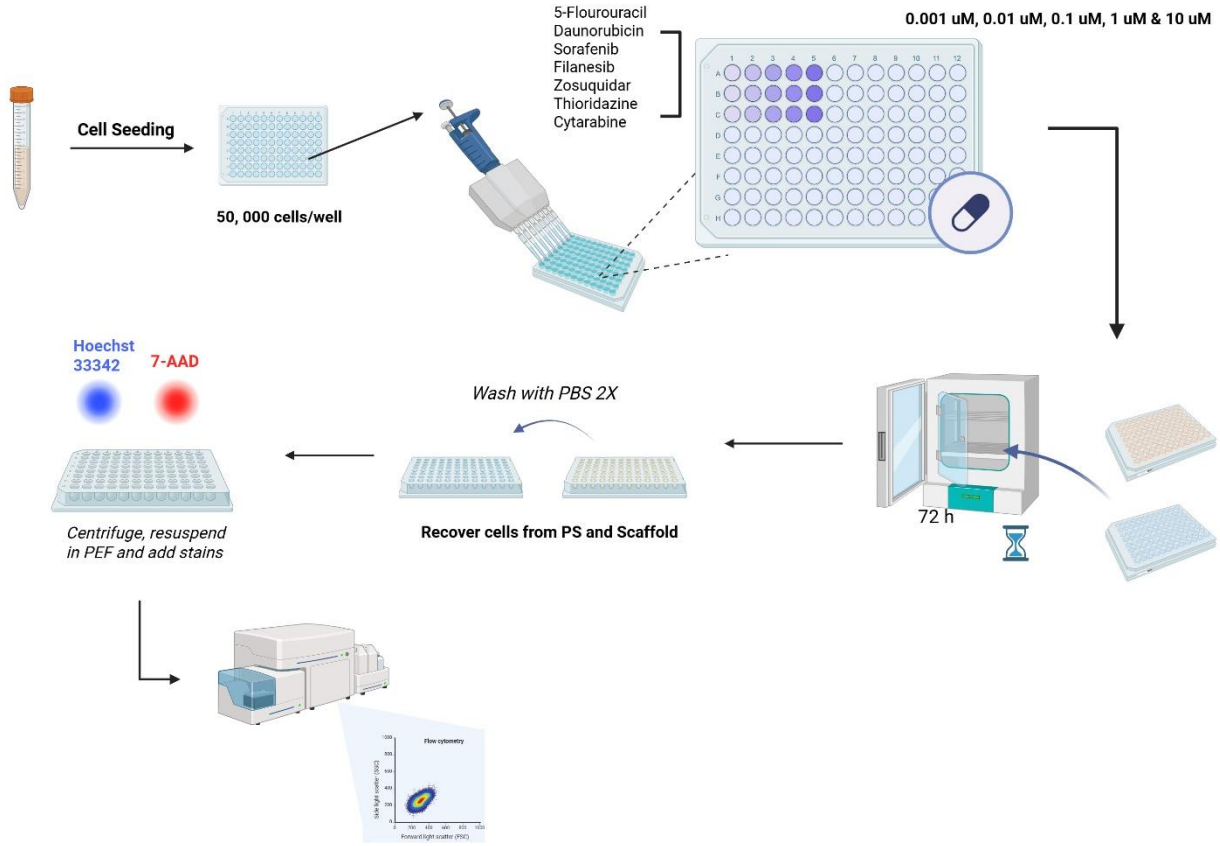

Figure 5. Flow cytometry–based dose–response drug screening of AML cells. AML cells were treated with increasing concentrations of 5-fluorouracil, daunorubicin, sorafenib, filanesib, zosuquidar, thioridazine and cytarabine to evaluate drug sensitivity across concentrations. Following treatment, cell viability was quantified using flow cytometry to determine the proportion of live and dead cells at each dose. Dose–response curves were generated to assess the relative cytotoxic effects of each compound and to enable comparison of drug efficacy across treatments.

3.10 Statistical Analysis

Data represented through graphical visualization and statistical analyses were performed using GraphPad Prism (Version 10.0; GraphPad Software Inc., La Jolla, CA, USA). Data is presented as the mean ± standard error of the mean (SEM) and standard deviation (SD). Three technical replicates were used to determine statistical significance. A one-way ANOVA was applied in the cell recovery experiment to evaluate culture condition as the independent variable, while a two-way ANOVA was used in the dose–response assay to examine the effects of both culture condition and drug treatment as independent variables, with multiple comparisons performed using Tukey's test.

Dose–response curves were generated using nonlinear regression (four-parameter logistic model) to accurately model sigmoidal relationships and calculate IC_{50} values; differences between polystyrene and scaffold conditions were assessed using an extra sum-of-squares F-test to determine whether separate curve fits significantly improved the model. Independent variables for the one-way ANOVA was culture condition while the independent variables for the two-way ANOVA were culture conditions and drug compounds.

Statistical testing assumptions passed normality test (Shapiro-Wilk) for one-way and two-way ANOVAS performed throughout experiments. Testing assumptions for linear and non-linear regression curves using residual plot with confidence intervals determined a good fit for dose standard curve and dose-response curves, making for a reliable fit.

The levels of statistical significance are indicated by asterisks, corresponding to P-values as follows: * for $P < 0.05$, ** for $P < 0.01$, and *** for $P < 0.001$. Error bars in the graphs indicate ± SEM.

CHAPTER 4

RESULTS

4.1 Design and Optimize an Effective Cell Quantification Procedure

4.1.1 Microscopy Imaging–Based Cell Count

To assess the stability of the Cell-Tracking Red fluorescent dye staining for visualizing over a 72 hour period, cells were cultured on polystyrene and scaffold across varying dilutions at two time periods on the Agilent BioTek Cytation C10 Confocal Imaging Reader. In polystyrene cultures, Cell Tracking Red Dye fluorescence intensity was higher at the 0-hour time point (Figure 6.1) compared with 24 hours, however cellular morphology was poorly resolved and less comparable to Hoechst nuclear staining. At the 0-hour timepoint for polystyrene, the 1:1,000 dilution fluorescence imaging demonstrated optimal clarity, characterized by prominent cellular signal and enhanced contrast relative to background. Greater colocalization between the Red Dye and Hoechst signal was observed at 24 hours in polystyrene (Figure 6.2), with the 1:1,000 dilution producing the most optimal imaging quality under these conditions.

Dual-Stain Signal Maintained at T0 Timepoint in Polystyrene

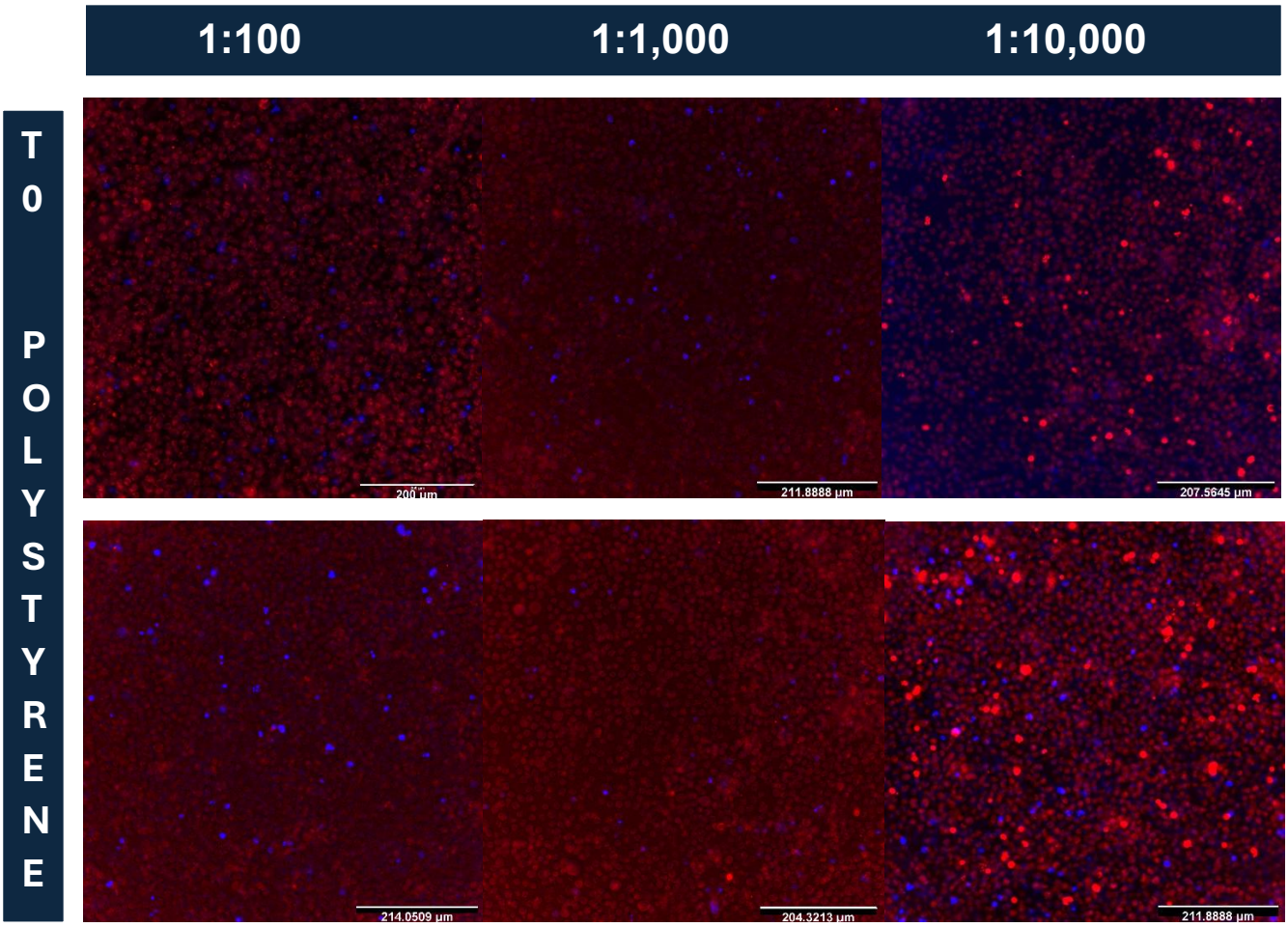

Figure 6.1. T0 dual stain of cell of Hoechst and Cell Tracker dye in polystyrene. Confocal microscopy imaged obtained with stain dilutions of 1:100, 1:1,000 and 1:10,000 from cell tracking red dye cells and a 1:10,000 dilution of Hoechst 33342 on T0 timepoint in polystyrene only. Images are taken in 20X magnification.

Dual-Stain Signal Remained Strong at T24 Timepoint in Polystyrene

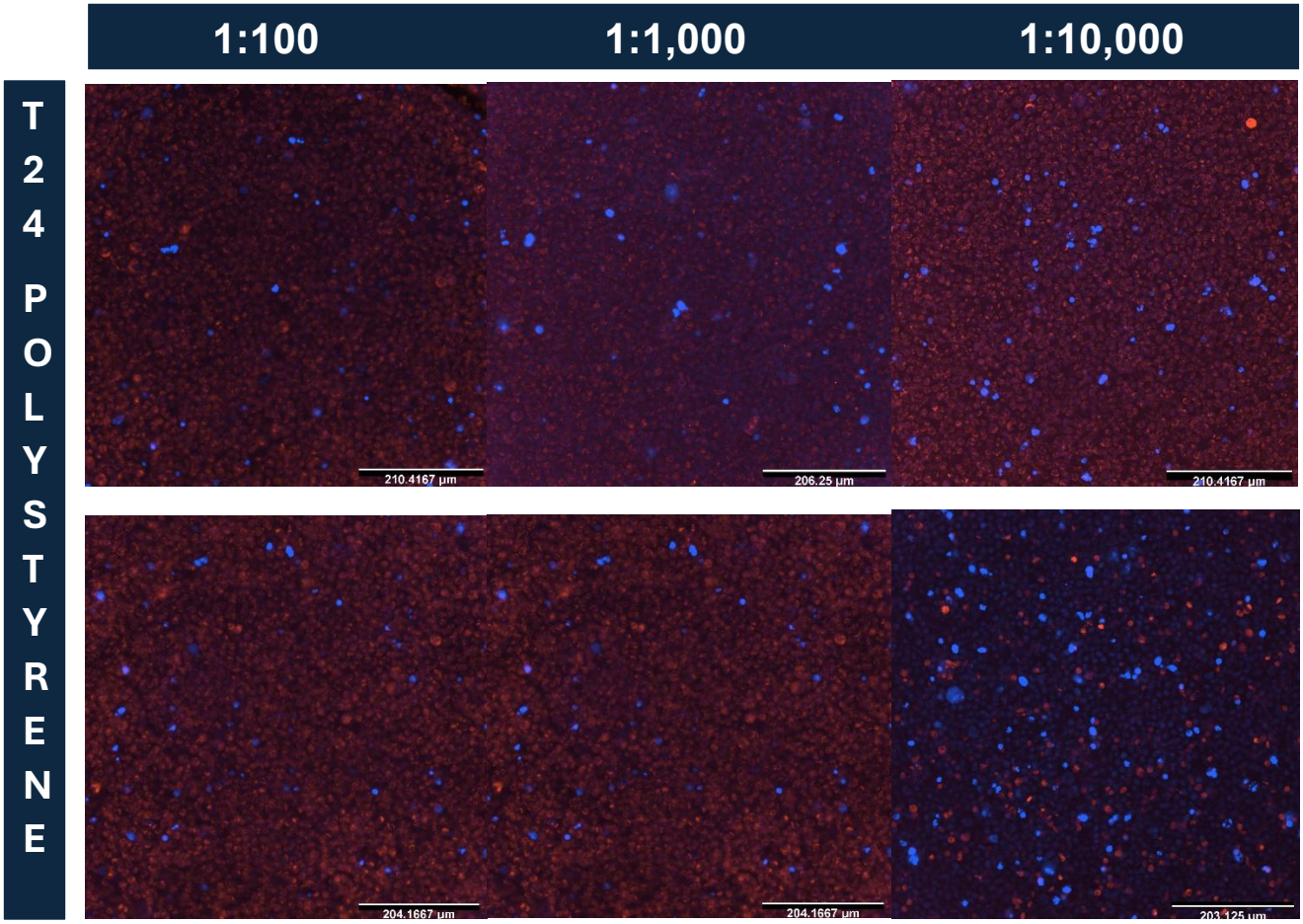

Figure 6.2. T24 dual stain of cell of Hoechst and Cell Tracker dye in polystyrene. Confocal microscopy imaged obtained with stain dilutions of 1:100, 1:1,000 and 1:10,000 from cell tracking red dye and a 1:10,000 dilution of Hoechst 33342 on T24hr timepoint in polystyrene only. Images are taken in 20X magnification.

In scaffold cultures, autofluorescence from scaffold components generated background interference, although dye signal remained detectable through the matrix. At the 0-hour scaffold condition (Figure 6.3), cells were most discernible at the 1:100 dilution, whereas after 24 hours (Figure 6.4) cells were visible at both 1:100 and 1:10,000 dilutions. Detecting the optimal concentration between 1:100 and 1:10,000 dilutions can be difficult to distinguish due to scaffold interference.

Autofluorescence in Scaffold Interferes with Hoechst and CellTracker Staining at T0 Timepoint

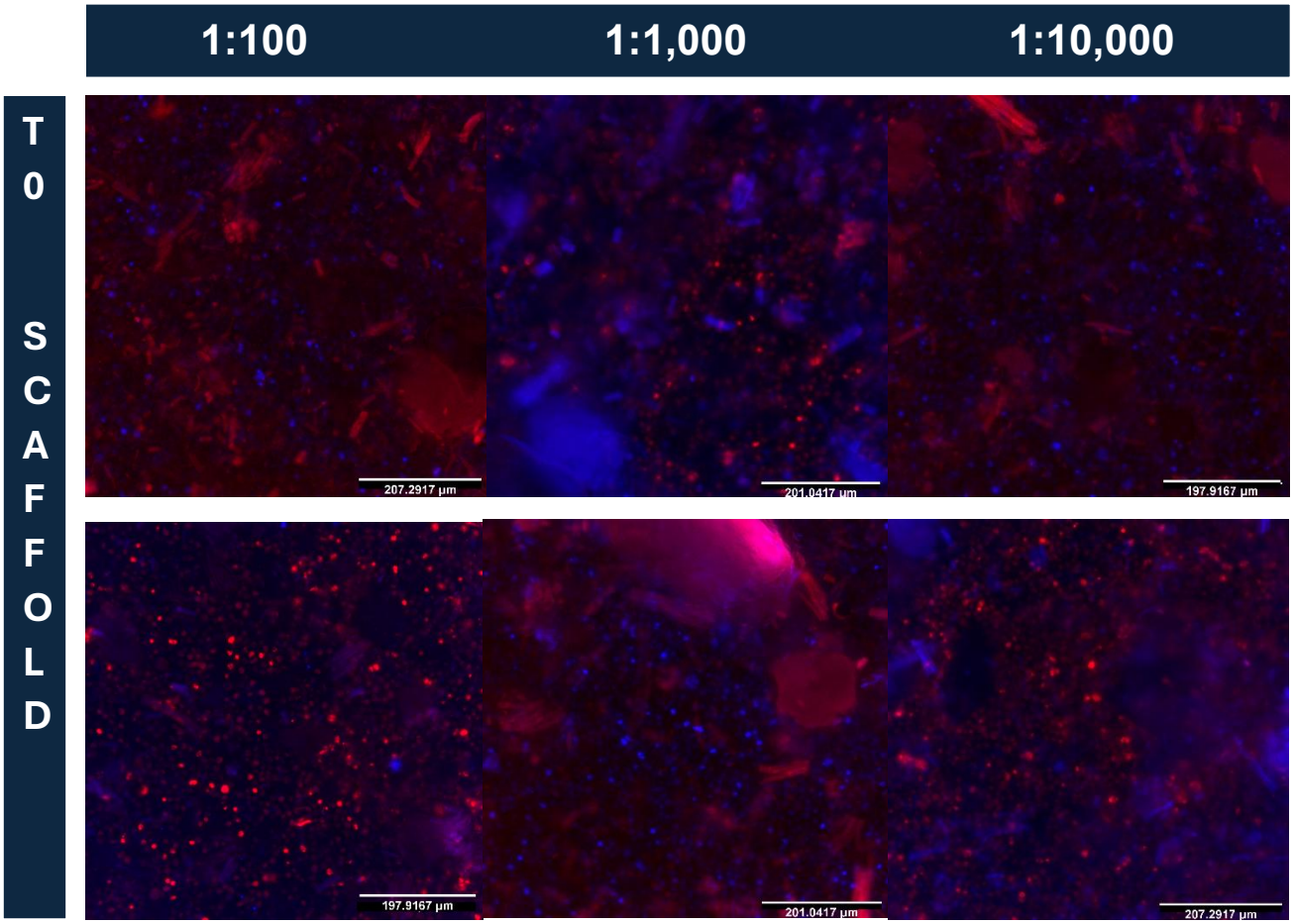

Figure 6.3. T0 dual stain of cell of Hoechst and Cell Tracker dye in scaffold. Confocal microscopy imaged obtained with stain dilutions of 1:100, 1:1,000 and 1:10,000 from cell tracking red dye and a 1:10,000 dilution of Hoechst 33342 on T0 timepoint in scaffold. Images are taken in 20X magnification.

Although OCI-AML2 cells cultured on scaffolds were successfully visualized by microscopy, automated image analysis using Agilent BioTek Gen5 software was not feasible as background scaffold components were detected as cells. Adjustment of cell size and morphology parameters did not improve discrimination between cells and scaffold. Manual counting in ImageJ was also impractical due to cell overlap and high cell density, precluding its use for high-throughput drug screening. Consequently, quantitative image-based cell counts and statistical analyses were not obtained, no significance testing was performed for microscopy-derived measurements.

Scaffold Artifacts Increase in Autoflourescence in Scaffold with Hoechst and CellTracker Staining at T24 Timepoint

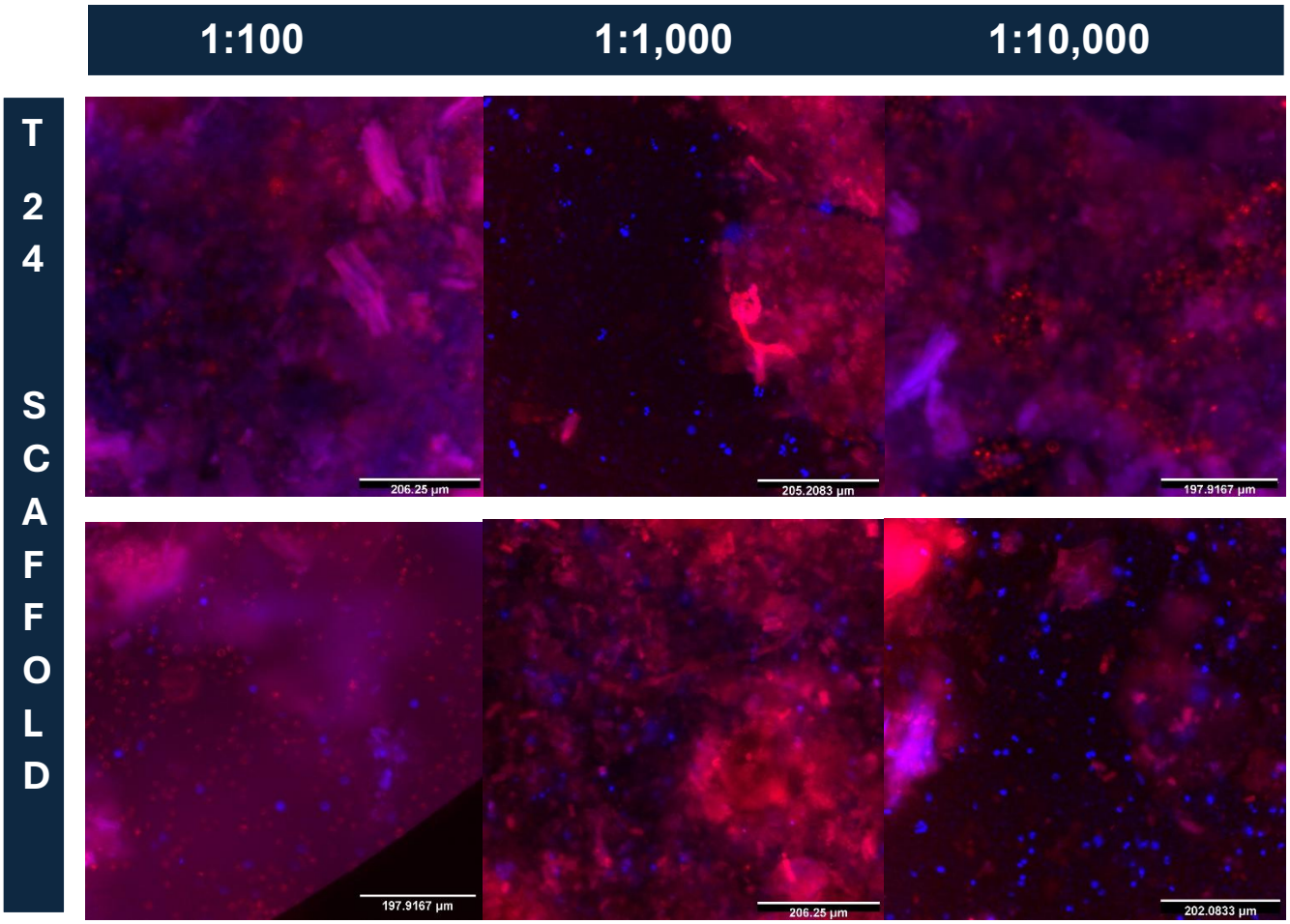

Figure 6.4. T24 dual stain of cell of Hoechst and Cell Tracker dye in scaffold. Confocal microscopy imaged obtained with stain dilutions of 1:100, 1:1,000 and 1:10,000 from cell tracking red dye and a 1:10,000 dilution of Hoechst on T24hr timepoint in scaffold. Images are taken in 20X magnification.

4.1.2 Plate Reader–Based Cell Quantification

An AlamarBlue-based plate reader assay was developed and validated for fluorescence-derived cell quantification, enabling comparison of metabolically active cell numbers between polystyrene and scaffold cultures. Fluorescence measurements were obtained using a plate reader to quantify cell densities of 50,000, 100,000, 200,000, and 400,000 cells (Figure 7B). A standard curve was generated with AlamarBlue to relate relative fluorescence units (RFU) to cell number across a range of 3,125–500,000 cells (Figure 7A) and the

resulting regression equation was used to convert sample RFU values into estimated cell counts. Both polystyrene and scaffold cultures were analyzed, with scaffold conditions demonstrating significantly greater metabolic activity than polystyrene. At each seeding density, scaffold cultures showed a statistically significant increase compared with polystyrene ($P < 0.01$). Statistical analyses were performed in GraphPad Prism using two-way ANOVA followed by Tukey's multiple comparisons test.

Metabolic Activity for OCI AML-2 Cells Increased on Scaffold Versus Polystyrene

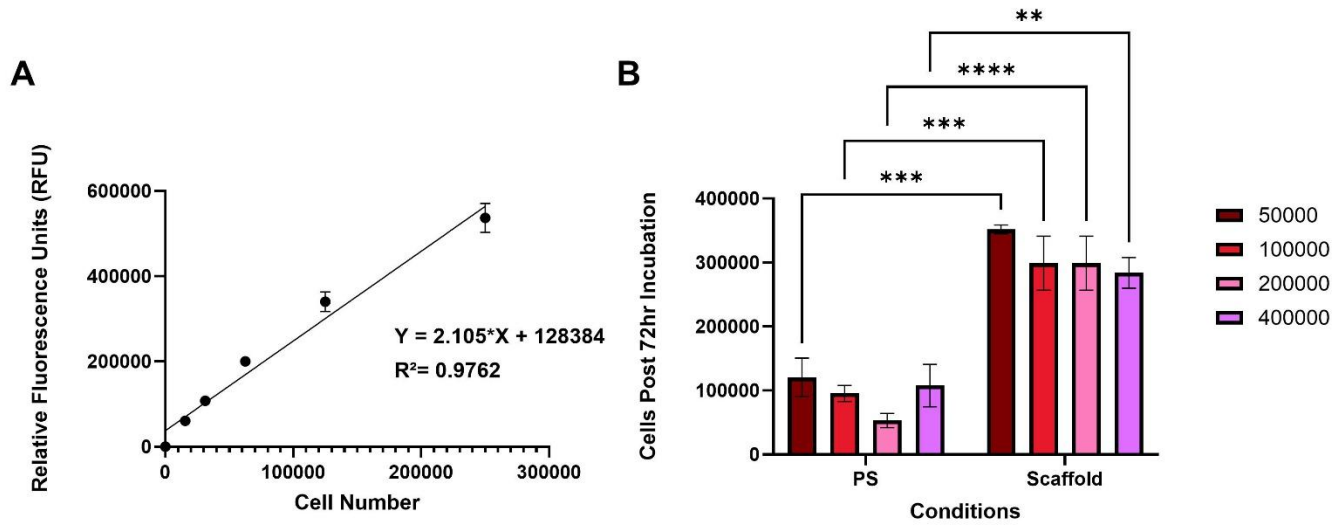

Figure 7. A) An Alamar Blue standard curve to assess metabolic activity following 72 hours of incubation. Standard curve ranged from 3125-500,000 cells with replicates of three, the r2 value is 0.09762. **B) Metabolic assay of metabolically active cells following 72-hour incubation in PS and scaffold.** Calculated based on equation from standard curve. Data represents n=3 independent samples per conditions. Values are mean ± SD. Statistical analysis by 2-way ANOVA with Tukey's multiple comparisons test.

In Figure 8A, a Hoechst 33342 standard curve (3,125–500,000 cells) was generated for live/dead discrimination, the resulting regression equation was used to convert relative fluorescence units (RFU) from the standarve curve into estimated total cell counts. Fluorescence measurements were obtained by plate reader to quantify total cell numbers at seeding densities of 50,000, 100,000, 200,000 and 400,000 cells.

Through a two-way ANOVA with Tukey's multiple comparisons test, comparison of polystyrene and scaffold cultures revealed no statistically significant differences, with a statistically significant difference determined as a P-value less than 0.05. Figure 7B illustrates that after 72 hours of incubation, polystyrene cultures exhibited higher total cell numbers at 50,000 and 400,000 seeding densities, whereas scaffold cultures showed greater cell numbers at 100,000 and 200,000 when looking at means of each replicate. Under typical growth conditions, higher initial seeding densities are expected to yield proportionally greater cell numbers however in this assay cell counts increased up to 200,000 cells and then declined at the 400,000 seeding density.

Reliable Viability Assessment Using Validated Hoechst Quantification

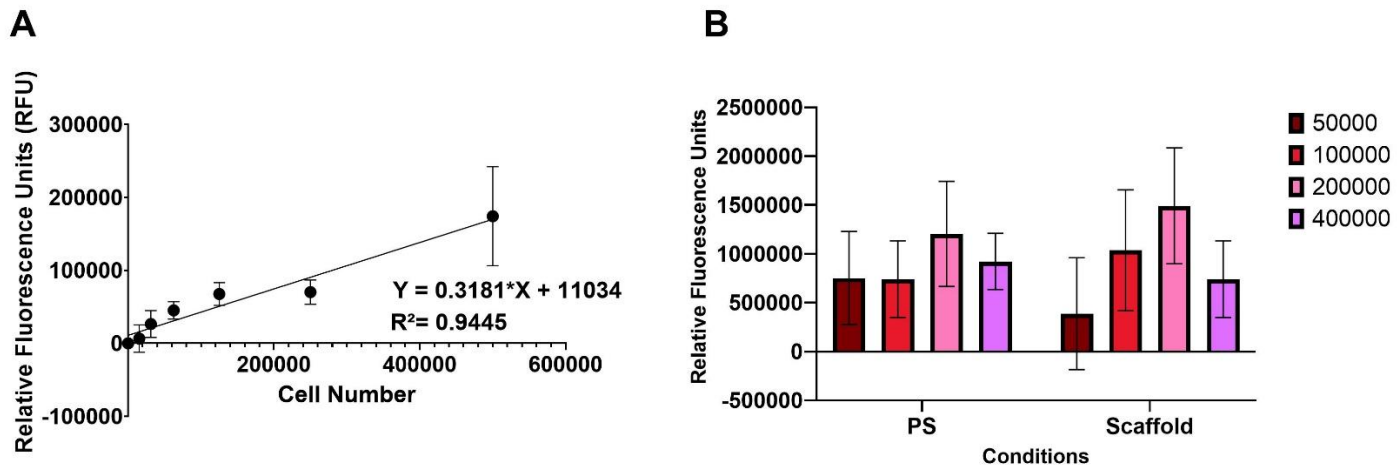

Figure 8. A) A Hoechst 33342 standard curve to assess total cell number following 72 hours of incubation. Standard curve ranged from 3125-500,000 cells with replicates of three, the r2 value is 0.09445. **B) Cell viability assay of total cells following72 hour incubation in PS and scaffold.** Calculated based on equation from standard curve. Data represents n=3 independent samples per condition. Values are mean ± SD. Statistical analysis by 2-way ANOVA with Tukey's multiple comparisons test.

Plate reader fluorescence was used to estimate dead cell numbers at seeding densities of 50,000, 100,000, 200,000 and 400,000 cells in Figure 9B. A propidium iodide (PI) standard curve spanning 3,125–500,000 cells (Figure 9A), was generated for viability discrimination and the derived regression model was applied to convert RFU values into dead cell counts. At the lowest seeding density (50,000 cells), higher levels of cell death were observed than

other seeding densities, scaffold cultures exhibit fewer dead cells than polystyrene at this density. In contrast at 200,000 cells, scaffold conditions showed increased cell death relative to polystyrene, other cell concentrations display a negligible difference between polystyrene and scaffold.

Standardized Propidium Iodide Assay for Dead Cell Quantification in PS versus Scaffold

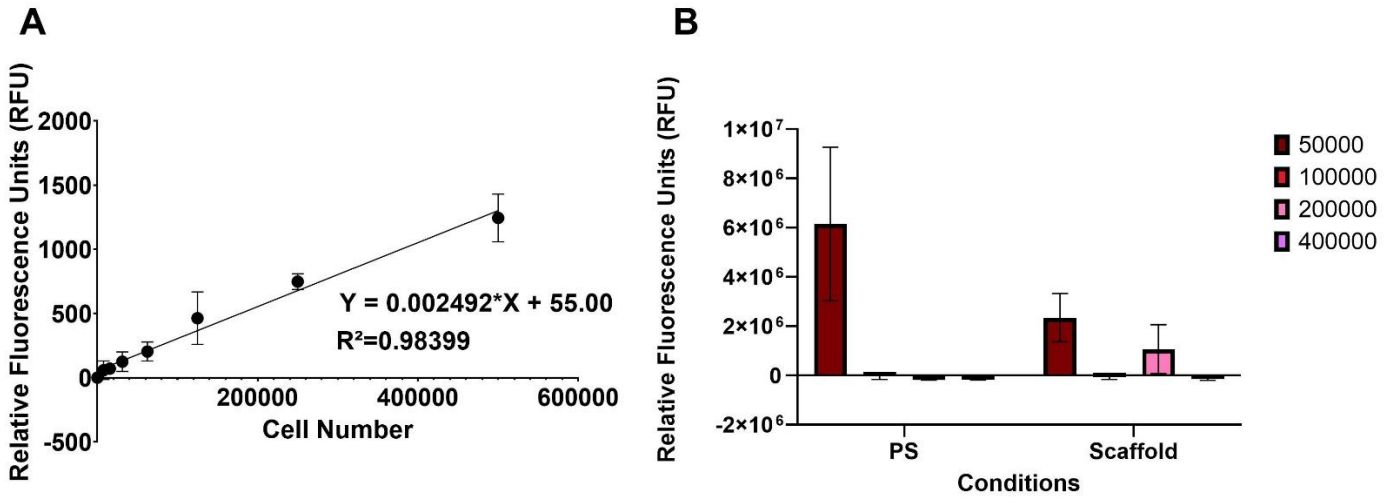

Figure 9. A) A propidium iodide standard curve (via RFU) to assess dead cell number following 72 hours of incubation. Standard curve ranged from 3125-500,000 cells with replicates of three, the r2 value is 0.9839. **B) Cell viability assay of dead cells following72 hour incubation in PS and scaffold.** Calculated based on equation from standard curve. Data represents n=3 independent samples per condition. Values are mean ± SD. Statistical analysis by 2-way ANOVA with Tukey's multiple comparisons test.

4.2 Optimization of Scaffold Cell Recovery and Viability Assay Validation

4.2.1 Evaluation of Cell Recovery from Scaffolds Across Varying Conditions

Cell recovery efficiency was evaluated using an OCI-AML2 viability assay on the Agilent NovoCyte Opteon Spectral Flow Cytometer after 1 hour of incubation. Cells were stained with Hoechst 33342 and 7-AAD to distinguish live and dead populations and quantify recovered cell numbers. Recovery agents tested included PBS, EDTA, cell dissociation buffer (CDB), accutase, and trypsin across polystyrene (Figure 10), crosslinked scaffold, and non-crosslinked scaffold conditions. Through a two-way ANOVA statistical analysis with Tukey's multiple comparisons test, comparison of scaffold versus polystyrene cultures for

each reagent showed no significant differences overall, except between polystyrene and non-crosslinked scaffold in the CDB condition (Figure 10C) defined by a P-value less than 0.05. Within scaffold conditions, non-crosslinked scaffolds consistently yielded higher recovered cell numbers than crosslinked scaffolds across all reagents (Figure 10A, B). Polystyrene cultures generally produced greater recovery than scaffold conditions for every reagent.

Using PBS as the reference control (Figure 10), it produced the greatest recovery at 1 hour and was significantly higher than accutase and trypsin ($P < 0.0001$) (Figure 10H, I). The elevated PBS recovery at this early time point likely reflects limited cell embedding within the scaffold after only 1 hour of culture; therefore, experiments were repeated following 72 hours of incubation. Statistical analyses were performed in GraphPad Prism using two-way ANOVA with Tukey's multiple comparisons test.

Various Recovery Agents Tested on PS, Crosslinked and Non-Crosslinked Scaffolds following 1 Hour Incubation with Comparison to PBS

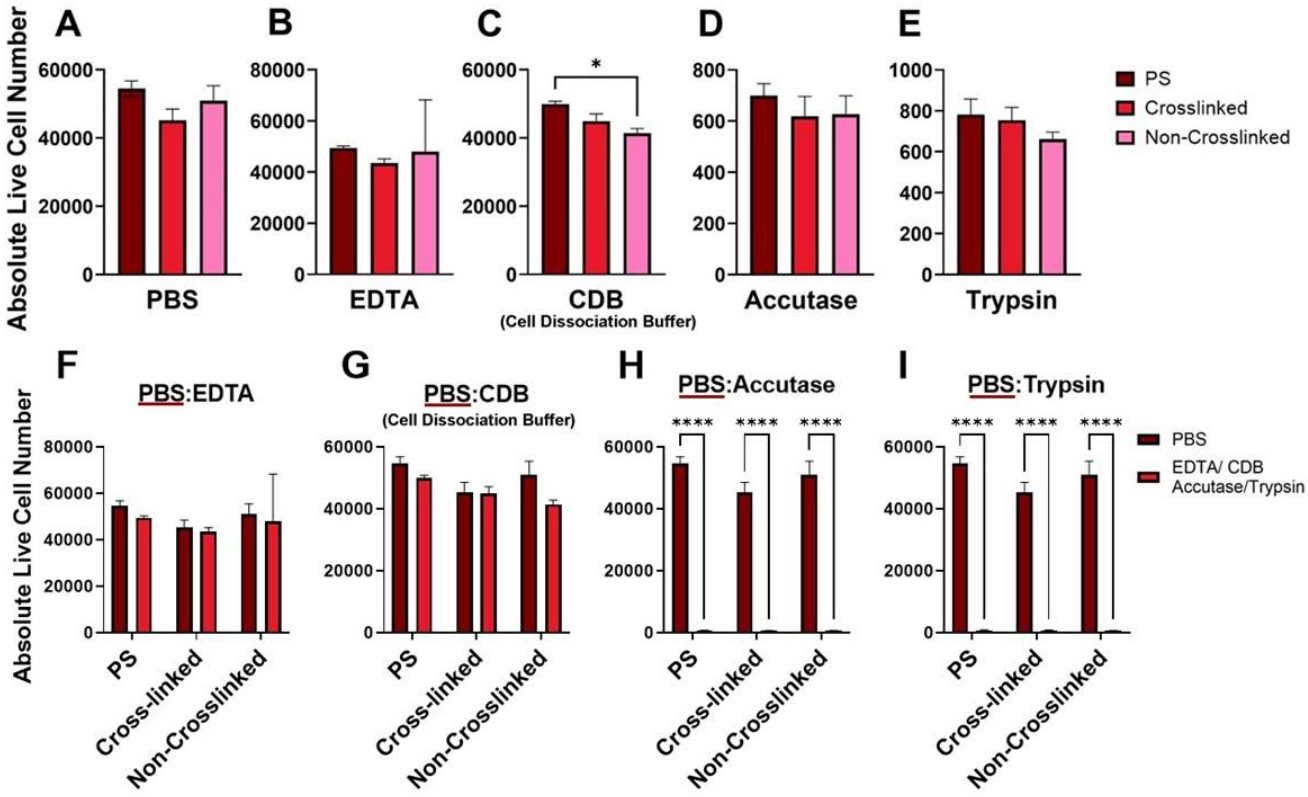

Figure 10. Cell viability for various cell recovery methods: A) PBS, B) EDTA, C) CDB, D) Accutase and E) Trypsin, were assessed after 1 hour of incubation in PS, Crosslinked and Non-Crosslinked scaffolds by counting absolute live cell count conducted through flow cytometry using stains Hoechst 3342 and 7AAD. **Cell viability for various cell recovery methods: F) EDTA, G) CDB, H) Accutase and I) Trypsin, were compared to control PBS in PS, Crosslinked and Non-Crosslinked scaffolds** by counting absolute live cell count conducted through flow cytometry using stains Hoechst 3342 and 7AAD. Values are mean ± SEM. Statistical analysis by 2-way ANOVA with Tukey's multiple comparisons test.

In Figure 11, cell recovery was evaluated again after 72 hours of incubation. PBS, EDTA, cell dissociation buffer (CDB), accutase, and trypsin were applied as recovery agents across polystyrene, crosslinked scaffold, and non-crosslinked scaffold conditions. Overall, comparisons with three technical replicates between scaffold and polystyrene cultures for each reagent showed no significant differences, except for accutase and trypsin (statistical analysis via a two-way ANOVA with Tukey's multiple comparisons test defined by a $P \leq 0.01$). Non-crosslinked scaffolds yielded higher cell recovery than crosslinked scaffolds with PBS, EDTA, and CDB, however with no statistical significance (Figure 11A, B, C). In contrast, with

accutase and trypsin (Figure 11D, E), crosslinked scaffolds produced significantly greater recovered cell numbers than non-crosslinked scaffolds ($P \leq 0.01$). Polystyrene cultures exhibited the greatest recovery across all reagents (Figure 11). Using PBS as the reference control demonstrated the highest overall recovery (Figure 11F, G), with significant differences relative to accutase and trypsin ($P \leq 0.01$) (Figure 11H, I). Consistent with the 1-hour recovery experiment, PBS was identified as the most effective recovery agent.

PBS Remains Most Effective Compared to Other Recovery Agents After 72 Hours

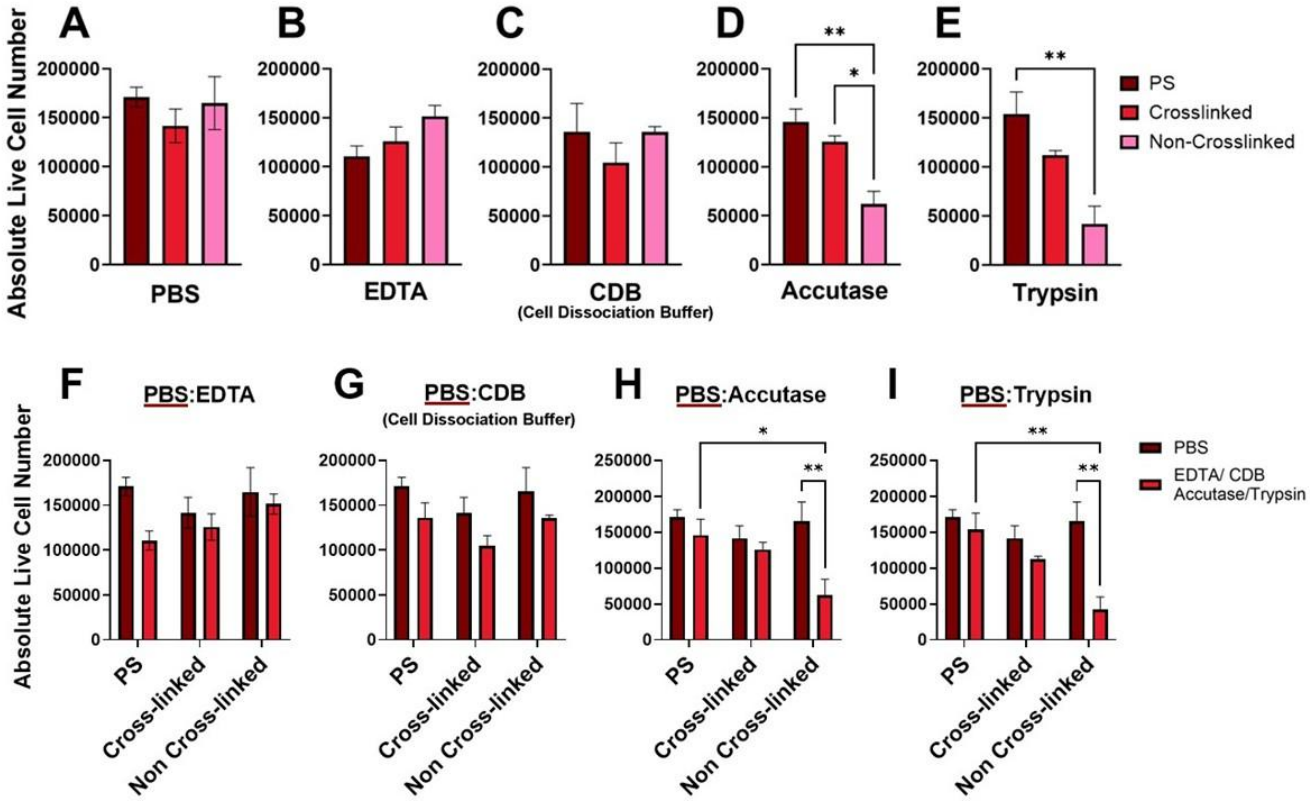

Figure 11. Cell viability for various cell recovery methods: A) PBS, B) EDTA, C) CDB, D) Accutase and E) Trypsin, were assessed after 72 hours of incubation in PS, Crosslinked and Non-Crosslinked scaffolds by counting absolute live cell count conducted through flow cytometry using stains Hoechst 3342 and 7AAD. **Cell viability for various cell recovery methods: F) EDTA, G) CDB, H) Accutase and I) Trypsin, were compared after 72 hours of incubation to control PBS in PS, Crosslinked and Non-Crosslinked scaffolds** by counting absolute live cell count conducted through flow cytometry using stains Hoechst 3342 and 7AAD. Values are mean ± SEM. Statistical analysis by 2-way ANOVA with Tukey's multiple comparisons test.

4.2.2 Viability Assay Validation

To establish a baseline of OCI-AML2 cell viability, OCI-AML2 were assessed by flow cytometry using Hoechst 33342 and 7-AAD staining to discriminate live and dead populations. Establishing baseline growth of leukemic cells enabled comparison with drug-treated conditions to assess treatment effects on cell survival over 72 hours. Drug responses are commonly evaluated at 24 hours, extending the treatment duration allowed assessment of longer-term effects on cell survival. Leukemic cells were seeded at 50,000 per condition in polystyrene (PS) and scaffold cultures under standard media or media containing 0.1% DMSO and incubated for 72 hours.

In Figure 12A, scaffold cultures yields higher live cell recovery than PS in both untreated and 0.1% DMSO conditions. Dead cell counts were lower in scaffold than PS under untreated media, whereas in 0.1% DMSO conditions scaffold cultures showed slightly higher dead cell numbers than PS (Figure 12B). These differences were not statistically significant for either live or dead cell counts assessed through a two-way ANOVA with Tukey's multiple comparisons test.

Live cell numbers were reduced in 0.1% DMSO relative to untreated conditions, while dead cell counts were higher in untreated media than in 0.1% DMSO. Figure 12C, percent viability showed a greater proportion of viable cells in scaffold cultures compared with PS.

Live Cells and Cell Viability Increased in Scaffold in both Media and Media (w/ 0.1% DMSO)

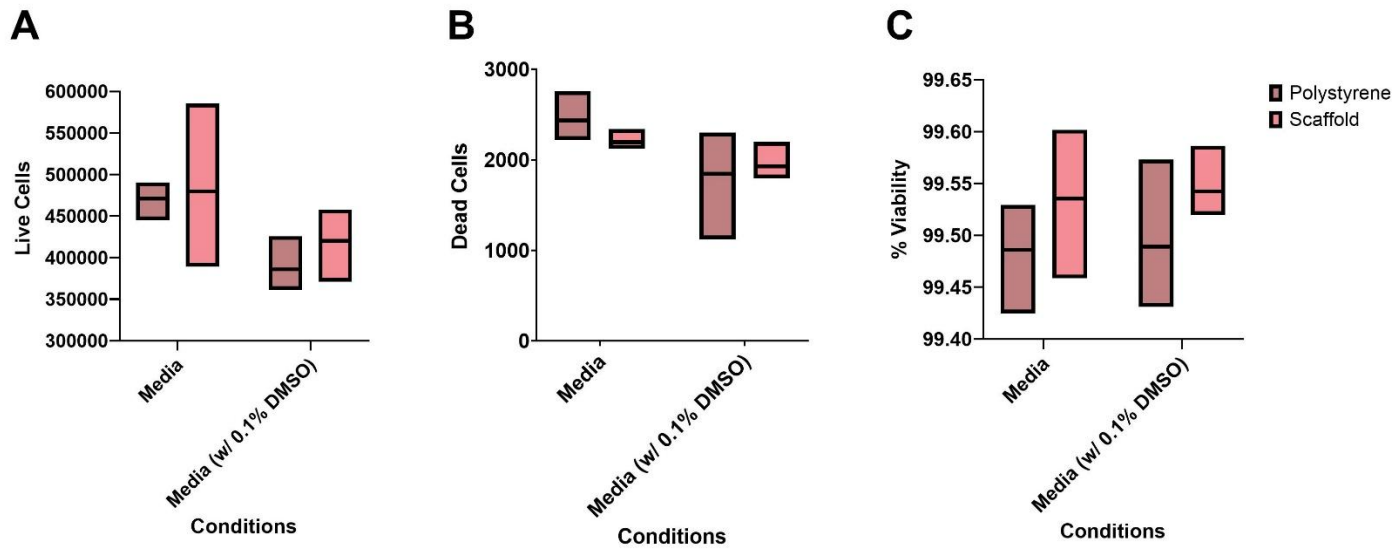

Figure 12. A) Cell viability of total cells establish baseline of OCI-AML2 cells following 72 hour incubation on polystyrene and scaffold. Absolute cell counts from Hoechst 33342 staining determined total number of cells**. B) Assessment of dead cells recovered from PS and scaffold are stained with dead cell stain 7-AAD**. **C) Percentage of viability analyzed through live/dead discrimination using formula and data acquired by gating live cell populations.** Values in replicates of three and are mean ± minimum and maximum. Statistical analysis by 2-way ANOVA with Tukey's multiple comparisons test.

4.3 Identification of Compounds Targeting OCI-AML2 Cells by Dose–Response Analysis

4.3.1 AML OCI-2 Response to Chemotherapeutic Treatment on Polystyrene and 2D Scaffolds

To evaluate a high-content flow cytometry–based approach for quantifying live cell numbers following chemotherapeutic treatment, OCI-AML2 cells were seeded in polystyrene and scaffold cultures to be treated for 72 hours with seven drugs (5-fluorouracil, daunorubicin, sorafenib, filanesib, zosuquidar, thioridazine, and cytarabine). Cell viability was subsequently assessed by live/dead gating using an Agilent NovoCyte Opteon 4-laser spectral flow cytometer and the NovoExpress software. Dose–response analyses were performed across three biological replicates to compare drug sensitivity of AML cells and if AML cells respond similarly over different time points. Biological replicates in this experiment are considered to be cells from different passage cycles and performed at

various time points. To determine statistical significance, nonlinear regression curves were compared between conditions along with an extra sum-of-squares F-test, where p value < 0.05 to be considered a statistically significant difference between curves. Dose–response curves were generated using nonlinear regression (four-parameter logistic model) to accurately model sigmoidal relationships and calculate IC_{50} values; differences between polystyrene and scaffold conditions were assessed using an extra sum-of-squares F-test to determine whether separate curve fits significantly improved the model.

For 5-fluorouracil, IC_{50} values varied between replicates but were generally higher in scaffold cultures than in polystyrene in two of three replicates (Replicate 1: 3.398 vs 1.047 μM (Figure 13A); Replicate 2: 1.134 vs 0.00045 μM (Figure 13B), indicating reduced sensitivity on scaffold. In Replicate 3 (Figure 13C) IC_{50} values were similar between conditions (0.980 vs 0.807 μM), suggesting minimal effect.

For Figure 13, daunorubicin IC_{50} values were consistently low in both platforms across all replicates, reflecting high potency. Scaffold cultures exhibited slightly lower IC_{50} values than polystyrene in each replicate (Replicate 1: 0.00041 vs 0.00172 μM (Figure 13D), Replicate 2: 0.00228 vs 0.00429 μM (Figure 13E), Replicate 3: 0.00046 vs 0.00039 μM(Figure 13F)), indicating comparable or slightly increased sensitivity in scaffold conditions.

For sorafenib in Figure 13, greater variability between conditions and replicates was observed. In replicate 1 (Figure 13G), scaffold IC_{50} was markedly higher than polystyrene (4.524 vs 0.273 μM), indicating reduced sensitivity on scaffold. Replicate 2 (Figure 13H) showed a measurable IC_{50} in polystyrene (0.381 μM) but an unstable fit in scaffold cultures. In Replicate 3 (Figure 13I), scaffold IC_{50} was substantially higher than polystyrene (561.8 vs 0.068 μM).

Differential Response Exhibited with Microenvironment-Dependent Resistance in Select Drugs and Condition-Insensitivity in High-Potency Drugs

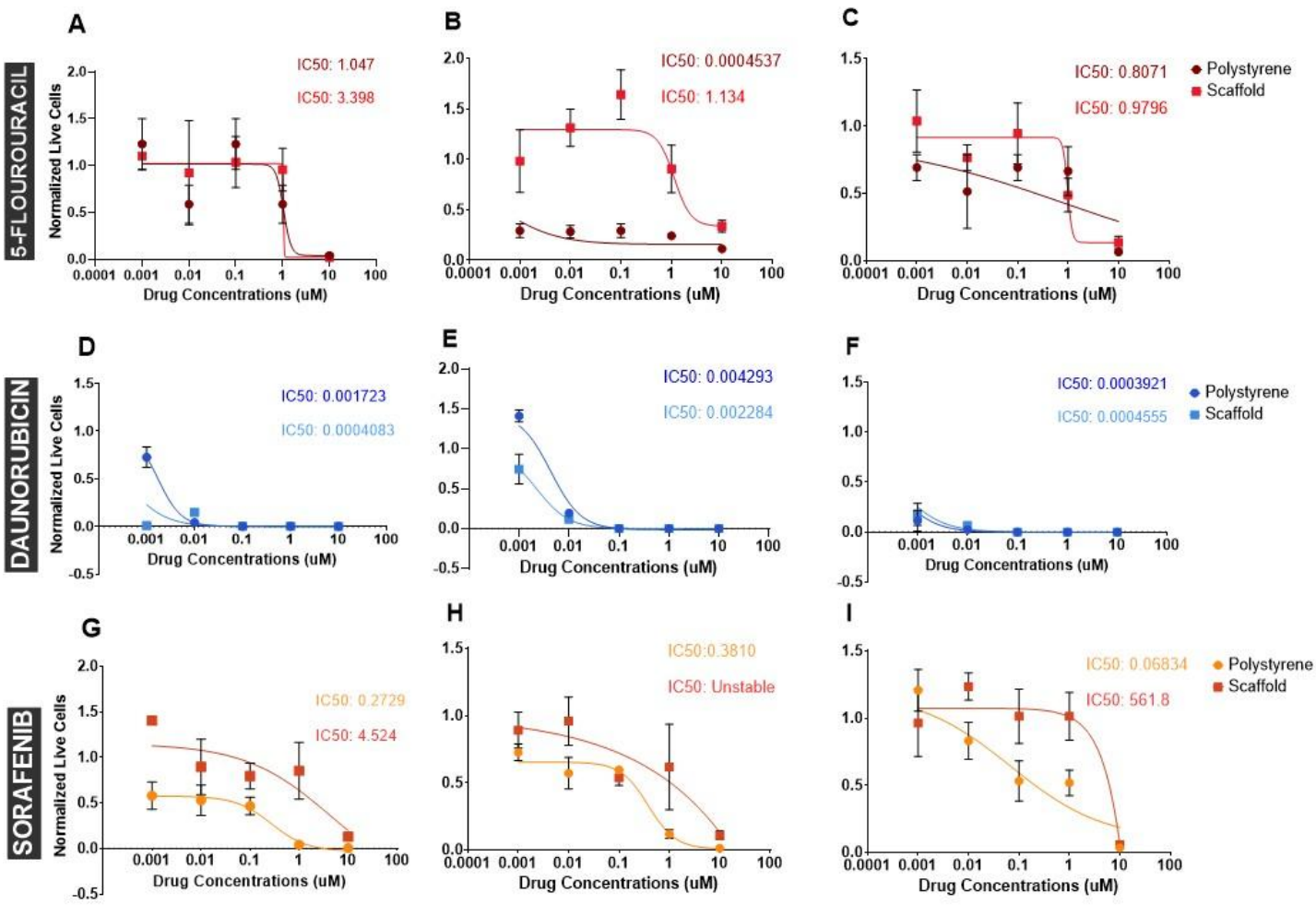

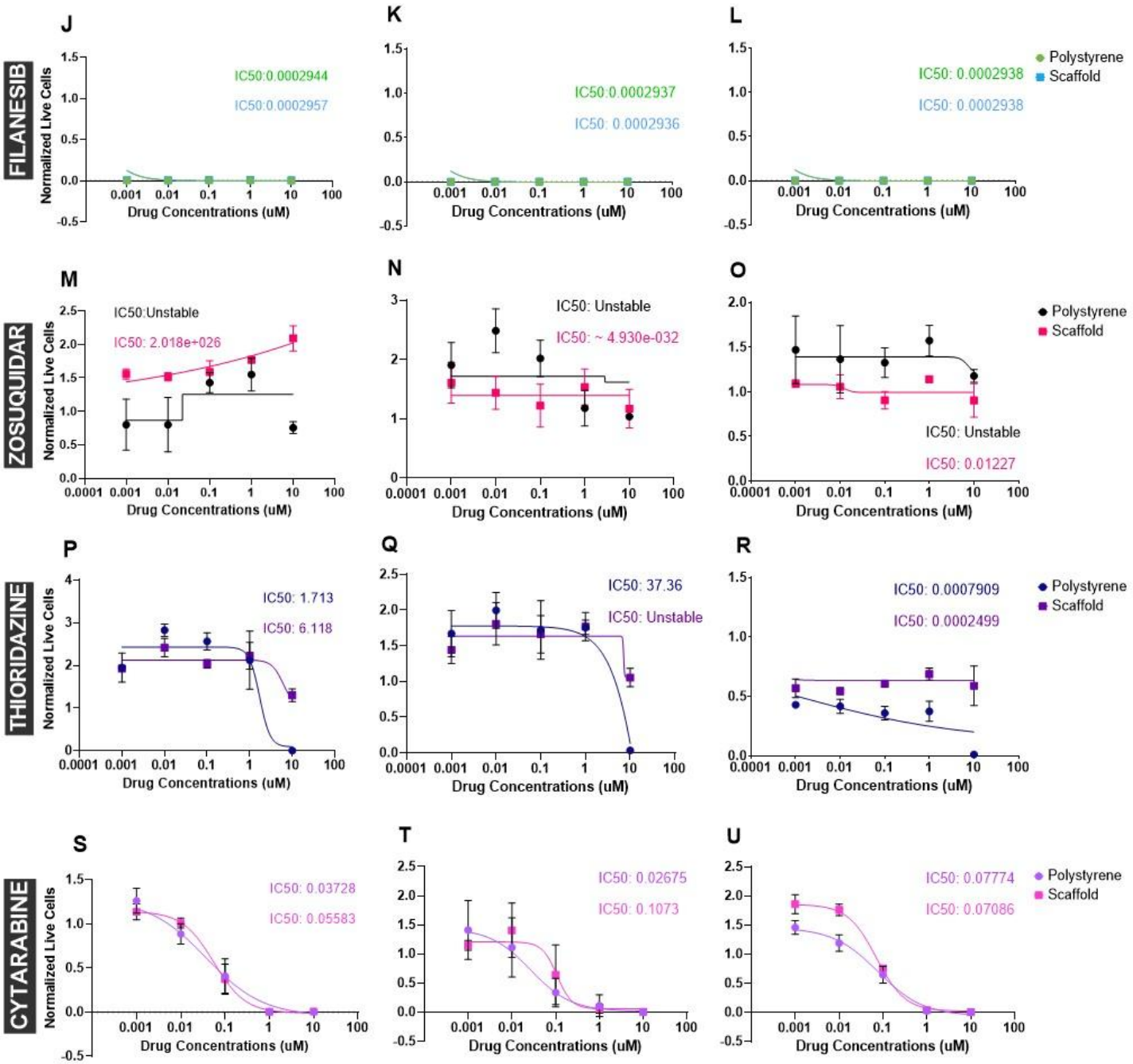

Figure 13. Dose–response and IC_{50} analysis of A-C) 5-Flourouracil, D-F) Daunorubicin, G-I) Sorafenib, J-L) Filanesib, M-O) Zosuquidar, P-R) Thioridazine and S-U) Cytarabine in AML cells cultured on polystyrene and crosslinked scaffold. Drug response after 72 hours of incubation in polystyrene (PS) and crosslinked scaffold conditions were evaluated at 0.001, 0.01, 0.1, 1, and 10 µM by quantifying absolute live cell counts using flow cytometry with Hoechst 33342 and 7-AAD staining. Values are normalized mean ± SEM, each graph representing a biological repeat. Dose–response curves were fitted by non-linear regression, and IC_{50} values derived from the fitted curves are indicated.

For filanesib (Figure 13J, K, L), both culture systems exhibited near-complete loss of viability at low micromolar concentrations, with highly consistent IC_{50} values across replicates (~2.9 × 10^{-4} μM). The overlap of the polystyrene and scaffold curves and nearly identical IC_{50} estimates indicate comparable drug sensitivity between the two culture conditions.

In contrast, zosuquidar (Figure 13M, N, O) did not present typical IC_{50} curves across all replicates. Cell viability remained relatively constant across the concentrations in both polystyrene and scaffold cultures, preventing reliable curve fitting and resulting in unstable IC_{50} estimates. This was consistent between culture conditions, indicating a lack of measurable cytotoxic response within the tested doses.

Thioridazine exhibited variable IC_{50} curves across replicates and culture systems. In replicate 1(Figure 13P), both conditions showed dose–response behavior, with a rightward shift in the scaffold curve corresponding to a higher IC_{50} (6.1 μM) compared with polystyrene (1.7 μM). Replicate 2 (Figure 13Q) demonstrated a clear dose–dependent decline in polystyrene viability (37.6 μM), whereas the scaffold data did not support stable IC_{50} estimation. In replicate 3 (Figure 13R), both conditions produced measurable IC_{50} values, again with greater sensitivity in polystyrene (7.9 × 10^{-4} μM) than scaffold (2.5 × 10^{-3} μM). A significant difference between culture conditions was observed at 10 μM, where cells in scaffold culture retained higher viability, whereas polystyrene cultures showed near-complete loss of viable cells. However, results remained inconsistent across all replicates to draw conclusions.

Cytarabine responses in Figure 13S, T, U were consistent across replicates and IC_{50} curves in both culture conditions. Although scaffold cultures required slightly higher drug concentrations to achieve comparable effects, the differences were minimal. IC_{50} values ranged from 0.00553–0.07086 μM in scaffold and 0.03728–0.07774 μM in polystyrene. Overall, cytarabine responses were comparable between scaffold and polystyrene conditions.

Table 2. Drug Effects Observed Summarized in Repeated Experiments. IC50 values on polystyrene and scaffold averages with ± 1 to summarize effective dosage. Statistical anaylsis was assessed through an extra sum-of-squares F-test for comparison as well as t-test where significance is defined as a p-value less than 0.05. Astericks (*) indicating large variability between biological repeats.

Drug	Average IC_{50} Polystyrene (μM)	Average IC_{50} Scaffold (μM)	Different IC_{50} Value	Effective Dosage (Scaffold Vs. PS)
5-Flourouracil	0.618 ± 0.313	1.837 ± 0.758	Yes	Higher
Cytarabine	0.0501 ± 0.0135	0.0273 ± 0.0218	No	Same
Daunorubicin	0.00213 ± 0.00116	0.00105 ± 0.0006	No	Same
Sorafenib	0.241 ± 0.091	283.16 ± 278.7*	Yes	Higher
Zosuquidar	N/A	N/A	N/A	N/A
Filanesib	0.00029 ± 0	0.00029 ± 0	No	Same
Thioridazine	13.1* ± 12.2*	3.35* ± 3.05*	Yes	Higher

4.3.2 Comparison of Drug Response Assays: Flow Cytometry Versus Plate Reader

Across the tested chemotherapeutic compounds on the flow cytometer, AML cells cultured on the crosslinked scaffold exhibited drug responses that were comparable to those in polystyrene, with compound-specific shifts in IC_{50} indicating condition-dependent differences in sensitivity (Figure 14).

For 5-fluorouracil (Figure 14A), IC_{50} values were similar between PS (1.249 μM) and scaffold (1.228 μM), indicating minimal effect of culture platform on sensitivity. Daunorubicin (Figure 14B) and filanesib (Figure 14G) likewise showed nearly identical IC_{50} values between conditions, suggesting preserved potency in scaffold culture as seen in figure 14.

In contrast, sorafenib (Figure 14C) and zosuquidar (Figure 14D) exhibited significantly higher IC_{50} values in scaffold relative to PS (sorafenib: 0.795 μM vs 0.135 μM, zosuquidar: 1.942 μM vs 0.151 μM). Cytarabine showed the opposite trend in figure 14F, with a lower IC_{50} in scaffold than PS (0.018 μM vs 0.026 μM), suggesting increased sensitivity in scaffold culture.

Thioridazine dose–response curves in figure 14E did not reach a stable inhibitory range, precluding reliable IC_{50} estimation in either condition.

Significance was assessed by running a nonlinear regression curve to compare curves for an extra sum-of-squares F-test, where p-value < 0.05 to be considered a statistically significant difference between the curves.

Consistent Drug Effects Observed in Replicated Experiments using Flow Cytometry

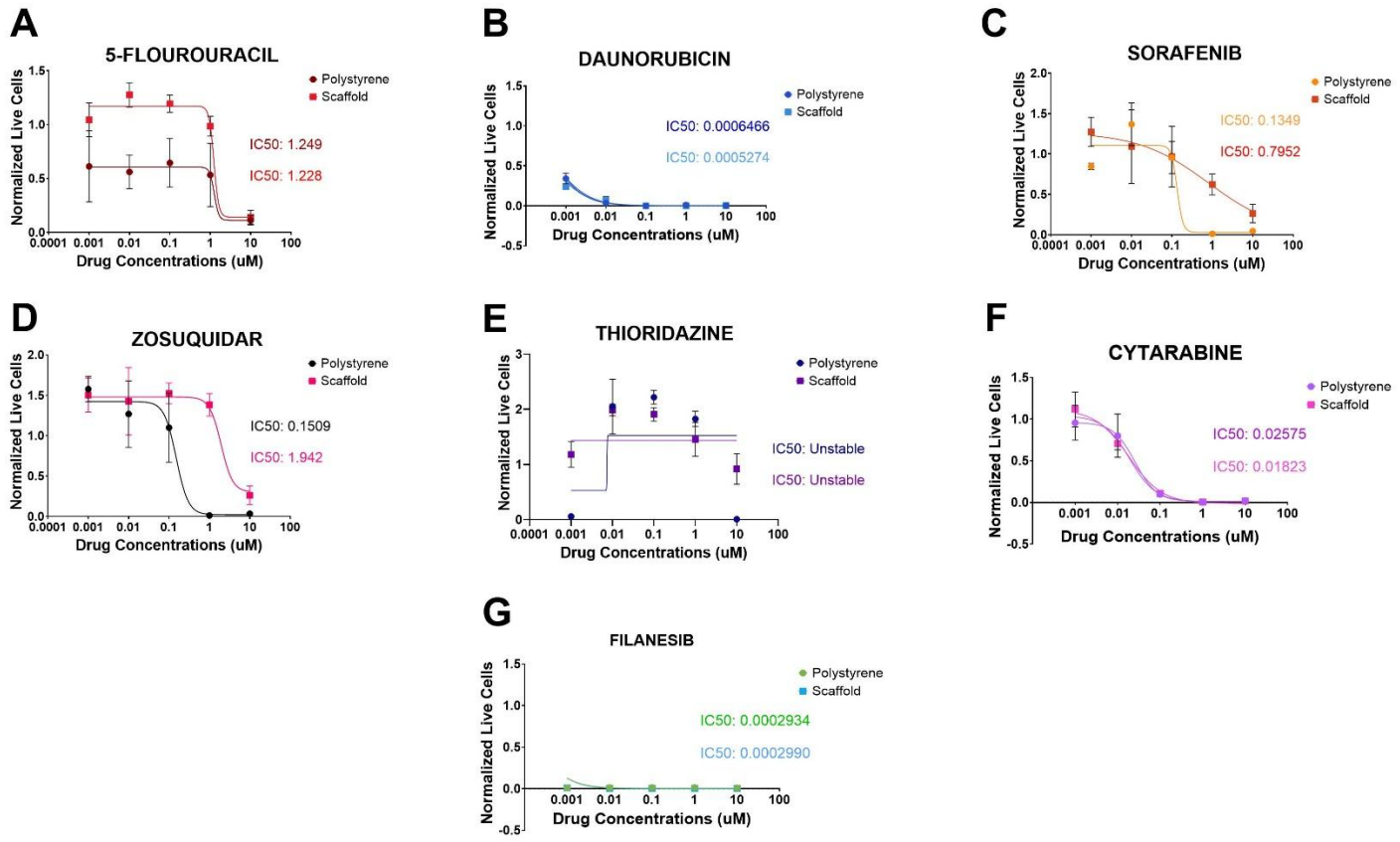

Figure 14. Dose–response curves and IC_{50} comparison of antileukemic compounds in AML cells cultured on polystyrene and crosslinked scaffold via Flow Cytometry. AML cells were treated for 72 hours with **A) 5-fluorouracil, B) daunorubicin, C) sorafenib, D) zosuquidar, E) thioridazine, F) cytarabine or G) filanesib** across the indicated concentration ranges. Drug response was quantified as normalized live cell counts by flow cytometry using Hoechst 33342 and 7-AAD staining. Symbols represent mean ± SEM for polystyrene and scaffold cultures. Dose–response curves were fitted by non-linear regression, and IC_{50} values derived from the fitted curves are shown for each condition; unstable fits are indicated where applicable.

A parallel AlamarBlue assay (Figure 15) was run alongside from the same samples on the Agilent Cytation C10 Imaging plate reader, AlamarBlue can assess the metabolic activity of cells though it is not a direct correlation to cell number. An AlamarBlue standard curve demonstrated a strong linear correlation between fluorescence intensity and cell number (R^2 = 0.9571), confirming the reliability of the assay for quantifying cell viability (Fig. 15A).

IC_{50} dose–response curves were generated using fluorescence reads from tested chemotherapeutic compounds, revealing differences to those generated via flow cytometry. Scaffold cultures were more sensitive to 5-fluorouracil (IC_{50} = 0.01728 μM vs 1.200 μM in polystyrene) (Figure 15B) and sorafenib (0.02523 μM vs 0.2868 μM) (Figure 15D). In contrast, daunorubicin showed greater potency in polystyrene (0.0004597 μM) than scaffold (0.002507 μM) in figure 15C. Filanesib exhibited nearly identical, highly potent IC_{50} values in both systems (~3×10^{-4} μM), indicating minimal effect (Figure 15E).

Zosuquidar (Figure 15F) and thioridazine (Figure 15G) displayed inconsistent or unstable IC_{50} behavior between conditions, with limited dose-dependent responses in at least one condition. In figure 15H cytarabine showed similar sensitivity in both cultures, with a slightly lower IC_{50} in scaffold (0.06935 μM) compared with polystyrene (0.09767 μM).

AlamarBlue Assay was Repeated Following Drug Treatment with Inaccurate Results

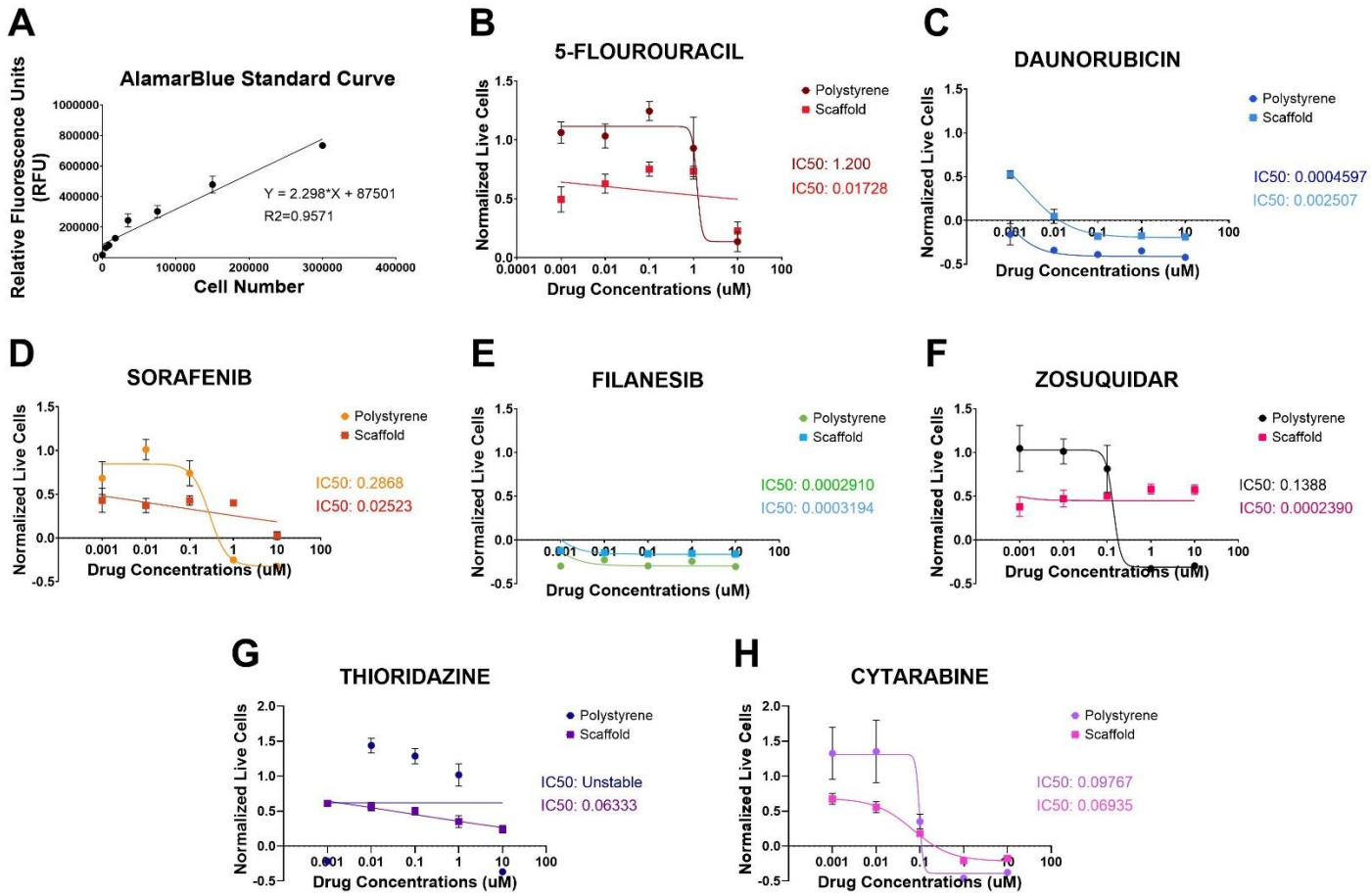

Figure 15. Dose–response curves and IC_{50} comparison of antileukemic compounds in AML cells cultured on polystyrene and crosslinked scaffold measured by alamarBlue assay. AML cells were treated for 72 hours with **B) 5-fluorouracil, C) daunorubicin, D) sorafenib, E) Filanesib, F) zosuquidar, G) thioridazine or H) cytarabine** across the indicated concentration ranges. Drug response was quantified as normalized metabolic activity using the **A) alamarBlue plate readout**. Symbols represent mean ± SEM for polystyrene and scaffold cultures. Dose–response curves were fitted by non-linear regression, and IC_{50} values derived from the fitted curves are shown for each condition; unstable fits are indicated where applicable.

CHAPTER 5

DISCUSSION

5.1 ECM-Mimicking Scaffold Fabrication and Niche Relevance

The bone marrow microenvironment, a dynamic three-dimensional network composed of diverse cell populations, ECM proteins, biochemical and mineralized elements, harbors specialized niches that provides structural support and regulate hematopoietic and leukemic cell behavior. Therein lies the extracellular matrix, the non-cellular components of the bone marrow that functions as mechanical support, adhesion sites and emits biochemical signalling that influence hematopoietic homeostasis. Interactions between this complex framework and hematopoietic stems cells shape cell survival, migration and differentiation[12] as well as malignant transformation. ECM can promote leukemic transformation and progression by enhancing survival signaling, altering differentiation pathways, and protecting emerging leukemic clones from apoptosis[117]. The remodeling by leukemic cells further reinforces these signals, contributing to the establishment of a permissive leukemic niche that supports malignant expansion and therapeutic resistance[26].

Understanding this complex microenvironment is crucial for gaining insight into the mechanisms that drive drug resistance in AML. However, a major limitation remains the ability to culture AML cells outside of their native bone marrow niche. Once removed from this environment, leukemic cells rapidly lose key cell–cell and cell–matrix interactions, soluble signaling cues and mechanical stimuli that regulate survival, proliferation and drug responsiveness as well failing to maintain phenotypic and functional characteristics[32].

While ex vivo drug screening on AML cells has been extensively researched, most studies rely on polystyrene culture systems. These conditions fail to mimic the native extracellular matrix, which may contribute to the poor translation of findings to in vivo outcomes observed in clinical trials[20]. Given the limited physiological relevance of polystyrene-based culture systems, previous work in our lab focused on developing a scaffold platform incorporating key components that fabricate the extracellular matrix. The optimized scaffold currently employed mimics the complex interplay between leukemic cells and their microenvironment. Due to its structural and material properties, conducting drug screening assays in a high-throughput format remains challenging. To overcome this limitation,

several techniques were explored to develop a scalable screening platform capable of testing large panels of compounds across different patient samples.

5.2 Potential and Limitations of High-Content Microscopy Imaging for Cell Quantification

Microscopy imaging, a form of high-content screening (HCS), is a fluorescence imaging technique that combines microscopy with quantitative image analysis to extract data at the single-cell level[88]. Unlike conventional high-throughput screening (HTS) methods such plate readouts based on metabolic activity or total fluorescence intensity, high-content imaging allows for direct visualization and quantification of individual cells within a culture system. High-content microscopy imaging (HCM) is able to consider cell number, viability, morphology and spatial organization through automated computational analysis with the appropriate set up parameters[122].

The use of the Agilent Cytation C10 Confocal Imaging Reader allowed for detailed visualization of cells stained with both the Abcam cell tracking red dye (Cat.# ab269446, Abcam) and Hoechst at 20X magnification. The cell tracking red dye effectively labeled the membranes of live cells through intracellular delivery via PolyNaut particles. This mechanism, which involves endocytosis and release of the dye from early endosomes into the cytosol, ensures that staining is largely restricted to the target cell, minimizing dye transfer between neighboring cells. Hoechst, being a nuclear-specific and cell-permeable dye, consistently stained all cell nuclei, providing a reliable marker for identifying cells in the imaging panels. Together, these dyes allowed for the differentiation of live and dead cells, with live cells exhibiting a combination of red and blue fluorescence and cells that were only Hoechst-positive likely representing dead or compromised cells.

Fluorescence staining was evaluated under both polystyrene and scaffold conditions over time, with long-term staining considered in the context of drug screening experiments where cells are incubated for up to 72 hours. The cells were not exposed to any drug treatment, as this experiment was conducted solely to evaluate the efficiency of the system. While the red dye intensity remained relatively stable over 24 hours, the distribution of the stain after this

period improved the ability to distinguish individual cells, suggesting that the dye is suitable for extended observation periods. This stability is particularly important for drug efficacy studies, as it allows for reliable tracking of cell viability without repeated staining.

The optimal stain concentration in polystyrene differed from that of the scaffold condition, at both T0 and T24 in polystyrene conditions the optimal stain concentration was 1:1000. Whereas in scaffold conditions, the optimal stain at T0 was 1:100 while at T24 was 1:100 or 1:10,000. At the T24 timepoint, cells were visualized at both 1:100 and 1:10,000 concentrations but lacked clear images of cells without background scaffold components auto fluorescing. Scaffold conditions may require a stronger concentration of the Abcam cell tracking red dye due to partial absorption by the scaffold though increasing the dye concentration may also lead to elevated background fluorescence, making cells less distinguishable. Scaffold artifacts cause autofluorescence from Hoechst 3342 absorption, therefore cells cannot be observed on the scaffold and quantitively measured using confocal imaging. Due to the difficulty in subtracting background fluorescence, automated image analysis could not be completed as the software could not accurately discriminate for cells despite setting up parameters based on cell shape and size therefore this technique was not best suited for accomplishing our objective.

Microscopy imaging is the screening technique of choice because it provides a more nuanced understanding of drug response by taking into account the heterogeneity of AML and its manifestation. Observing morphology, viability and phenotypic change can identify resistant or surviving subpopulations as well as how cells interact with their surrounding microenvironment[25]. An ideal screening method would be observing cells in this scaffold composition while subjected to chemotherapeutic compounds as removing the cells from this environment may disrupt critical cell–matrix interactions, potentially missing important biological insights to obtain a more physiologically relevant assessment of drug response within complex culture systems.

This can be further optimized to reduce background fluorescence or dampen it to the extent of quantifying cells in our scaffold. Autofluorescence dampening reagents for microscopy

imaging are commercially available however was not explored in the time frame of our experiment. While investigating other scaffold culturing systems, those studied do not present this unique challenge as their culture systems are either using a premanufactured scaffold such as Matrigels or has not yet attempted confocal imaging on scaffold for high-throughput screening purposed.

5.3 Plate Reader Approaches for High-Throughput Cell Quantification

For high-throughput screening, plate reader assays are the most commonly used method for their rapid evaluation of cellular responses in large scale drug screens. This approach is typically dependent on assessing cell viability, metabolic activity and proliferation through colorimetric, fluorescent or luminescent readouts[11]. These assays are specifically selected for their speed and scalability, producing a quick evaluation of numerous drug conditions in a high-throughput manner where hits are required to be identified. As an initial drug screening procedure, plate reads can generate readouts based on a fluorescence signature. Although, this can generate bulk data it is important to note they may not provide the most accurate results as plate reader-based metabolic, or cell viability assays are indirect measure of cell number. Despite this, it is still employed to identify hit compounds in early-stage drug discovery investigation and preclinical screening[125].

Implementing a plate reader in the context of our project, which utilizes a tissue-engineered scaffold designed to closely mimic the bone marrow microenvironment, presents several unique challenges. The scaffold's structural and material properties can interfere with conventional plate reader measurements by scattering light, absorbing assay reagents, or generating background signals. Optimization of this system was attempted using a diverse number of techniques and various stains were tested such as Alamar blue, Hoechst, PI, and 7-AAD as well measuring with and without scaffold and ensuring top and bottom reads.

In an Alamar blue staining, a reliable indicator of metabolic activity, a redox reaction occurs when cells are exposed to the stain. When active component resazurin, in the indicator dye, accepts electrons — it is reduced from its oxidized non-fluorescent blue form to a pink, fluorescent resorufin which occurs within the mitochondria to reflect cellular metabolic

activity. At an excitation/emission wavelength of 530/590, OCI-AML2 metabolic activity was measured in various cell seeding densities with a standard curve as a reference point for converting relative fluorescence units (RFU) into the 'supposed' cell number. The standard curve exhibited an R^2 value of 0.9762, ensuring the reliability of the cell count. OCI-AML2 metabolic activity was significant with an increase on the scaffold, implying the scaffold may provide an environment for the cells to be better supported than on polystyrene. All seeding densities displayed an increase than polystyrene conditions.

To further evaluate the accuracy of the plate reader Hoechst 33342, cell permeable nucleic acid stain, was utilized to quantify cell number. By binding to the to the minor groove of double-stranded DNA, there is fluorescent detection of nuclei and provides a more direct measurement of cell presence compared to metabolic assays. As the dye readily penetrates live cells and produces strong fluorescence upon binding DNA, it is commonly used for nuclear staining and cell counting applications[61]. To investigate the reliability and accuracy of the plate reader, we aimed to determine whether direct nuclei staining could provide a more reliable indicator of cell number within these two diverse culture conditions. This comparison was particularly important given that scaffold-based cultures can influence metabolic activity and may therefore confound metabolic viability assays.

The resulting R^2 value of 0.9445 suggests that the staining approach produced a reasonably consistent signal across conditions, indicating that the dye was effectively detecting cellular DNA. Despite this correlation, the readout did not clearly reflect the expected seeded cell densities. No statistically significant differences were observed between polystyrene and scaffold conditions. Interestingly, polystyrene cultures showed higher detected cell numbers at the 50,000 and 400,000 seeding densities, whereas scaffold cultures displayed relatively higher signals at the intermediate densities of 100,000 and 200,000 cells. Although Hoechst staining demonstrated adequate fluorescence and absorption by cells, the variability in measured cell numbers suggests that plate reader–based cell quantification may still be influenced by the scaffold microenvironment, limiting its reliability as a standalone method for accurate cell quantification in this system. An alternative

interpretation is that differences in cell counts between scaffold and polystyrene conditions may reflect enhanced cell proliferation within the scaffold environment.

To perform a differential stain, we assessed Propidium iodide (PI) staining as a membrane integrity dye that is membrane-impermeable and therefore cannot enter, viable cells. Instead, PI selectively penetrates cells with compromised plasma membranes, such as dead or late-stage apoptotic cells. Once inside the cell, PI binds to DNA and emits strong red fluorescence when excited, allowing these non-viable cells to be readily detected and quantified. While looking at our PI standard curve to detect dead cells, the same pattern is observed where our R^2 value remains in the standard range, but the cell quantity varies between polystyrene and scaffold conditions even in the negative range with no significance. In both conditions, few dead cells were detected, which may be attributed to the absence of drug treatment or potentially to inaccurate signal detection during measurement

These inconsistencies may be attributed to the structural complexity of the scaffold environment. The three-dimensional architecture of the scaffold may influence dye penetration, fluorescence detection or signal distribution during plate reader measurements however this was also observed in polystyrene conditions indicating the plate reader analysis did not perform as expected.

5.4 Optimization of Cell Recovery from Scaffold Cultures for Flow Cytometry Analysis

As fluorescence plate reader assays are not well suited for screening within three-dimensional matrices, the analysis was shifted toward a cell recovery approach with cells subsequently analyzed by flow cytometry following culture under polystyrene and scaffold conditions. Previous research has demonstrated that ECM scaffolds can influence stem cell fate through the combined effects of biochemical signals, biological components and biophysical properties of the matrix[17].

A study examining embryonic stem cell derived ECM scaffolds have exhibited that matrix modification such as crosslinking can alter cellular differentiation outcomes[96]. Crosslinking

is process that improves structural integrity of ECM-based scaffolds by linking ECM components together, enhancing scaffold mechanical strength and preventing degradation for the better support of cells over extended culture periods. Stiffness, porosity and binding availability shape how cells interact with their environment through the modulation of physical and biochemical cues[95]. Crosslinking was considered in our experimentation due to long term culturing for up to 72 hours, requiring our scaffold to remain intact and persist through the cell recovery process. Supporting evidence suggests crosslinking plays a critical role in modulating the dynamic interface between cells and the ECM, making it a useful strategy for evaluating scaffold composition and structure[101] to determine how these factors influence cellular responses.

As crosslinking strengthens cell–matrix interactions within the scaffold microenvironment, cells are likely to adhere more strongly to the matrix. Consequently, efficient cell recovery becomes critical for downstream analysis. In this study, various recovery agents were evaluated to determine the potential influence of altered cellular mechanical properties on adhesion and recovery efficiency, as these factors may affect how strongly cells interact with the scaffold matrix.

In this study, recovery efficiency was assessed using OCI-AML2 cells stained with Hoechst 33342 and 7-AAD to distinguish live and dead populations after 1 and 72 hours of incubation. Several commonly used recovery agents—PBS, EDTA, cell dissociation buffer (CDB), accutase, and trypsin—were tested across standard polystyrene plates, crosslinked scaffolds and non-crosslinked scaffolds to evaluate their effectiveness.

Overall, recovery was similar between scaffold and polystyrene cultures. Notably, non-crosslinked scaffolds consistently yielded higher recovered cell numbers than crosslinked scaffolds for most reagents, suggesting that the looser scaffold structure facilitates cell detachment. Polystyrene cultures generally produced higher recovery than scaffolds across reagents, with PBS providing the greatest recovery at 1 hour, significantly exceeding accutase and trypsin ($P < 0.0001$). The elevated PBS recovery likely reflects limited cell

embedding at this early time point. Recovery after longer culture periods (72 hours) was performed to account for increased cell-matrix interactions.

Recovery following 72 hours, cell recovery across PBS, EDTA, CDB, accutase, and trypsin was generally similar between scaffold and polystyrene cultures, except for accutase and trypsin ($P \leq 0.01$). Non-crosslinked scaffolds yielded higher recovery with PBS, EDTA, and CDB, suggesting that a looser matrix facilitates detachment. Accutase and trypsin recovered more cells from crosslinked scaffolds, indicating that enzymatic agents are more effective for denser matrices[82]. Polystyrene consistently gave the highest recovery, with PBS remaining the most effective agent overall. Greater cell recovery in polystyrene may be attributed to lower adhesion, whereas scaffold-based cultures promote integrin-mediated attachment to matrix proteins, reducing cell retrieval[44]. These findings highlight that scaffold structure and recovery method jointly influence cell retrieval, establishing an effective protocol and laying the foundation for future drug screening.

5.5 Validating Scaffold Functionality via Cell Viability

Although optimized recovery has been achieved, with polystyrene yielding the highest cell numbers, scaffold-based recovery will inherently be lower therefore assessing viability of recovered cells remains more significant. Before initiating the drug treatment experiment, control experiments were performed to establish a baseline of OCI-AML2 cell viability over the 72-hour treatment time frame. Extending the treatment period to 72 hours allowed assessment of longer-term effects on OCI-AML2 cell survival as early drug discovery experiments have a duration of 24 hours to capture initial cytotoxic or signalling effects observing for apoptosis markers and signaling pathway changes[123].

Cells seeded at 50,000 per condition in polystyrene (PS) and 2D scaffold cultures under standard media or 0.1% DMSO showed that scaffold cultures consistently yielded higher numbers of live cells compared with PS while dead cell counts were generally lower in scaffolds under untreated conditions, though it was not significant. Under 0.1% DMSO, dead cell numbers in scaffolds were slightly higher than PS but these differences were not statistically significant. Significance being defined as $P \leq 0.05$. Viability percentage was

consistently higher in scaffold cultures compared with PS, suggesting that the 2D scaffold environment may provide enhanced support for cell survival over extended culture times.

These findings, supported by past evidence, indicates that various AML cell lines (e.g. K-562, HL60 and Kasumi-6) work favourably in scaffolds by supporting leukemic growth, in particular scaffolds containing ECM proteins such as collagen and fibronectin[78]. Thus, highlighting scaffold-based systems can maintain cell viability comparable or slightly superior to conventional polystyrene, establishing a reliable baseline for subsequent drug treatment experiments.

5.6 Flow Cytometry–Driven Drug Screening in Scaffold and Polystyrene AML Cultures

A high-content flow cytometry approach was used to quantify OCI-AML2 cell survival following 72-hour treatment with multiple chemotherapeutic agents in both polystyrene and scaffold cultures. By distinguishing live and dead populations through viability gating, this method enabled reliable dose–response analysis across biological replicates derived from different passage cycles and experimental time points. Overall, the results demonstrate that flow cytometry can effectively quantify drug-induced changes in AML cell viability while allowing comparison between conventional culture systems and ECM-inspired scaffold environments.

Drug sensitivity differed depending on the compound and culture platform. For 5-fluorouracil, IC_{50} values were generally higher in scaffold cultures in two of three replicates, suggesting reduced drug sensitivity when cells were cultured within the scaffold environment. In colorectal cancer (CRC), increased expression of extracellular matrix protein 1 (ECM1) in patients resistant to 5-fluorouracil (5-FU) suggests that extracellular matrix–associated signaling can contribute to reduced chemotherapy sensitivity and poorer clinical outcomes[65]. Similarly, in AML, interactions between leukemic cells and the extracellular matrix within the bone marrow niche are known to promote survival and resistance to chemotherapeutic agents[13]. However, the difference observed in one replicate

indicates that this effect may vary depending on experimental conditions or biological differences between passages

In contrast, daunorubicin showed consistently low IC_{50} values across both platforms, highlighting its strong cytotoxic potency against AML cells. The slightly lower IC_{50} values observed in scaffold cultures suggest that the scaffold environment does not confer resistance to this drug and may even modestly enhance sensitivity. These findings suggest that highly potent chemotherapeutic agents remain effective regardless of culture platform, consistent with clinical studies reporting significant improvements in complete remission (CR), overall survival (OS), and event-free survival (EFS)[34].

Responses to sorafenib were more variable. Scaffold cultures frequently displayed higher IC_{50} values than polystyrene, indicating reduced sensitivity under scaffold conditions. Given that sorafenib targets multiple signaling pathways, these differences may reflect the influence of cell–matrix interactions on kinase signaling and survival pathways within the scaffold environment[41].

For filanesib, both culture systems demonstrated nearly identical dose–response curves and highly consistent IC_{50} values, indicating that scaffold culture did not alter the drug's cytotoxic activity and aligning with studies that outline the critical role of kinesin spindle protein (KSP) in AML cells. Filanesib inhibits cell cycle progression and induces apoptosis through the mitochondrial pathway, suggesting its activity may remain effective across different culture conditions since KSP function is not directly associated with the ECM. Alternatively, zosuquidar failed to produce clear dose–response relationships in either condition, as cell viability remained relatively stable across the tested concentrations. This suggests limited cytotoxic activity within the dose range examined.

Thioridazine responses were more inconsistent across replicates. At higher concentrations (10 μM), scaffold cultures retained a significantly greater cell viability compared with polystyrene, suggesting potential protective effects of the scaffold environment. Although thioridazine targets DRD2 and shows selectivity for the MLL-AF6 variant[9], variability between replicates limited definitive conclusions about potential scaffold-mediated protection and

its effects may not be scaffold-associated. Finally, cytarabine responses were largely comparable between platforms, with similar IC_{50} ranges observed in both scaffold and polystyrene cultures, indicating that the scaffold environment did not substantially alter sensitivity to this commonly used AML therapeutic[90].

Drugs such as 5-fluorouracil and sorafenib, which target proliferative and signaling pathways, showed reduced sensitivity in scaffold cultures, suggesting that extracellular matrix-associated interactions may activate compensatory survival pathways that diminish drug efficacy. In contrast, the consistent potency of daunorubicin and filanesib across both platforms indicates that agents targeting fundamental intracellular processes, such as DNA integrity and mitotic machinery, are less susceptible to microenvironment-mediated resistance. Cytarabine's comparable activity further supports the idea that certain standard chemotherapeutics remain effective regardless of extracellular context. The lack of response observed with zosuquidar suggests that inhibition of drug efflux alone is insufficient to induce cytotoxicity in this system, while the variability seen with thioridazine underscores the complexity of targeting stem-like or niche-dependent AML populations.

Together, these results emphasize the importance of incorporating physiologically relevant models, such as ECM-mimicking scaffolds, to better capture microenvironment-driven drug resistance and improve the predictive value of preclinical drug screening.

5.7 Flow Cytometry and Plate Reader Reveal Assay-Dependent Differences in AML Drug Response on Scaffolds

Comparison of the two screening approaches highlighted important differences in how drug responses were captured, despite both assays being performed on the same treatment conditions and samples in parallel. Flow cytometry analysis indicated that AML cells cultured on the crosslinked scaffold generally exhibited drug sensitivities comparable to those observed in polystyrene, with compound-specific shifts in IC_{50} reflecting condition-dependent responses. For example, 5-fluorouracil showed nearly identical IC_{50} values between polystyrene (1.249 μM) and scaffold (1.228 μM), while daunorubicin and filanesib also demonstrated consistent potency across both platforms. In contrast, sorafenib and

zosuquidar displayed higher IC_{50} values in scaffold cultures relative to polystyrene, suggesting reduced sensitivity in the scaffold environment, whereas cytarabine showed slightly greater sensitivity in scaffold. Thioridazine dose–response curves did not reach a stable inhibitory range, preventing reliable IC_{50} estimation. These measurements were derived from direct quantification of live and dead cell populations, allowing nonlinear regression analysis and statistical comparison of dose–response curves using an extra sum-of-squares F-test.

In parallel, the same treated samples were evaluated using an AlamarBlue assay on the Agilent Cytation C10 imaging plate reader to assess metabolic activity as a proxy for cell viability. Although the AlamarBlue standard curve demonstrated a strong linear correlation between fluorescence intensity and cell number ($R^2 = 0.9571$), IC_{50} values generated from fluorescence readings showed greater variability compared with those obtained by flow cytometry. Scaffold cultures appeared markedly more sensitive to 5-fluorouracil and sorafenib in the AlamarBlue assay, while daunorubicin appeared more potent in polystyrene, trends that differed from those observed by flow cytometry. Filanesib remained consistently potent across both platforms, but compounds such as zosuquidar and thioridazine displayed unstable or inconsistent dose–response behaviour. These discrepancies likely reflect the indirect nature of metabolic assays, where fluorescence intensity represents cellular metabolic activity rather than a direct measurement of viable cell number.

Although the plate reader assay indicated significant effects for all drugs except thioridazine and filanesib, these results are unreliable because the fluorescence readouts corresponded to negative metabolic activity in the figures. Significance was determined via nonlinear regression and comparison of dose–response curves using an extra sum-of-squares F-test. However, these measurements do not provide a dependable assessment of drug response. Flow cytometry enables direct single-cell quantification of viability and population changes, providing more consistent and interpretable dose–response relationships.

Collectively, these results support the use of flow cytometry as a more reliable platform for drug screening in scaffold-based AML culture systems, particularly when evaluating compounds that may alter cellular metabolism independently of cell survival.

CHAPTER 6

CONCLUDING REMARKS

6.1 Conclusion

Acute myeloid leukemia (AML) progression and therapeutic resistance are profoundly shaped by interactions between leukemic cells and the extracellular matrix (ECM), which together form a protective niche within the bone marrow. These ECM-mediated signals enhance leukemic cell survival and diminish drug sensitivity, contributing to treatment failure and relapse. Traditional preclinical drug screening platforms, which predominantly use two-dimensional polystyrene cultures, fail to capture this microenvironmental complexity and may therefore underestimate niche-driven drug resistance.

Scaffold-based culture systems offer a more physiologically relevant representation of ECM architecture and cell–matrix interactions, influencing leukemic cell behavior and therapeutic response. However, accurately quantifying drug effects in such complex environments remains challenging, as standard assays including plate-based viability measurements, flow cytometry and high-content microscopy, each present specific strengths and limitations.

In this work, we addressed these challenges by optimizing and comparing complementary screening methods for assessing AML drug responses in both conventional polystyrene and ECM-mimicking scaffold cultures. Our results identified these constraints and guided the optimization of the experimental methodology, ultimately leading to the use of flow cytometry for more reliable assessment of AML cell responses.

It was observed that crosslinking scaffold structure dictate cell–matrix interactions and recovery efficiency, influencing cell survival on 2D scaffold environments by supporting higher OCI-AML2 viability over extended culture periods compared with polystyrene. This approach not only enhanced cell viability but also confirmed the distinct responses of cells in the scaffold environment compared to conventional polystyrene cultures across varying drug treatment concentrations.

We established a framework for evaluating drug sensitivity under microenvironment-relevant conditions. Leukemic cells exhibited variable response under scaffold conditions, potent agents like daunorubicin, filanesib, and cytarabine maintained efficacy regardless of

culture platform while 5-fluorouracil, sorafenib, and thioridazine showed reduced sensitivity in scaffold cultures. Highlighting that the ECM functions as an active, mechanism-specific regulator of AML drug response, rather than a passive protective barrier capturing compound-specific and microenvironment-dependent effects.

This approach enables more accurate assessment of ECM-associated drug resistance and provides a foundation for improving preclinical screening strategies, ultimately supporting the development of more effective AML therapeutics.

6.2 Future Directions

Building on the current findings, future studies will extend these experiments to primary patient AML samples to evaluate whether the methods established here yield consistent results in a clinically relevant context. Screening these samples will provide critical insight into the effects of therapeutics on leukemic stem cells including impacts on survival, proliferation, differentiation and underlying molecular mechanisms. To better understand the basis of differential drug responses, RNA sequencing can be employed to identify genes associated with resistance while complementary protein expression assays may reveal how specific therapeutics contribute to drug resistance mechanisms in AML cells.

Additionally, a broader drug screening approach will be undertaken including compounds not FDA approved, still in development and those that failed clinical trials to identify therapies that may perform more effectively in physiologically relevant scaffold environments. This approach could serve as a preclinical screening platform, allowing clinical trials to advance more efficiently by progressing only compounds that demonstrate efficacy within the scaffold-based system. It will elucidate how genetic differences between patients influence treatment response, providing a foundation for personalized medicine approaches. Collectively, these studies aim to refine therapeutic strategies, improve targeting of leukemic stem cells, and enhance remission outcomes for AML patients.

APPENDIX

Appendix 1. Sample CFU Results

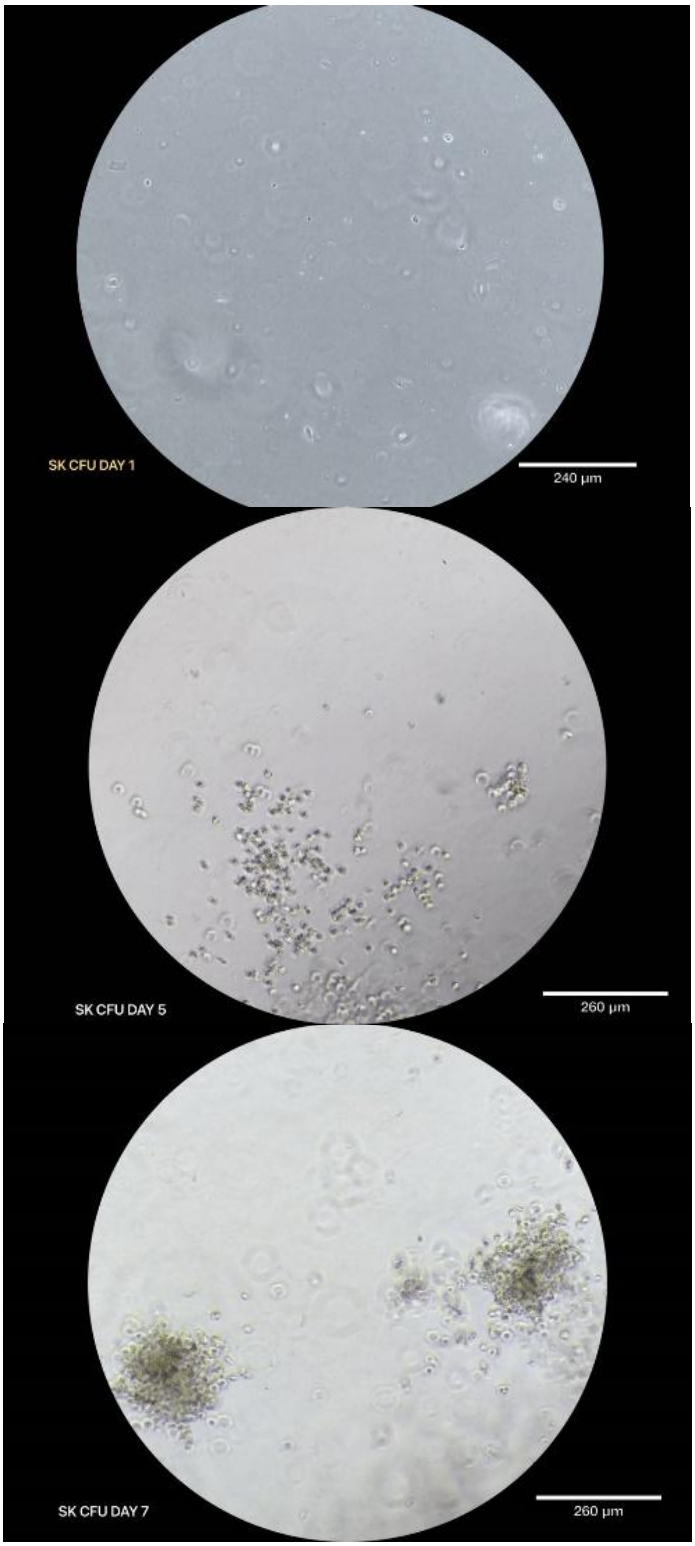

Supplemental Figure 1. Colony formation from 500 OCI-AML-2 cells cultured in MethoCult H4434. Representative images show colony development at different time points during incubation: A) day 0, immediately following cell plating, B) day 5, and C) day 7. Progressive colony growth and increased cellular clustering can be observed over time, reflecting the proliferative capacity of OCI-AML-2 cells within the semisolid methylcellulose medium. All images were acquired using phase-contrast microscopy at 10× magnification.

Appendix 2. 7AAD Standard Curve and Dead Cell Count

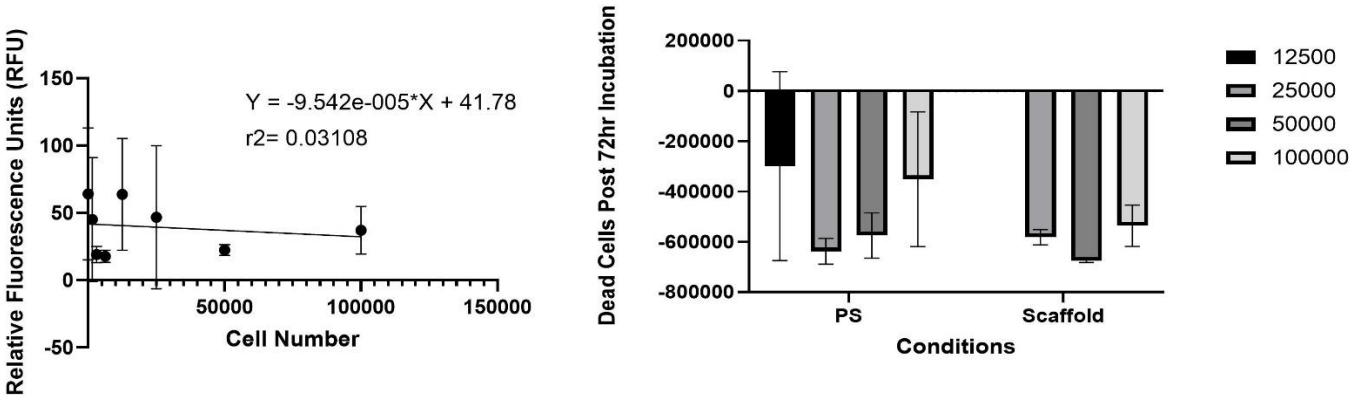

Supplemental Figure 2. Evaluation of fluorescence-based cell quantification and cell death following 72-hour incubation. (Left) Correlation between relative fluorescence units (RFU) and seeded cell number measured using a fluorescence-based assay. Linear regression analysis ($Y = -9.542 \times 10^{-5}X + 41.78$, $R^2 = 0.03108$) indicates a weak relationship between fluorescence signal and cell number under the tested conditions. (Right) Quantification of dead OCI-AML-2 cells after 72 hours of incubation under two culture conditions: standard polystyrene (PS) and scaffold. Cells were seeded at increasing densities (12,500; 25,000; 50,000; and 100,000 cells). Bars represent mean values with error bars indicating variability between replicates.

Appendix 3. Gating Strategy for Live/Dead Discrimination

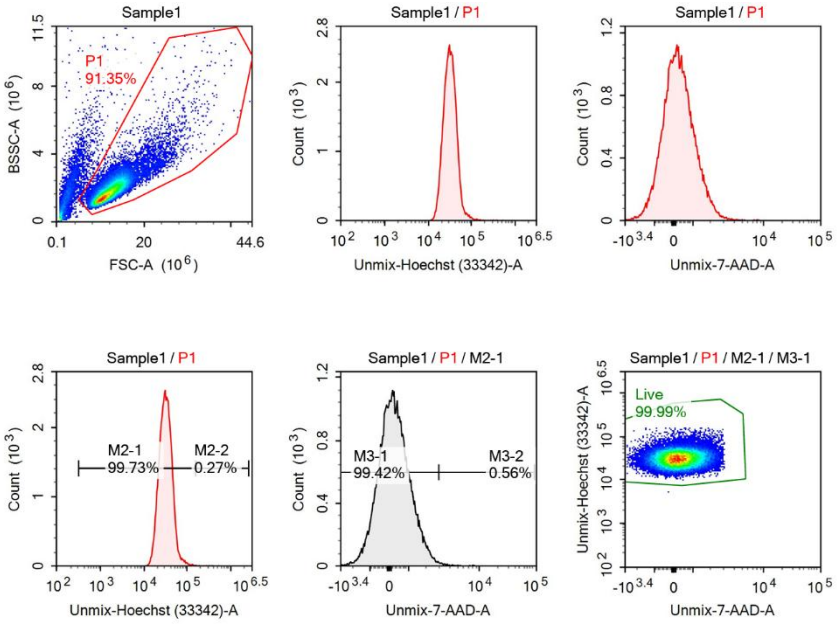

Supplemental Figure 3. Flow cytometry gating strategy for live/dead discrimination following drug treatment. Cells were first gated based on forward scatter area (FSC-A) versus side scatter area (SSC-A) to select the main cell population (P1). Within the P1 population, Hoechst (33342) staining was used to identify nucleated cells, while 7-AAD staining was used to discriminate dead cells. Sequential gating was applied to isolate Hoechst-positive events (M2-1), followed by exclusion of 7-AAD–positive cells (M3-2) to identify the live cell population. The final live cell gate ($Hoechst^+/7\text{-}AAD^-$) represents viable cells.

REFERENCES

1. Abarrategi A et al. Versatile humanized niche model enables study of normal and malignant human hematopoiesis. Journal of Clinical Investigation. 2017;127(2):543–548. https://doi.org/10.1172/JCI89364

2. Adnane L, Trail PA, Taylor I, Wilhelm SM. Sorafenib (BAY 43-9006, Nexavar®), a Dual-Action Inhibitor That Targets RAF/MEK/ERK Pathway in Tumor Cells and Tyrosine Kinases VEGFR/PDGFR in Tumor Vasculature. 2006. p 597–612. https://doi.org/10.1016/S0076-6879(05)07047-3

3. Algarín EM, Hernández-García S, Garayoa M, Ocio EM. Filanesib for the treatment of multiple myeloma. Expert Opinion on Investigational Drugs. 2020;29(1):5–14. https://doi.org/10.1080/13543784.2020.1703179

4. Alice Pievani et al. Acute myeloid leukemia shapes the bone marrow stromal niche <i>in vivo</i> Haematologica. 2020;106(3):865–870. https://doi.org/10.3324/haematol.2020.247205

5. Al-Mawali A. Leukemic Stem Cells Shows the Way for Novel Target of Acute Myeloid Leukemia Therapy Citation: Al-Mawali A (2013) Leukemic Stem Cells Shows the Way for Novel. J Stem Cell Res Ther. 2013 [accessed 2026 Feb 17];3:4. https://doi.org/10.4172/2157-7633.1000151

6. Alves AC et al. The daunorubicin interplay with mimetic model membranes of cancer cells: A biophysical interpretation. Biochimica et Biophysica Acta (BBA) - Biomembranes. 2017;1859(5):941–948. https://doi.org/10.1016/j.bbamem.2017.01.034

7. Antebi B et al. Stromal-cell-derived extracellular matrix promotes the proliferation and retains the osteogenic differentiation capacity of mesenchymal stem cells on three-dimensional scaffolds. Tissue Engineering - Part C: Methods. 2015 [accessed 2026 Feb 28];21(2):171–181. https://scholar.google.com/scholar_url?url=https://journals.sagepub.com/doi/pdf/10.1089/ten.tec.2014.0092&hl=en&sa=T&oi=ucasa&ct=ufr&ei=hm6kabitNNiM6rQP1pLi2Qk&scisig=AFtJQiwOcwSVv-1jh9GDGjWJQ1IL. https://doi.org/10.1089/ten.tec.2014.0092

8. Aslostovar L et al. A phase 1 trial evaluating thioridazine in combination with cytarabine in patients with acute myeloid leukemia. Blood Advances. 2018;2(15):1935–1945. https://doi.org/10.1182/bloodadvances.2018015677

9. Aslostovar L et al. A phase 1 trial evaluating thioridazine in combination with cytarabine in patients with acute myeloid leukemia. Blood Advances. 2018 [accessed 2026 Feb 28];2(15):1935–1945. https://dx.doi.org/10.1182/bloodadvances.2018015677.
https://doi.org/10.1182/bloodadvances.2018015677

10. Aslostovar L et al. Abnormal dopamine receptor signaling allows selective therapeutic targeting of neoplastic progenitors in AML patients. Cell Reports Medicine. 2021;2(2):100202. https://doi.org/10.1016/j.xcrm.2021.100202

11. Banks MN, Cacace AM, O'Connell J, Houston JG. High-Throughput Screening: Evolution of Technology and Methods. Pharmaceutical Sciences Encyclopedia. 2010 Mar 15 [accessed 2026 Feb 26]:1–44. https://onlinelibrary.wiley.com/doi/full/10.1002/9780470571224.pse014.
https://doi.org/10.1002/9780470571224.pse014

12. Behrmann L, Wellbrock J, Fiedler W. Acute Myeloid Leukemia and the Bone Marrow Niche—Take a Closer Look. Frontiers in Oncology. 2018;8. https://doi.org/10.3389/fonc.2018.00444

13. Blair A, Sutherland HJ. Primitive acute myeloid leukemia cells with long-term proliferative ability in vitro and in vivo lack surface expression of c-kit (CD117). Experimental Hematology. 2000 [accessed 2026 Feb 28];28(6):660–671. https://doi.org/10.1016/S0301-472X(00)00155-7

14. Blair HA. Daunorubicin/Cytarabine Liposome: A Review in Acute Myeloid Leukaemia. Drugs. 2018;78(18):1903–1910. https://doi.org/10.1007/s40265-018-1022-3

15. Blanco TM, Mantalaris A, Bismarck A, Panoskaltsis N. The development of a three-dimensional scaffold for ex vivo biomimicry of human acute myeloid leukaemia. Biomaterials. 2010;31(8):2243–2251. https://doi.org/10.1016/j.biomaterials.2009.11.094

16. Bonnet D, Dick JE. Human acute myeloid leukemia is organized as a hierarchy that originates from a primitive hematopoietic cell. Nature Medicine 1997 3:7. 1997 [accessed 2026 Apr 15];3(7):730–737. https://www.nature.com/articles/nm0797-730. https://doi.org/10.1038/nm0797-730

17. Brown BN et al. Surface characterization of extracellular matrix scaffolds. Biomaterials. 2010 [accessed 2026 Feb 27];31(3):428–437. https://pubmed.ncbi.nlm.nih.gov/19828192/. https://doi.org/10.1016/j.biomaterials.2009.09.061

18. Busch C, Nyamondo K, Wheadon H. Complexities of modeling the bone marrow microenvironment to facilitate hematopoietic research. Experimental Hematology. 2024 [accessed 2026 Apr 15];135. https://www.exphem.org/action/showFullText?pii=S0301472X24000924. https://doi.org/10.1016/j.exphem.2024.104233

19. Busch C, Nyamondo K, Wheadon H, O'gorman P. Complexities of modeling the bone marrow microenvironment to facilitate hematopoietic research. Experimental Hematology. 2024 [accessed 2026 Feb 28];135:104233. https://doi.org/10.1016/j.exphem.2024.104233. https://doi.org/10.1016/j.exphem.2024.104233

20. Cairns L V, Clarke K, Catherwood M, Mills KI. Multiplex Drug Screening Identifies a Novel Therapeutic Backbone for the Treatment of Acute Myeloid Leukaemia. Blood. 2022 [accessed 2026 Feb 25];140(Supplement 1):7814–7815. https://dx.doi.org/10.1182/blood-2022-163107. https://doi.org/10.1182/blood-2022-163107

21. Carrillo E et al. 5-Fluorouracil derivatives: a patent review (2012 – 2014). Expert Opinion on Therapeutic Patents. 2015;25(10):1131–1144. https://doi.org/10.1517/13543776.2015.1056736

22. Carter BZ et al. Inhibition of KSP by ARRY-520 induces cell cycle block and cell death via the mitochondrial pathway in AML cells. Leukemia. 2009;23(10):1755–1762. https://doi.org/10.1038/leu.2009.101

23. Chen W et al. Neurotransmitters in tumors: chemical cross-talk shaping tumor progression. Biomarker Research. 2025;13(1):125. https://doi.org/10.1186/s40364-025-00835-6

24. Cros E, Jordheim L, Dumontet C, Galmarini CM. Problems Related to Resistance to Cytarabine in Acute Myeloid Leukemia. Leukemia & Lymphoma. 2004;45(6):1123–1132. https://doi.org/10.1080/1042819032000159861

25. Dhaliwal A et al. Profiling stem cell states in three-dimensional biomaterial niches using high content image informatics. Acta Biomaterialia. 2016 [accessed 2026 Feb 25];45:98–109. https://pubmed.ncbi.nlm.nih.gov/27590870/. https://doi.org/10.1016/j.actbio.2016.08.052

26. Döhner H et al. Expression of a specific extracellular matrix signature is a favorable prognostic factor in acute myeloid leukemia. Leukemia Research Reports. 2018 [accessed 2026 Feb 25];9(4):9–13. https://doi.org/10.1182/blood-2016-08-733196. https://doi.org/10.1182/blood-2016-08-733196

27. Ermens AA, Kroes AC, Lindemans J, Abels J. 5-Fluorouracil treatment of rat leukemia and a reappraisal of its application in human leukemia. Anticancer research. 1986;6(4):797–800.

28. Fernandez HF et al. Anthracycline Dose Intensification in Acute Myeloid Leukemia. New England Journal of Medicine. 2009;361(13):1249–1259. https://doi.org/10.1056/NEJMoa0904544

29. Floren M, Gillette JM. Acute myeloid leukemia: Therapy resistance and a potential role for tetraspanin membrane scaffolds. The International Journal of Biochemistry & Cell Biology. 2021;137:106029. https://doi.org/10.1016/j.biocel.2021.106029

30. Gadaleta-Caldarola G et al. Sorafenib: 10 years after the first pivotal trial. Future Oncology. 2015;11(13):1863–1880. https://doi.org/10.2217/fon.15.85

31. Garcia-Saez I, Skoufias DA. Eg5 targeting agents: From new anti-mitotic based inhibitor discovery to cancer therapy and resistance. Biochemical Pharmacology. 2021;184:114364. https://doi.org/10.1016/j.bcp.2020.114364

32. Gattazzo F, Urciuolo A, Bonaldo P. Extracellular matrix: A dynamic microenvironment for stem cell niche. Biochimica et Biophysica Acta (BBA) - General Subjects. 2014 [accessed 2026 Feb 25];1840(8):2506–2519. https://doi.org/10.1038/nrm3620. https://doi.org/10.1016/j.bbagen.2014.01.010

33. Goda C et al. ARTICLE Cellular taxonomy of the preleukemic bone marrow niche of acute myeloid leukemia. [accessed 2026 Feb 28]. https://doi.org/10.1038/s41375-024-02415-3. https://doi.org/10.1038/s41375-024-02415-3

34. Gong Q et al. High Doses of Daunorubicin during Induction Therapy of Newly Diagnosed Acute Myeloid Leukemia: A Systematic Review and Meta-Analysis of Prospective Clinical Trials. 2015 [accessed 2026 Feb 28]. https://clinicaltrials.gov/,. https://doi.org/10.1371/journal.pone.0125612

35. Gong Q et al. High Doses of Daunorubicin during Induction Therapy of Newly Diagnosed Acute Myeloid Leukemia: A Systematic Review and Meta-Analysis of Prospective Clinical Trials. PLOS ONE. 2015;10(5):e0125612. https://doi.org/10.1371/journal.pone.0125612

36. Hansen RM, Quebbeman E, Anderson T. 5-Fluorouracil by Protracted Venous Infusion. Oncology. 1989;46(4):245–250. https://doi.org/10.1159/000226725

37. Harvestine JN, Saiz AM, Leach JK. Cell-secreted extracellular matrix influences cellular composition sequestered from unprocessed bone marrow aspirate for osteogenic grafts. Biomaterials Science. 2019 [accessed 2026 Apr 18];7(5):2091–2101. https://pubs.rsc.org/en/content/articlehtml/2019/bm/c8bm01478g. https://doi.org/10.1039/C8BM01478G

38. Hasserjian RP. Acute myeloid leukemia: Advances in diagnosis and classification. International Journal of Laboratory Hematology. 2013 [accessed 2026 Feb 17];35(3):358–366. https://onlinelibrary.wiley.com/doi/pdf/10.1111/ijlh.12081. https://doi.org/10.1111/ijlh.12081

39. Hasskarl J. Sorafenib: Targeting Multiple Tyrosine Kinases in Cancer. 2014. p 145–164. https://doi.org/10.1007/978-3-642-54490-3_8

40. Hou H-A et al. Genetic Alterations and Their Clinical Implications in Acute Myeloid Leukemia. Myeloid Leukemia - Basic Mechanisms of Leukemogenesis. 2011 Dec 14 [accessed 2026 Apr 15]. https://www.intechopen.com/chapters/25043. https://doi.org/10.5772/26421

41. Hu S et al. Activity of the Multikinase Inhibitor Sorafenib in Combination With Cytarabine in Acute Myeloid Leukemia. JNCI: Journal of the National Cancer Institute. 2011 [accessed 2026 Feb 28];103(11):893–905. https://dx.doi.org/10.1093/jnci/djr107. https://doi.org/10.1093/jnci/djr107

42. Jagannathan-Bogdan M, Zon LI. Hematopoiesis. Development. 2013;140(12):2463–2467. https://doi.org/10.1242/dev.083147

43. Jusoh N et al. Microfluidic vascularized bone tissue model with hydroxyapatite-incorporated extracellular matrix. Lab on a chip. 2015 [accessed 2026 Feb 28];15(20):3984–3988. https://pubmed.ncbi.nlm.nih.gov/26288174/. https://doi.org/10.1039/c5lc00698h

44. Kadry YA, Calderwood DA. Chapter 22: Structural and signaling functions of integrins. Biochimica et biophysica acta. Biomembranes. 2020 [accessed 2026 Apr 18];1862(5):183206. https://pmc.ncbi.nlm.nih.gov/articles/PMC7063833/. https://doi.org/10.1016/J.BBAMEM.2020.183206

45. Kersten B et al. CD45RA, a specific marker for leukaemia stem cell sub-populations in acute myeloid leukaemia. British Journal of Haematology. 2016 [accessed 2026 Feb 18];173(2):219–235. /doi/pdf/10.1111/bjh.13941. https://doi.org/10.1111/bjh.13941

46. Khoury HJ et al. A phase 1 dose-escalation study of ARRY-520, a kinesin spindle protein inhibitor, in patients with advanced myeloid leukemias. Cancer. 2012;118(14):3556–64. https://doi.org/10.1002/cncr.26664

47. Kim. Defective expression of deoxycytidine kinase in cytarabine-resistant acute myeloid leukemia cells. International Journal of Oncology. 2009;34(4). https://doi.org/10.3892/ijo_00000245

48. Klamer S, Voermans C. Cell Adhesion & Migration The role of novel and known extracellular matrix and adhesion molecules in the homeostatic and regenerative bone marrow microenvironment. 2015 [accessed 2026 Apr 15]. https://www.tandfonline.com/action/journalInformation?journalCode=kcam20. https://doi.org/10.4161/19336918.2014.968501

49. Klein G. The extracellular matrix of the hematopoietic microenvironment. Experientia 1995 51:9. 1995 [accessed 2026 Feb 28];51(9):914–926. https://link.springer.com/article/10.1007/BF01921741. https://doi.org/10.1007/BF01921741

50. Kobayashi N et al. Integrin α7 and Extracellular Matrix Laminin 211 Interaction Promotes Proliferation of Acute Myeloid Leukemia Cells and Is Associated with Granulocytic Sarcoma. Cancers. 2020 [accessed 2026 Apr 17];12(2):363. https://pmc.ncbi.nlm.nih.gov/articles/PMC7072541/. https://doi.org/10.3390/CANCERS12020363

51. Konopleva M, Tabe Y, Zeng Z, Andreeff M. Therapeutic targeting of microenvironmental interactions in leukemia: mechanisms and approaches. Drug resistance updates : reviews and commentaries in antimicrobial and anticancer chemotherapy. 2009 [accessed 2026 Apr 17];12(0):103. https://pmc.ncbi.nlm.nih.gov/articles/PMC3640296/. https://doi.org/10.1016/J.DRUP.2009.06.001

52. Kopp HG, Avecilla ST, Hooper AT, Rafii S. The bone marrow vascular niche: home of HSC differentiation and mobilization. Physiology. 2005 [accessed 2026 Feb 17];20(5):349–356. https://doi.org/10.1152/physiol.00025.2005

53. De Kouchkovsky I, Abdul-Hay M. ‘Acute myeloid leukemia: a comprehensive review and 2016 update’ Blood Cancer Journal. 2016 [accessed 2026 Feb 17];6:441. www.nature.com/bcj. https://doi.org/10.1038/bcj.2016.50

54. Kufe DW, Major PP. Studies on the mechanism of action of cytosine arabinoside. Medical and Pediatric Oncology. 1982;10(S1):49–67. https://doi.org/10.1002/mpo.2950100708

55. Kumar B et al. Acute myeloid leukemia transforms the bone marrow niche into a leukemia-permissive microenvironment through exosome secretion. Leukemia. 2018;32(3):575–587. https://doi.org/10.1038/leu.2017.259

56. Ladikou EE, Sivaloganathan H, Pepper & A, Chevassut & T. Acute Myeloid Leukaemia in Its Niche: the Bone Marrow Microenvironment in Acute Myeloid Leukaemia. 1912 [accessed 2026 Feb 28]. https://doi.org/10.1007/s11912-020-0885-0. https://doi.org/10.1007/s11912-020-0885-0

57. Lai WY et al. Reconstitution of bone-like matrix in osteogenically differentiated mesenchymal stem cell-collagen constructs: A three-dimensional in vitro model to study hematopoietic stem cell niche. Journal of Tissue Engineering. 2013 [accessed 2026 Feb 28];4(1):1–14. https://scholar.google.com/scholar_url?url=https://journals.sagepub.com/doi/pdf/10.1177/2041731413508668&hl=en&sa=T&oi=ucasa&ct=ufr&ei=QlekafO2Mtil6rQP6o2D2Aw&scisig=AFtJQix4Ia8rrye1JWKFfuLx5ahK. https://doi.org/10.1177/2041731413508668

58. Lancet JE et al. Phase I/II Study of the P-Glycoprotein (Pgp) Inhibitor Zosuquidar Administered by Continuous Infusion (CIV) with Daunorubicin (DNR) and Cytarabine (ARA-C) as Primary Therapy in Older Patients with Pgp-Positive Acute Myeloid Leukemia (AML). Blood. 2007;110(11):299–299. https://doi.org/10.1182/blood.V110.11.299.299

59. Lane SW, Scadden DT, Gilliland DG. The leukemic stem cell niche: current concepts and therapeutic opportunities. Blood. 2009 [accessed 2026 Apr 16];114(6):1150. https://pmc.ncbi.nlm.nih.gov/articles/PMC2723012/. https://doi.org/10.1182/BLOOD-2009-01-202606

60. Lee JY, Hong S-H. Hematopoietic Stem Cells and Their Roles in Tissue Regeneration. International Journal of Stem Cells. 2020;13(1):1–12. https://doi.org/10.15283/ijsc19127

61. LEMA C, VARELA-RAMIREZ A, AGUILERA RJ. Differential nuclear staining assay for high-throughput screening to identify cytotoxic compounds. Current cellular biochemistry. 2011 [accessed 2026 Feb 26];1(1):1. https://pmc.ncbi.nlm.nih.gov/articles/PMC4816492/

62. Li AJ, Dhanraj JP, Lopes G, Parker JL. Clinical trial risk in leukemia: Biomarkers and trial design. Hematological Oncology. 2021;39(1):105–113. https://doi.org/10.1002/hon.2818

63. Li D et al. A novel extracellular matrix-based leukemia model supports leukemia cells with stem cell-like characteristics. Leukemia Research. 2018 [accessed 2026 Apr 17];72:105–112. https://www.sciencedirect.com/science/article/abs/pii/S0145212618301905. https://doi.org/10.1016/J.LEUKRES.2018.08.012

64. Lindblad O et al. Aberrant activation of the PI3K/mTOR pathway promotes resistance to sorafenib in AML. Oncogene. 2016;35(39):5119–5131. https://doi.org/10.1038/onc.2016.41

65. Long S et al. ECM1 regulates the resistance of colorectal cancer to 5-FU treatment by modulating apoptotic cell death and epithelial-mesenchymal transition induction. Frontiers in Pharmacology. 2022 [accessed 2026 Feb 28];13:1005915. https://doi.org/10.3389/fphar.2022.1005915

66. Longley DB, Harkin DP, Johnston PG. 5-Fluorouracil: mechanisms of action and clinical strategies. Nature Reviews Cancer. 2003;3(5):330–338. https://doi.org/10.1038/nrc1074

67. Löwenberg B et al. High-Dose Daunorubicin in Older Patients with Acute Myeloid Leukemia. New England Journal of Medicine. 2009;361(13):1235–1248. https://doi.org/10.1056/NEJMoa0901409

68. Lymperi S, Ferraro F, Scadden DT. The HSC niche concept has turned 31 Has our knowledge matured? 2010 [accessed 2026 Feb 17]. https://doi.org/10.1111/j.1749-6632.2009.05223.x

69. Magina KN et al. Cytarabine dose in the consolidation treatment of AML: a systematic review and meta-analysis. Blood. 2017;130(7):946–948. https://doi.org/10.1182/blood-2017-04-777722

70. Man CH et al. Sorafenib treatment of FLT3-ITD+ acute myeloid leukemia: favorable initial outcome and mechanisms of subsequent nonresponsiveness associated with the emergence of a D835 mutation. Blood. 2012;119(22):5133–5143. https://doi.org/10.1182/blood-2011-06-363960

71. Marcelletti JF, Sikic BI. Continuous 72-h infusion of zosuquidar with chemotherapy in patients with newly diagnosed acute myeloid leukemia stratified for leukemic blast P-glycoprotein phenotype. Cancer Chemotherapy and Pharmacology. 2024;93(6):595–604. https://doi.org/10.1007/s00280-024-04656-6

72. Maynard RS, Hellmich C, Bowles KM, Rushworth SA. Acute Myeloid Leukaemia Drives Metabolic Changes in the Bone Marrow Niche. Frontiers in Oncology. 2022 [accessed 2026 Feb 28];12:924567. www.frontiersin.org. https://doi.org/10.3389/fonc.2022.924567

73. Mendelson A, Frenette PS. Hematopoietic stem cell niche maintenance during homeostasis and regeneration. Nature Medicine. 2014;20(8):833–846. https://doi.org/10.1038/nm.3647

74. Mendelson A, Frenette PS. Hematopoietic stem cell niche maintenance during homeostasis and regeneration. Nature Medicine. 2014;20(8):833–846. https://doi.org/10.1038/nm.3647

75. Menon K et al. Development and molecular characterization of polymeric micro-nanofibrous scaffold of a defined 3-D niche for in vitro chemosensitivity analysis against acute myeloid leukemia cells. International Journal of Nanomedicine. 2015 May:3603. https://doi.org/10.2147/IJN.S80397

76. Morrison SJ, Scadden DT. The bone marrow niche for haematopoietic stem cells. Nature 2014 505:7483. 2014 [accessed 2026 Feb 28];505(7483):327–334. https://www.nature.com/articles/nature12984. https://doi.org/10.1038/nature12984

77. Morrison SJ, Scadden DT. The bone marrow niche for haematopoietic stem cells. [accessed 2026 Feb 17]. https://doi.org/10.1038/nature12984

78. Mortera Blanco T, Mantalaris A, Bismarck A, Panoskaltsis N. The development of a three-dimensional scaffold for ex vivo biomimicry of human acute myeloid leukaemia. 2009 [accessed 2026 Feb 27]. https://doi.org/10.1016/j.biomaterials.2009.11.094

79. Murphy T, Yee KWL. Cytarabine and daunorubicin for the treatment of acute myeloid leukemia. Expert Opinion on Pharmacotherapy. 2017;18(16):1765–1780. https://doi.org/10.1080/14656566.2017.1391216

80. Nair MS et al. Development and molecular characterization of polymeric micro-nanofibrous scaffold of a defined 3-D niche for in vitro chemosensitivity analysis against acute myeloid leukemia cells. International Journal of Nanomedicine. 2015 [accessed 2026 Feb 27];10(1):3603–3622. https://www.dovepress.com/development-and-molecular-characterization-ofnbsppolymeric-micro-nanof-peer-reviewed-fulltext-article-IJN. https://doi.org/10.2147/IJN.S80397

81. Niu J, Peng D, Liu L. Drug Resistance Mechanisms of Acute Myeloid Leukemia Stem Cells. Frontiers in Oncology. 2022 [accessed 2026 Feb 17];12:896426. www.frontiersin.org. https://doi.org/10.3389/fonc.2022.896426

82. Oryan A et al. Chemical crosslinking of biopolymeric scaffolds: Current knowledge and future directions of crosslinked engineered bone scaffolds. International Journal of Biological Macromolecules. 2018 [accessed 2026 Feb 27];107(PartA):678–688. https://pubmed.ncbi.nlm.nih.gov/28919526/. https://doi.org/10.1016/j.ijbiomac.2017.08.184

83. Pal R, Mamidi MK, Das AK, Bhonde R. Diverse effects of dimethyl sulfoxide (DMSO) on the differentiation potential of human embryonic stem cells. Archives of toxicology. 2012 [accessed 2026 Apr 18];86(4):651–661. https://pubmed.ncbi.nlm.nih.gov/22105179/. https://doi.org/10.1007/S00204-011-0782-2

84. Park B, Yoo KH, Kim C. Hematopoietic stem cell expansion and generation: the ways to make a breakthrough. Blood Research. 2015;50(4):194. https://doi.org/10.5045/br.2015.50.4.194

85. Pelcovits A, Niroula R. Acute Myeloid Leukemia: A Review. [accessed 2026 Feb 17]. https://seer.cancer.gov/statfacts/

86. Pinho S, Frenette PS. Haematopoietic stem cell activity and interactions with the niche. Nature Reviews Molecular Cell Biology. 2019;20(5):303–320. https://doi.org/10.1038/s41580-019-0103-9

87. Ravandi F et al. Final report of phase II study of sorafenib, cytarabine and idarubicin for initial therapy in younger patients with acute myeloid leukemia. Leukemia. 2014;28(7):1543–1545. https://doi.org/10.1038/leu.2014.54

88. Rimon N, Schuldiner M. Getting the whole picture: combining throughput with content in microscopy. Journal of Cell Science. 2011 [accessed 2026 Feb 25];124(22):3743–3751. https://dx.doi.org/10.1242/jcs.087486. https://doi.org/10.1242/jcs.087486

89. Robak T et al. Novel and Emerging Drugs for Acute Myeloid Leukemia: Pharmacology and Therapeutic Activity. Current Medicinal Chemistry. 2011;18(5):638–666. https://doi.org/10.2174/092986711794480104

90. Robak T, Wierzbowska A. Current and emerging therapies for acute myeloid leukemia. Clinical Therapeutics. 2009 [accessed 2026 Feb 28];31(PART. 2):2349–2370. https://pubmed.ncbi.nlm.nih.gov/20110045/. https://doi.org/10.1016/j.clinthera.2009.11.017

91. Roboz GJ. Current treatment of acute myeloid leukemia. Current Opinion in Oncology. 2012;24(6):711–719. https://doi.org/10.1097/CCO.0b013e328358f62d

92. Ross DD. Modulation of drug resistance transporters as a strategy for treating myelodysplastic syndrome. Best Practice & Research Clinical Haematology. 2004;17(4):641–651. https://doi.org/10.1016/j.beha.2004.08.014

93. S Z, K H. Cardiotoxicity induced by antineoplastic drug Daunorubicin and its amelioration: A review of literature. Blood, Heart and Circulation. 2019;3(1). https://doi.org/10.15761/BHC.1000153

94. Sachlos E et al. Identification of Drugs Including a Dopamine Receptor Antagonist that Selectively Target Cancer Stem Cells. Cell. 2012;149(6):1284–1297. https://doi.org/10.1016/j.cell.2012.03.049

95. Sallent I, Capella-Monsonís H, Zeugolis DI. Production and Characterization of Chemically Cross-Linked Collagen Scaffolds. Methods in molecular biology (Clifton, N.J.). 2019 [accessed 2026 Feb 27];1944:23–38. https://pubmed.ncbi.nlm.nih.gov/30840233/. https://doi.org/10.1007/978-1-4939-9095-5_3

96. Sart S et al. Crosslinking of extracellular matrix scaffolds derived from pluripotent stem cell aggregates modulates neural differentiation. Acta Biomaterialia. 2016 [accessed 2026 Feb 27];30:222–232. https://pubmed.ncbi.nlm.nih.gov/26577988/. https://doi.org/10.1016/j.actbio.2015.11.016

97. Schimmer AD. Novel Mitochondrial Mechanisms of Cytarabine Resistance in Primary AML Cells. Cancer Discovery. 2017;7(7):670–672. https://doi.org/10.1158/2159-8290.CD-17-0476

98. Shah JJ et al. ARRY-520 Shows Durable Responses in Patients with Relapsed/Refractory Multiple Myeloma in a Phase 1 Dose-Escalation Study. Blood. 2011;118(21):1860–1860. https://doi.org/10.1182/blood.V118.21.1860.1860

99. Shah JJ et al. A Phase 1 and 2 study of Filanesib alone and in combination with low-dose dexamethasone in relapsed/refractory multiple myeloma. Cancer. 2017;123(23):4617–4630. https://doi.org/10.1002/cncr.30892

100. Sorbera LA, Castaner J, Silvestre JS, Bayes M. Zosuquidar Trihydrochloride. Drugs of the Future. 2003;28(2):0125. https://doi.org/10.1358/dof.2003.028.02.719469

101. Subbiah R et al. Tunable Crosslinked Cell-Derived Extracellular Matrix Guides Cell Fate. Macromolecular bioscience. 2016 [accessed 2026 Feb 27];16(11):1723–1734. https://pubmed.ncbi.nlm.nih.gov/27557868/. https://doi.org/10.1002/mabi.201600280

102. Tang G et al. Advances in research on potential inhibitors of multiple myeloma. European Journal of Medicinal Chemistry. 2023;262:115875. https://doi.org/10.1016/j.ejmech.2023.115875

103. Tang R et al. Zosuquidar restores drug sensitivity in P-glycoprotein expressing acute myeloid leukemia (AML). BMC Cancer. 2008;8(1):51. https://doi.org/10.1186/1471-2407-8-51

104. Terpstra W et al. Fluorouracil selectively spares acute myeloid leukemia cells with long- term growth abilities in immunodeficient mice and in culture. Blood. 1996 [accessed 2026 Apr 17];88(6):1944–1950. https://dx.doi.org/10.1182/blood.V88.6.1944.bloodjournal8861944. https://doi.org/10.1182/BLOOD.V88.6.1944.BLOODJOURNAL8861944

105. Terpstra W et al. Fluorouracil selectively spares acute myeloid leukemia cells with long-term growth abilities in immunodeficient mice and in culture. Blood. 1996;88(6):1944–50.

106. Thomas D, Majeti R. Biology and relevance of human acute myeloid leukemia stem cells. Blood. 2017 [accessed 2026 Feb 17];129(12):1577–1585. https://dx.doi.org/10.1182/blood-2016-10-696054. https://doi.org/10.1182/blood-2016-10-696054

107. Till JE, Mcculloch EA. A Direct Measurement of the Radiation Sensitivity of Normal Mouse Bone Marrow Cells. Vol 14 1961.

108. Tina. Topoisomerase IIα expression in acute myeloid leukaemia cells that survive after exposure to daunorubicin or ara-C. Oncology Reports. 2009;22(06). https://doi.org/10.3892/or_00000597

109. Tissot F et al. 3220 – THE BONE MARROW EXTRACELLULAR MATRIX REMODELLING DURING ACUTE MYELOID LEUKAEMIA. Experimental Hematology. 2024 [accessed 2026 Apr 17];137:104540. https://www.sciencedirect.com/science/article/pii/S0301472X24003990. https://doi.org/10.1016/J.EXPHEM.2024.104540

110. Tregnago C et al. Thioridazine requires calcium influx to induce MLL-AF6–rearranged AML cell death. Blood Advances. 2020;4(18):4417–4429. https://doi.org/10.1182/bloodadvances.2020002001

111. Urs 1# ^ AP, Goda C, Kulkarni R. Remodeling of the bone marrow microenvironment during acute myeloid leukemia progression. Ann Transl Med. 2024 [accessed 2026 Feb 28];12(4). https://dx.doi.org/10.21037/atm-23-1824. https://doi.org/10.21037/atm-23-1824

112. Urs AP, Goda C, Kulkarni R. Remodeling of the bone marrow microenvironment during acute myeloid leukemia progression. Annals of Translational Medicine. 2024;12(4):63–63. https://doi.org/10.21037/atm-23-1824

113. Valencia-Lazcano AA et al. 5-Fluorouracil nano-delivery systems as a cutting-edge for cancer therapy. European Journal of Medicinal Chemistry. 2023;246:114995. https://doi.org/10.1016/j.ejmech.2022.114995

114. Vincelette ND, Yun S. Assessing the Mechanism of Cytarabine-Induced Killing in Acute Leukemia. Blood. 2014;124(21):5210–5210. https://doi.org/10.1182/blood.V124.21.5210.5210

115. Walter RB et al. Shortcomings in the clinical evaluation of new drugs: acute myeloid leukemia as paradigm. Blood. 2010;116(14):2420–2428. https://doi.org/10.1182/blood-2010-05-285387

116. Wang A, Zhong H. Roles of the bone marrow niche in hematopoiesis, leukemogenesis, and chemotherapy resistance in acute myeloid leukemia. 2018 [accessed 2026 Feb 17]. https://www.tandfonline.com/action/journalInformation?journalCode=yhem20. https://doi.org/10.1080/10245332.2018.1486064

117. Wang A, Zhong H. Roles of the bone marrow niche in hematopoiesis, leukemogenesis, and chemotherapy resistance in acute myeloid leukemia. 2018 [accessed 2026 Feb 25]. https://www.tandfonline.com/action/journalInformation?journalCode=yhem20. https://doi.org/10.1080/10245332.2018.1486064

118. Wang A, Zhong H. Roles of the bone marrow niche in hematopoiesis, leukemogenesis, and chemotherapy resistance in acute myeloid leukemia. Hematology. 2018;23(10):729–739. https://doi.org/10.1080/10245332.2018.1486064

119. Wang LD, Wagers AJ. Dynamic niches in the origination and differentiation of haematopoietic stem cells. Nature Reviews Molecular Cell Biology. 2011;12(10):643–655. https://doi.org/10.1038/nrm3184

120. Wang X et al. High-dose cytarabine monotherapy is superior to standard-dose cytarabine- based multiagent sequential treatment cycle for consolidation treatment in adult (14-59 years) AML patients according to European Leukemia Net 2022 risk stratification. Frontiers in Oncology. 2023 [accessed 2026 Apr 17];12:1070588. https://pmc.ncbi.nlm.nih.gov/articles/PMC9885085/. https://doi.org/10.3389/FONC.2022.1070588

121. Wang Z, Xu C, Wang Q, Wang Y. Repurposing of nervous system drugs for cancer treatment: recent advances, challenges, and future perspectives. Discover Oncology. 2025;16(1):396. https://doi.org/10.1007/s12672-025-02067-4

122. Way GP et al. Evolution and impact of high content imaging. SLAS Discovery. 2023 [accessed 2026 Feb 25];28:292–305. http://creativecommons.org/licenses/by/4.0/. https://doi.org/10.1016/j.slasd.2023.08.009

123. Welch J et al. Identification of AML/MDS Drug Sensitization By In Vivo Chemotherapy Administration. Blood. 2020 [accessed 2026 Feb 27];136(Supplement 1):32–33. https://dx.doi.org/10.1182/blood-2020-142165. https://doi.org/10.1182/blood-2020-142165

124. Woessner R et al. ARRY-520, a novel KSP inhibitor with potent activity in hematological and taxane-resistant tumor models. Anticancer research. 2009;29(11):4373–80.

125. Xiang W, Lam YH, Periyasamy G, Chuah C. Application of High Throughput Technologies in the Development of Acute Myeloid Leukemia Therapy: Challenges and Progress. International Journal of Molecular Sciences. 2022;23(5):2863. https://doi.org/10.3390/ijms23052863

126. Xu X et al. Venetoclax Overcomes Sorafenib Resistance in Acute Myeloid Leukemia by Targeting BCL2. Biology. 2023;12(10):1337. https://doi.org/10.3390/biology12101337

127. Xu X, Zhang J-F. Cross-linked Electrospun Fibrous Scaffolds for Tissue Engineering. Current Tissue Engineering (Discontinued). 2012 [accessed 2026 Apr 18];1(1):2–14. https://www.eurekaselect.com/article/45462. https://doi.org/10.2174/2211542011201010002

128. Yao Y et al. Leukemia stem cell-bone marrow microenvironment interplay in acute myeloid leukemia development. Experimental Hematology & Oncology 2021 10:1. 2021 [accessed 2026 Apr 16];10(1):39-. https://link.springer.com/article/10.1186/s40164-021-00233-2. https://doi.org/10.1186/S40164-021-00233-2

129. Yu VWC, Scadden DT. Hematopoietic Stem Cell and Its Bone Marrow Niche. 2016. p 21–44. https://doi.org/10.1016/bs.ctdb.2016.01.009

130. Zhang N, Yin Y, Xu SJ, Chen WS. 5-Fluorouracil: Mechanisms of Resistance and Reversal Strategies. Molecules. 2008 [accessed 2026 Apr 17];13(8):1551. https://pmc.ncbi.nlm.nih.gov/articles/PMC6244944/. https://doi.org/10.3390/MOLECULES13081551

131. Zhang P et al. The physical microenvironment of hematopoietic stem cells and its emerging roles in engineering applications. [accessed 2026 Feb 28]. https://doi.org/10.1186/s13287-019-1422-7. https://doi.org/10.1186/s13287-019-1422-7

132. Zhang W et al. Sorafenib induces apoptosis of AML cells via Bim-mediated activation of the intrinsic apoptotic pathway. Leukemia. 2008;22(4):808–818. https://doi.org/10.1038/sj.leu.2405098

133. Zhou J. Identification and targeting leukemia stem cells: The path to the cure for acute myeloid leukemia. World Journal of Stem Cells. 2014 [accessed 2026 Feb 17];6(4):473. https://doi.org/10.4252/wjsc.v6.i4.473

134. Zoabi M et al. Reduced elastin in multiple myeloma niche promotes cell proliferation. Experimental Cell Research. 2025 [accessed 2026 Feb 28];444(2). https://pubmed.ncbi.nlm.nih.gov/39725193/. https://doi.org/10.1016/j.yexcr.2024.114395